Міністерство освіти і науки України
Національний технічний університет «Дніпровська політехніка»

Гірничий інститут, гірничий факультет
(інститут, факультет)

Кафедра підземної розробки родовищ
(повна назва)

ПОЯСНЮВАЛЬНА ЗАПИСКА
дипломної роботи
магістра
(назва освітньо-кваліфікаційного рівня)

галузь знань 18 Виробництво та технології
(шифр і назва галузі знань)

спеціальність 184 Гірництво
(код і назва спеціальності)

спеціалізація Розробка родовищ та видобування корисних копалин
(код і назва спеціалізації)

освітній рівень вища освіта
(назва освітнього рівня)

кваліфікація 2147.1 Гірничий інженер, дослідник
(код і назва кваліфікації)

на тему: Дослідження зменшення сили різання гранітного зразка, підданого мікрохвильовому опроміненню з варіюванням тривалості опромінення

Виконавець:

студент II **курсу, групи** 184м-16-11-ГФ

(підпис) Маловик А. В.
(прізвище та ініціали)

Керівники	Посада, прізвище, ініціали	Оцінка	Підпис
роботи	проф. Бондаренко В.І.		
розділів:			
Дослідницький	проф. Бондаренко В.І.		
Технологічний	проф. Бондаренко В.І.		

Рецензент			

Нормоконтроль	проф. Бондаренко В.І.		

Дніпро
2018

Міністерство освіти і науки України
Національний технічний університет «Дніпровська політехніка»

ЗАТВЕРДЖЕНО:
завідувач кафедри

_____
(повна назва)

_____ _____
(підпис) (прізвище, ініціали)

«_____»_____20___року

ЗАВДАННЯ
на виконання кваліфікаційної роботи магістра

спеціальності 184 Гірництво
(код і назва спеціальності)

студенту 184м-16-11-ГФ Маловик А. В.
(група) (прізвище та ініціали)

Тема дипломної роботи Дослідження зменшення сили різання гранітного зразка, підданого мікрохвильовому опроміненню з варіюванням тривалості опромінення

1 ПІДСТАВИ ДЛЯ ПРОВЕДЕННЯ РОБОТИ

Наказ ректора Державного НТУ "ДП" від _____**№**_____

2 МЕТА ТА ВИХІДНІ ДАНІ ДЛЯ ПРОВЕДЕННЯ РОБІТ

Об'єкт досліджень процес різання гранітних блоків, опромінених мікрохвилями, на лабораторному стенді для вимірювання сил різання.
Предмет досліджень сили різання у трьох напрямах та їх вплив на процес екскавації під час різання порід.
Мета дослідження зменшення сили різання гранітного зразка, підданого мікрохвильовому опроміненню з варіюванням тривалості опромінення, для визначення ефективності впливу мікрохвиль на породу та подальшої модернізації та автоматизації механічних способів екскавації.
Вихідні дані для проведення роботи проведення експериментів на дослідницькому стенді в ТУ «Фрайберзька гірнича академія»

3 ОЧІКУВАНІ НАУКОВІ РЕЗУЛЬТАТИ

Наукова новизна полягає у встановленні залежності сил різання, зносу ріжучого інструменту, енергоспоживання від відстані між різами робочого інструменту породи, поглибленні в породу та тривалість мікрохвильового опромінення.

Практична цінність полягає в розробці регресійних моделей, що дозволяють визначити залежність зусиль різання від відстані між різами та тривалості мікрохвильового опромінення; розробці мап зусиль та знаходження оптимальних параметрів різання скельних порід.

4 ВИМОГИ ДО РЕЗУЛЬТАТІВ ВИКОНАННЯ РОБОТИ

Обгрунтованість і достовірність наукових положень, висновків і рекомендацій, сформульованих в роботі, обумовлена: коректною постановкою завдань використанням фундаментальних положень механіки руйнування гірських порід і впливу мікрохвиль на породу.

5 ЕТАПИ ВИКОНАННЯ РОБОТИ

Найменування етапів робіт	Термін виконання
Стан питання мета і задачі дослідження	16.10.17 – 21.10.17
Аналіз методів розрахунку максимальних зусиль	22.10.17 – 03.11.17
Планування та проведення експериментів	04.11.17 – 10.12.17
Обробка масиву даних	11.12.17 – 19.12.17
Аналіз та розрахунок ключових параметрів процесу різання	20.12.17 – 02.01.18
Розробка регресійних моделей та мап сил	03.01.18 – 21.01.18

6 РЕАЛІЗАЦІЯ РЕЗУЛЬТАТІВ ТА ЕФЕКТИВНІСТЬ

Економічний ефект застосування мікрохвильового опромінення масиву гірських порід дозволить знизити міцність масиву і в результаті перейти від буровзривних методів видобутку до механічних, як результат оптимізувати безперервний процес відобутку.

Соціальний ефект застосування мікрохвиль дозволить відмовитись від вибухівки і буровзривних методів видобутку, що є незаперечно забруднює навколишнє середовище шумом, вібраціями та токсичними газами.

7 ДОДАТКОВІ ВИМОГИ

Відповідність оформлення згідно ДСТУ 3008-95. Документація. Звіти у сфері науки і техніки. Структура і правила оформлення.

Завдання видав _____ Бондаренко В.І.
(підпис) (прізвище, ініціали)

Завдання прийняв до виконання _____ Маловик А. В.
(підпис) (прізвище, ініціали)

Дата видачі завдання: 16.10.2017 р.

Термін подання дипломної роботи до ЕК 21.01.2018 р.

Дніпро
2018

ЗАГАЛЬНА ХАРАКТЕРИСТИКА РОБОТИ

Актуальність теми. Попит на безвибухові методи розробки міцних гірських порід постійно зростає. Це обумовлено цілим рядом причин, серед яких є наступні: зростаючий тиск на гірничодобувну промисловість та пов'язані з нею галузі промисловості органів влади та зацікавлених сторін. До того ж, механічні методи розробки скельних гірських порід демонструють ряд переваг в порівнянні з буровзривним методом.

Використання вибухових речовин створює ряд небезпечних факторів для працівників, навколишнього середовища та суміжних територій. А саме, викиди токсичних газів, землетруси, високий рівень шуму, погіршення стабільності гірських виробок. Крім того, велика частина видобувних робіт відбувається в політично нестабільних регіонах. Це може спричинити проблеми безпеки, пов'язані з придбанням, транспортуванням та зберіганням вибухових речовин. Більш цього, невибухові методи можуть бути впроваджені в методи розробки безперервної дії, це може бути інтегровано краще в гірничо-збагачувальний комплекс.

Саме тому механічні методи стають все більше і більше привабливими для гірничих підприємств. Проте вони показують високий рівень зносу та низіка швидкість просування фронту робіт в дуже твердих та абразивних породах. У випадку, якщо машини працювати в таких умовах можуть, механічні методи дуже негнучкі та не підходять для виробничих операцій. Для того, щоб збільшити діапазон застосування механічних методів, одним з можливих рішень є мікрохвильове випромінювання для зменшення різальної стійкості гірського масиву. Мікрохвильове випромінювання досліджується вже понад 70 років. В кінці 1960-х рр. була розглянута концепція використання мікрохвильової енергії в шахті. Проте, в контексті виробництва база знань обмежена. Тому в цій роботі аналізується ефект мікрохвильового опромінення щодо покращення ефективності різання, що є актуальною науковою задачею.

Мета роботи – дослідження зменшення сили різання гранітного зразка, підданого мікрохвильовому опроміненню з варіюванням тривалості опромінення,

для визначення ефективності впливу мікрохвиль на породу та подальшої модернізації та автоматизації механічних способів екстакавації.

Ідея роботи полягає у використанні мікрохвильового випромінювання для нагріву мінеральних включень з різними показниками діелектричної проникності, що призводить до виникнення тріщин і ослаблення скельного масиву.

Об'єкт досліджень – процес різання гранітних блоків, опромінених мікрохвилями, на лабораторному стенді для вимірювання сил різання.

Предмет досліджень – сили різання у трьох напрямах та їх вплив на процес екскавації під час різання порід.

Наукове значення роботи полягає у встановленні залежності сил різання, зносу ріжучого інструменту, енергоспоживання від відстані між різами робочого інструменту породи, поглибленні в породу та тривалість мікрохвильового опромінення.

Практичне значення роботи полягає в розробці регресійних моделей, що дозволяють визначити залежність зусиль різання від відстані між різами та тривалості мікрохвильового опромінення; розробці мап зусиль та знаходження оптимальних параметрів різання скельних порід.

Методи досліджень. Для вирішення сформульованих задач використовувався комплексний метод. Даний метод містить: теоретичні дослідження процесу екскавації скельних гірських порід та впливу мікрохвиль на гірські породи; методи фізичного моделювання, які використовувалися при розрахунках екскавованої породи; метод науково обґрунтованої постановки експерименту з використанням теорії регресійного аналізу і математичної статистики; експериментальні дослідження процесу різання граніту, опроміненого мікрохвилями різної тривалості.

РЕФЕРАТ

У **вступі** обґрунтовано актуальність теми магістерської роботи.

Перший розділ присвячений огляду та аналізу принципів екскавації твердих скельних порід. У ньому приведені поняття базових фізико-механічних властивостей гірських порід (модуль Юнга, пористість, щільність, одноосьова міцність на стиск та індекс абразивності), а також пояснення параметрів різання та їх вплив на ефективність (швидкість, глибина, відстань між різами та кути робочого інструменту).

Наведено приклади екскавації скельних гірських порід загальноприйнятими методами: буровзривний метод, використання тунелепрохідницьких машин та прохідницьких комбайнів. На ряду з ними представлені нові технології механічного видобутку твердих порід: використання дисків по технології «undercutting», тунелерозширювальні машини, активоване/осцилююче дискове різання, використання міні дисків, технологія ICUTROC, ударна дія, використання високонапірних струменів води або лазеру та підвердження мікрохвилям поперед екскавації.

У розділі приведені основні принципи та формули, пов’язані з мікрохвильовим опроміненням. Також, описані сьогоденні можливості та використання мікрохвиль у гірничій справі. Мікрохвильове опромінення має великий потенціал для використання у гірській промисловості. Мікрохвилі можуть використовуватися під час розморожування мерзлих ґрунтів; розм'якшення порід, розклад руди на мінерали; витяг металів з відходів і шламу; для подрібнення, вилуговування, магнітного поділу і високотемпературної сушки.

Сформульовано наукову задачу, визначено об'єкт і предмет досліджень, складено мету й задачі досліджень.

У **другому розділі** описуються методи дослідження, застосовувані до результатів випробувань процесу, і отримання регресійних моделей.

Основним принципом руйнування гірських порід є подолання зв'язку між частинками для дезінтеграції породи. Напруги, що перевищують міцність гірських

порід в масиві, є основою механічного руйнування гірських порід, вони призводять до виникнення та поширення тріщин, а також утворення стружки.

Під час різання на ріжучому інструменті діють тривимірні сили F_x, F_y, F_z.

Ріжуче зусилля F_x відбувається паралельно напрямку різання, F_x в основному відповідає за фактичну фрагментацію породи. Нормальна сила F_z спрямована перпендикулярно траєкторії різання та утримує ріжучий інструмент в скелі. Бокове зусилля F_y діє перпендикулярно траєкторії різання та утримує ріжучий інструмент в лінії різання. Повна сила F_{Total} може бути визначена наступним чином:

$$F_{Total} = \sqrt{F_x^2 + F_y^2 + F_z^2} \quad (1)$$

У цьому дослідженні найбільший інтерес представляють середні і максимальні сили (або пікові), оскільки вони використовуються для визначення параметрів екскаваційного обладнання.

В якості можливого методу аналізу пікових зусиль було прийнято рішення використовувати метод максимумів для аналізу даних. У цьому методі в якості амплітуд сил вибираються відмінності між піками σ_{maxi} та середнім значенням σ_μ. Крім того, повинні враховуватися тільки ті піки, що перевищують середнє значення.

У методі максимумів передбачається, що розподіл мінімумів і розподіл максимумів симетричні щодо σ_μ. Даний метод може вважатися вірним тільки у випадку, якщо здобутий масив даних відповідає нормальному закону розподілу. Перевірка масиву на нормальний закон розповсюдження приведена у даному розділі.

Під час процесу різання відстежується, вимірюється і обробляється кілька параметрів, таких як споживання енергії, знос робочого інструменту та розподіл часток за розмірами.

В поточній роботі досліджується питоме енергоспоживання процесу різання. Питоме споживання енергії дорівнює кількості енергії, споживаної для видобутку кубічного метра породи. Щоб визначити питому енергію E_{sp} в лабораторному тесті, використовувалось наступне рівняння:

$$E_{sp} = \frac{l_{1c} \cdot \sum \bar{F}_x}{3600 \cdot V_{cut}} \quad \left[\frac{\text{кВт} \cdot \text{год}}{\text{м}^3}\right] \tag{2}$$

де l_{1c} – довжина різу [м];

$\bar{F}_x$ – середнє ріжуче зусилля одного різу [кН];

V_{cut} – об’єм видобутої породи $\sum \bar{F}_x$ [м^3].

Інша форма споживання енергії, яка може бути оцінена, – це енергія, споживана мікрохвильовою установкою під час процесу опромінення.

$$E_{mic} = \frac{\sum E_{P_i}}{3600} \quad [\text{кВт} \cdot \text{год}] \tag{3}$$

де E_{P_i} – енергія, що витрачається на опромінення, в секунду [кДж/с].

Близько 80% всіх відмов видобувних машин викликані зносом деталей. Особливо інтенсивному стиранню піддаються робочі інструменти обладнання.

Деякі загальні ефекти зносу інструменту включають в себе підвищені зусилля різання, підвищені температури різання і погану обробку поверхні. Крім того, це може привести до зламу машини та викликати зміну геометрії інструменту.

Продуктивність видобутку і коефіцієнт зносу є основними темами багатьох досліджень. Однак знос повинний бути врахованим і аналізуватися під час експериментального аналізу. Таким чином, знос – це питання споживання матеріалу, а також важливий показник проведення гірських порід.

У цьому дослідженні застосовано незвичайний метод оцінки зносу. Це пов'язано з умовами експерименту. Основна процедура полягає у визначенні відношення різниці у вазі ріжучого інструменту до і після процесу різання щодо шляху різання:

$$W = \frac{m_i - m_{i+1}}{l_{cl}} \quad \left[\frac{\text{г}}{\text{м}}\right] \tag{4}$$

де m_i – маса різця до слою [г];

m_{i+1} – маса різця після слою [г];

l_{cl} – довжина різу [м].

Іншим важливим параметром, дослідженим в роботі, є розмір часток у відбитій породі. Розмір частинок грає важливу роль і безпосередньо впливає на безпеку здоров'я. Дрібні частинки легко вдихаються і можуть осідати в дихальних

шляхах в залежності від їх розміру, щільності, форми, властивостей заряду і поверхні, а також від характеру дихання людини. Численні дослідження та організації, наприклад Адміністрація безпеки та гігієни праці (OSHA) вказує, що розмір часток, які можуть досягати глибокої частини легенів, становить менш ніж 10 мкм. Однак розмір часток, які вдихаються, досягає 100 мкм. На жаль, в ході дослідження не було можливості визначити кількість часток, розмір яких менш ніж 63 мкм.

Крім того, більше подрібнення означає створення більшої площі поверхні, що, у свою чергу, вимагає більш високого споживання енергії. Менш подрібнений матеріал вказує на краще використання енергії, яке повинно приводити до меншого споживання енергії або більшого обсягу добутого матеріалу.

Процедура розробки регресійної моделі $y = f(x_1, x_2, x_3)$ була описана у другому розділі. Для розрахунку регрессіонної моделі, перш за все, необхідно створити таблицю з вихідними даними. У ній повинні бути змінні параметри (x_1, x_2, x_3) і експериментальні значення y.

Наступний крок – створення рівняння множинної регресії. Дослідження показують, що більшість експериментальних результатів можна описати як повний кубічний многочлен. Поліноміальна регресія трьохфакторної моделі може бути описана як:

$$y = b_0 + b_1x_1 + b_2x_2 + b_3x_3 + b_{12}x_1x_2 + b_{13}x_1x_3 + b_{23}x_2x_3 + b_{123}x_1x_2x_3 + b_{11}x_1^2 + b_{22}x_2^2 + b_{33}x_3^2 + b_{111}x_1^3 + b_{222}x_2^3 + b_{333}x_3^3. \quad (5)$$

Для визначення повного рівняння було використано метод множинного регресійного аналізу.

Для виконання регресійного моделювання існують два різних способи. Перший – взяття повного полінома та аналіз важливості членів рівняння в міру зменшення їх числа. Друге починається з простого рівняння з мінімальною кількістю членів, збільшуючи кількість змінних шляхом поступового додавання і обчислення важливості.

$$y = b_0 + b_1x_1 + b_2x_2 + b_3x_3 \quad (6)$$

Коефіцієнти b_i визначаються системою рівнянь, яка ґрунтується на методі виключення Гауса.

$$\begin{cases} nb_0 + b_1\sum x_1 + b_2\sum x_2 + b_3\sum x_3 = \sum y \\ b_0\sum x_1 + b_1\sum x_1^2 + b_2\sum x_1x_2 + b_3\sum x_1x_3 = \sum yx_1 \\ b_0\sum x_2 + b_1\sum x_1x_2 + b_2\sum x_2^2 + b_3\sum x_2x_3 = \sum yx_2 \\ b_0\sum x_3 + b_1\sum x_1x_3 + b_2\sum x_2x_3 + b_3\sum x_3^2 = \sum yx_3 \end{cases} \quad (7)$$

Розраховані коефіцієнти b_i повинні бути включені в рівняння (6). Наступним кроком проводиться визначення залишкової дисперсії регресії:

$$S_{res}^2 = \frac{\sum_{g=1}^{n}\left(Y_{gi} - y_i\right)^2}{n - (k+1)} \quad (8)$$

де y_i – розрахований результат параметру рівняння (6);

Y_{gi} – експериментальне значення;

$(k+1)$ – число коефіцієнтів в рівнянні (6);

n – розмір вибірки.

Надалі, додається наступний член многочлена до рівняння:

$$y = b_0 + b_1x_1 + b_2x_2 + b_3x_3 + b_{12}x_1x_2 \quad (9)$$

Для нового рівняння весь процес слід повторити. Після цього статистична значимість різниці дисперсій між многочленами може бути оцінена.

$$\frac{S_{res_j}^2}{S_{res_{j+1}}^2} > F_{1-p} \quad (10)$$

де F_{1-p} – значення розподілу Фішера, $m_1 = n - (k+1),\ m_2 = \infty$;

(більше значення S_{res}^2 повинно буті у чисельнику).

Якщо умова (10) виконана, то член додається до многочлена. Коли він є хибним, член повинен бути пропущений. Всі члени рівняння повинні бути оброблені і перевірені.

Визначення коефіцієнта кореляції проводиться за формулою:

$$R = \sqrt{1 - \frac{\sum_{g=1}^{n}\left(Y_{gi} - y_i\right)^2}{\sum_{g=1}^{n}\left(Y_{gi} - Y_g\right)^2}} \tag{11}$$

де Y_g – середнє експериментальне значення.

В результаті має бути отримано рівняння, що описує експериментальний результат з максимальною точністю.

У **третьому розділі** приведено та описано лабораторне обладнання та робочі зразки, використані в експериментах, а також наведені умови, за яких вони були проведені. Іншою частиною розділу являється обробка та аналіз результатів експериментального дослідження: ріжучі зусилля, питома енергія, знос і розподіл часток.

Ріжучі випробування проводилися з використанням випробувальної установки HXS 1000-50. Установка була розроблена для визначення сил та об'єму різання з використанням різних ріжучих інструментів під час роботи з блоками (зразками) в експериментальних умовах.

Машина була виготовлена ASW-GmbH Naumburg для проведення ріжучих випробувань в Технічному університеті «Фрайберзька гірнича академія», Німеччина.

Параметри різання налаштовуються за допомогою панелі управління. Рух інструменту по осі Y виконується шляхом переміщення траверсу, а по осі Z рух здійснюється шляхом регулювання робочого моста на потрібну висоту. Ріжуче переміщення виконується рухом робочого столу в напрямку X.

Вимірювальна система ріжучої сили, яка використовується в машині, може вимірювати сили в діапазоні від -50 до +50 кН (± 30 кН в напрямку Y). Похибка вимірювання дорівнює 0,5% (0,25 кН). Це допустима похибка в разі різання скельних порід.

Для дослідження були взяті три гранітних блоки, надані Гірничим університетом Леобену, Австрія. Хімічний склад був перевірений фірмою Baustoffprüfstelle Wismar GmbH.

Всі блоки мали розміри 500×500×300 мм та зернисту текстуру з ксеноморфними кристалами. Основні компоненти – це кварц, плагіоклазний польовий шпат, біотит, мусковіт і хлорит, апатит, епідот, титаніт і ксенотим. Крім того, міцність зразків на стиск дорівнює 202,7 МПа.

Згодом блоки піддавалися мікрохвильовому опроміненню, яке мало місце в Гірничому університеті Леобену, Австрія. Експерименти проводилися з безперервною потужністю 25 кВт і часом випромінювання 30 і 45 секунд. До і під час опромінення була виміряна температуру зразків. Після 30 секунд температура підвищилася з 220 °C до 3000 °C і до 5000 °C через 45 секунд. Процес опромінення призвів до утворення тріщин довжиною до 15 см.

В результаті випробувань були отримані діаграми відношення сили та часу для напрямків X, Y і Z, які використовувалися для подальшого аналізу. Також були проаналізовані швидкість зносу, розподіл часток за розмірами та споживання енергії.

Процес різання граніту супроводжували гучний шум, значний рівень вібрації та утворення невеликої пилової хмари попереду ріжучого інструменту. Дисперсія частинок під час різання була направлена у сторону напрямку різання. Ріжучий інструмент нагрівався у процесі різання, але температура дозволяла тримати інструмент руками без дискомфорту.

Зразок, опромінений протягом 45 секунд був зруйнований експериментами, що викликало передчасне припинення дослідження.

Після закінчення експериментів було застосовано статистичний аналіз експериментальних даних. Результат процесу різання, експортованого в Excel (як масиви даних), має понад 43 000 строк для кожного різу.

Сили

Вплив відстані між різами

Згідно з результатам, залежність сил від відстані відносно мала, з точки зору досліджуваних значень. Сили процесу різання з відстанню між зрізами 8 мм на 13% нижче, ніж з 12 мм.

Вплив відстані від початкової поверхні

Аналіз впливу відстані від початкової поверхні показує, що, проникаючи глибше в зразок, сили трохи збільшуються. Зростання для кожного наступного шару становить близько 3%. Це збільшення також пов'язане зі зменшенням розтріскування зразка і зносом різця. Оскільки всі зразки показують аналогічне збільшення сил зі збільшенням глибини, зменшення впливу випромінювання здається малоймовірним. Однак слід сказати, що кількісна оцінка глибини проникнення випромінювання в опроміненому протягом 45 секунд блоці не може бути виконана через його руйнування.

Вплив тривалості опромінення

Результати показують вплив мікрохвильового випромінювання на сили різання. Розраховано, що 45-секундний опромінений зразок в середньому потребує на 22% нижчі сили в порівнянні з неопроміненим зразком. Однак, під час експериментів з зразком, опроміненим протягом 30 секунд, спостерігалися дещо вищі зусилля в порівнянні з неопроміненим блокомю

Питома енергія

Вплив відстані між різами

В середньому питома витрата енергії на процес різання з відстанню між зрізами 8 мм була на 20% вище, ніж при різанні з відстанню 12 мм між різами.

Вплив відстані від початкової поверхні

Залежно від відстані від початкової поверхні і тривалості мікрохвильового опромінення питома витрата енергії коливається від 30 до 60 кВт · год/м^3. Питома енергія збільшується під час процесу різання після збільшення глибини відносно початкової поверхні.

Вплив тривалості опромінення

З результатів видно, що питома енергія, необхідна для різання 45 с обробленого блоку, є найнижчою. Порівняння питомого енергоспоживання процесу різання з інтервалом 8 мм показує (шари порівнюються відповідно):

- питома витрата енергії на 45 с опромінений блок нижче на 29,8%, 20,3% і 9,4%, в порівнянні з неопроміненим;

- 45-секундний опромінений блок вимагає на 27,01%, 17,05% і 13,99% менше енергії ніж 30 с опромінений зразок;
- різниця між питомим енергоспоживанням 30 с опроміненого блоку і неопроміненим блоком незначна (в діапазоні 2,8-13,2%).

Для інтервалу 12 мм ці цифри виглядають наступним чином:

- неопромінений блок вимагає на 7,4%, 32,8% і 6,3% більше енергії в порівнянні з блоком, опроміненим протягом 45 секунд;
- питома енергія, що витрачається на різання 30-секундного обробленого блоку, вище на 15,46%, 26,40% і 26,16%, ніж для 45 с обробленого блоку;
- блоки з тривалістю обробки 30 секунд і неопромінений не показали суттєвої різниці в питомому енергоспоживанні, за винятком шарів 4-го і 7-го, для яких питома енергія необробленого блока перевищує на 26,84% і 34,10% відповідно.

За даними, зібраними під час мікрохвильового опромінення, було розраховано споживання енергії, що витрачається на мікрохвильову обробку.

Беручи до уваги енергію, яка споживається процесом опромінення видно, що для опромінення протягом 45 секунд потрібно 4,96 кВтг, а це на 22% більше, ніж для 30 секунд (3,86 кВт · год).

Знос

Для збору даних про знос інструменту під час процесу різання використовувалося кілька ріжучих інструментів. Кожен інструмент був долучений тільки в процесі з такими ж параметрами різання (швидкість різання, глибина різання, відстань між зрізами та тривалість мікрохвильового опромінення).

Вплив відстані між різами

За результатами вимірів було розраховано, що для блоку, обробленого мікрохвилями протягом 45 секунд, швидкість зносу при різанні з кроком 8 мм становила близько 0,011 г/м, а під час різання з кроком 12 мм швидкість зносу перебувала в діапазоні 0,016-0,019 г/м .

Блок, опромінений протягом 30 секунд, показав швидкість зносу 0,011-0,017 г/м для різання з кроком між різами 8 мм і 0,011-0,045 г/м з кроком 12 мм.

Швидкість зносу при різанні неопроміненого зразка з кроком 8 мм між зрізами становила 0,012-0,015 г/м, а під час різання з кроком 12 мм – 0,012-0,019 г/м.

Крім того, слід зазначити, що вплив відстані між різами на знос при різанні опромінених блоків вище, ніж при різанні неопроміненого блоку. Різниця між різами 8 і 12 мм становить близько 15% для неопроміненого блоку, в середньому 30% протягом роботи з 30 с опроміненим блоком і понад 35% протягом 45 с опроміненим блоком.

Вплив відстані від початкової поверхні

Що стосується впливу відстані від початкової поверхні на знос, то її неможливо чітко ідентифікувати. Як видно з розрахунків, зміна швидкості зносу з кожним наступним зрізаним шаром не спостерігалася, а функція швидкості зносу описується майже як лінійна залежність. Виняток становлять шари 5 і 7 для 30 секундного блоку, які навряд чи можна статистично пояснити без додаткових досліджень однорідності зразка.

Вплив тривалості опромінення

Після різання 40 м неопроміненого граніту з відстанню між зрізами 8 мм інструмент зносився на 0,56 г, при тому, що знос інструменту для 45 та 30 секунд опромінених блоків складає 0,6 г та 0,72 г відповідно. Водночас, різання 30 м неопроміненого граніту з відстанню між зрізами 12 мм зносили інструмент на 0,62 г, 45 с обробленого блоку – приблизно на 0,66 г і 30 с опроміненого – на 0,62 г.

Розподіл часток

Вплив відстані між різами

Як видно з результатів, вплив відстані між різами для частинок розміром менше за 100 мкм становить менш ніж 3%. Але з проходженням 50% матеріалу видно, що процес різання з кроком 12 мм створює менше дрібних часток, що позитивно впливає на умови різання, подальшу обробку і транспортування.

Вплив відстані від початкової поверхні

Дисперсію розподілу розміру часток по відношенню до шару можна знайти в роботі. Відхилення результатів просіювання (розмір часток понад 1 мм) для різних шарів 45-секундного опроміненого блоку становлять 43,84 ± 1,77% (відстань між

різами 8 мм) і 37,34 ± 1,08% (відстань між різами 12 мм). Ці результати для 30-секундного обробленого блоку становлять 53,28 ± 5,73% і 45,48 ± 2,98%. Крім того, відхилення для неопроміненого зразка становлять 50,86 ± 1,9% і 40,86 ± 2,98%.

Вплив тривалості опромінення

Вплив тривалості опромінення мікрохвилями на розподіл часток було приведено в роботі. Опромінений протягом 45 секунд блок мав більший розмір зерна щодо інших зразків, він складається з 50% частинок діаметром понад 1,51 мм (2,39 мм для 12 мм кроку між різами), при тому, що неопромінений і 30-секундний опромінений зразки мають 0,85 мм (1,43 мм) і 0,97 мм (2,05 мм) відповідно. В цьому випадку мікрохвильова обробка має позитивний ефект, оскільки процес різання після опромінення протягом 45 секунд створює менший обсяг дрібних частинок.

У **четвертому розділі** представлені результати розробки моделей регресії для безлічі факторів, досліджених в поточному дослідженні.

Вихідні дані для розробки регресійної моделі наведені в Додатку С. Моделі регресії і наведені рівняння описують залежність відповідної сили F від тривалості опромінення T, відстані між зрізами S і відстані від початкової поверхні D. Використовується метод множинного регресійного аналізу, тобто виконується визначення повного рівняння регресії.

У цьому дослідженні було прийнято рішення розпочати регресійний аналіз з простого рівняння, а потім збільшити кількість змінних до тих пір, поки не буде знайдений максимальний коефіцієнт регресії. В якості простого рівняння була обрана формула (6).

Система рівнянь (7) для $F_{x_{mean}}$ набуває вигляду:

$$\begin{pmatrix} 34 & 750 & 340 & 640 \\ 340 & 26550 & 7500 & 13800 \\ 340 & 7500 & 3536 & 6400 \\ 640 & 13800 & 6400 & 14464 \end{pmatrix} \cdot \begin{pmatrix} b_0 \\ b_1 \\ b_2 \\ b_3 \end{pmatrix} = \begin{pmatrix} 223.96 \\ 4771.2 \\ 2270.36 \\ 4412.28 \end{pmatrix}$$

Після рішення системи лінійних рівнянь і визначення коефіцієнтів b_i формула (6) має вигляд:

$$F_{x_{mean}} = 3.147157421 - 0.014377651 \cdot T + 0.226176471 \cdot S + 0.079437322 \cdot D$$

Наступний крок – обчислення залишкової дисперсії регресії і коефіцієнта кореляції. Залишкова дисперсія дорівнює 0,36, а коефіцієнт кореляції дорівнює 0,84. Після аналізу всіх членів многочлена (5) було розраховано, що остаточне рівняння регресійної моделі середніх сил різання має вигляд

$$F_{x_{mean}} = 3.470653993 + 0.095667514 \cdot T + 0.226176471 \cdot S + 0.05046748 \cdot D - 0.00282456 \cdot T^2 \quad (12)$$

Візуалізація регресійної моделі (12) для середніх сил різання $F_{x_{mean}}$ показана на рис. 6.

Ця ж процедура була реалізована для визначення $F_{x_{max}}$, $F_{y_{mean}}$, $F_{y_{max}}$, $F_{z_{mean}}$ та $F_{z_{max}}$.

$$F_{x_{max}} = 11.573862984 + 0.097032916 \cdot T + 0.494558824 \cdot S + 0.133780488 \cdot D - 0.003142205 \cdot T^2$$

$$F_{y_{mean}} = 3.344489479 + 0.078016994 \cdot T - 0.059117647 \cdot S + 0.022825203 \cdot D - 0.002132336 \cdot T^2$$

$$F_{z_{mean}} = 5.307086322 + 0.321586213 \cdot T + 0.595147059 \cdot S + 0.155172764 \cdot D - 0.009474243 \cdot T^2$$

$$F_{y_{max}} = 6.602914873 + 0.131420958 \cdot T + 0.136911765 \cdot S + 0.065813008 \cdot D - 0.003580608 \cdot T^2$$

$$F_{z_{max}} = 11.065932568 + 0.457940041 \cdot T + 1.200882353 \cdot S + 0.298069106 \cdot D - 0.013046364 \cdot T^2$$

Важливим фактом є те, що регресійні моделі можуть бути застосовні тільки в установлених межах змінних факторів.

Слід зазначити, що кожне рівняння регресійних моделей має однакові поліноми, але різні коефіцієнти. Моделі регресій є квадратичними залежностями від тривалості мікрохвильової обробки. Встановлена лінійна залежність регресійних моделей від відстані від початкової поверхні. Крім того, існує лінійна залежність регресійних моделей від кроку між зрізами, оскільки використовується тільки два інтервали.

У той же час знаки перед коефіцієнтами повторюються, за винятком коефіцієнта при S (відстань між різами) регресійної моделі середньої бічної сили $F_{y_{mean}}$. Поясненням цієї ситуації може бути те, що при зменшенні відстані між різами урівноважуюча бічна сила (спрямована в протилежному напрямку) зменшується. Однак це спостереження не повторюється в максимальних бічних силах.

Мапи сил

Щоб проілюструвати вплив мікрохвильової обробки при руйнуванні гірських порід, було здійснено моделювання мап сил. Ця процедура дозволяє візуалізувати діючу силу в 3D-середовищі.

Для створення мап сил використовувалися дані, зібрані DEWE 5000. Процедура містить реалізацію змінного усереднення. Ця функція використовується для оцінки значення поверхні на певному вузлі сітки. Вона працює як обчислення середнього значення відомих значень поверхні в сусідніх контрольних точках. Фактично, вона проектує сусідні відомі значення на розташовані вузли сітки. Згодом комплексне наближення проводиться шляхом усереднення значень, зазвичай зважуючи найближчі точки більшою мірою, ніж віддалені точки.

Представлені мапи сил мають координати X і Y з даних як вісь X і вісь Y відповідно. Вісь Z представлена силами F_x, F_y, F_z та F_{Total} для другого шару і усередненими 2-4 рівнями для кожного блоку.

У вигляді пунктирної лінії візуалізується межа між відстанню 8 і 12 мм. На мапах сили з кроком між різами 8 мм лежать у верхній частині відповідно до кордону.

Слід зазначити, що для всіх мап сил відстань 8 мм показує більш низькі навантаження і піки у порівнянні з 12 мм. Однак, при зображенні бічних сил F_y – протилежно. Цей факт підтверджує припущення, що зменшення інтервалів в експериментальному діапазоні може збільшити бічні сили, що виникають при різанні.

У **висновку** зазначено, що дана робота розглядає актуальну наукову задачу, в ній описуються дослідження, виконані з використанням потужного мікрохвильового

опромінення в якості перспективного рішення при видобутку скельних порід. Рішення складається з використання мікрохвильової енергії для зменшення опору різання граніту. Крім того, в дослідженні показані залежності сил, зносу, споживання енергії та розподілу часток за розмірами від відстані між різами, часу опромінення мікрохвилями і відстані від початкової поверхні.

Мінерали граніту мають різні діелектричні властивості. Це призводить до нагрівання деяких частин зразка, що викликає його розтріскування. Цей факт має позитивні ефекти у вигляді зменшення сили різання. В ході досліджень сила різання була зменшена на 22% після 45-секундного мікрохвильового опромінення. Це означає, що питоме споживання енергії також скоротилося; аналіз показує зменшення на 20-40% (для різних умов різання) для зразка, обробленого протягом 45 секунд. Однак час опромінення в 30 секунд не мав явного позитивного впливу на сили та питоме споживання енергії. Різниця в швидкості зносу по відношенню до мікрохвильового опромінення була чітко видна. Залежність між розподілом часток за розмірами і мікрохвильовим випромінюванням помітна тільки при часі опромінення рівному 45 секунд, також аналіз показує менший обсяг дрібних частинок.

Дослідження включало аналіз двох положень відстані між різами, рівних 8 мм і 12 мм. Аналіз показує, що при відстані в 8 мм сили різання зменшуються приблизно на 13%, а знос інструменту відбувається повільніше. Однак, збільшення відстані до 12 мм позитивно впливає на питому витрату енергії та розподіл часток. Результати показують зниження питомого енергоспоживання на 20%, а матеріал менш переподрібнений при відстані між різами в 12 мм.

Отримано регресійні моделі, що описують залежності середніх і пікових сил різання від часу опромінення, відстані від початкової поверхні зразка і відстані між різами. Були створені мапи сил, що характеризують розподіл сили в розрізі.

В цілому, супутнє опромінення мікрохвильовою енергією породи для різання граніту показало гарні результати у разі опромінення протягом 45 секунд.

TABLE OF CONTENTS

INTRODUCTION

The demand for non-explosive hard rock excavation grows constantly. There are several reasons for it, one of which is the increasing pressure on mining and related industries by environmental authorities and stakeholders. In addition, mechanical hard rock excavation shows a number of advantages on drilling and blasting.

The usage of explosives creates a number of hazards for the workforce, environment, and adjacent communities. Namely, toxic gases emission, ground vibrations, high noise level, impairment to roof and wall stability. Furthermore, a major part the global mining activities take place in politically unstable regions. This may cause security issues associated with purchasing, transportation and storage of explosives. In addition, non-explosive excavation techniques could be operated continuously, which can be easier integrated in mining operation complex.

Therefore, mechanical excavation methods become more and more attractive to mining operators. However, mechanical methods show high wear and limited advance rates in very hard and abrasive rocks or, if machines can operate under such conditions, they are very inflexible and unsuited for production operations (Tunnel Boring machines). In order to increase the range of applicability of mechanical methods, one of the possible solutions is microwave irradiation to reduce the cutting resistance of the rock massive. Microwave irradiation is under research for over 70 years [1]. In late 1960s, the concept of using microwave energy in mining was examined [2]. However, in the context of roadheading and production, the knowledgebase is limited. Therefore, in this thesis, the effect of microwave irradiation with regard to cutting efficiency is analyzed.

1. ISSUE ANALYSIS

From the ancient times, mining was a part of human lives. Not much is left from the Bronze Age, but fragments discussing mining can be found in works of Greek and Roman authors. As modern beginning for mining is considered year 1556 when German doctor and scientist Georgius Agricola (Georg Bauer) published his book *De Re Metallica*. The next step in the mining was made only 100 years after, in 1670, when gunpowder was introduced, and in 1698, with Thomas Savery's fire engine invention. The next step to modern and safety mining was done after additional 150 years. In 19th century, safety fuse by William Bickford and dynamite by Alfred Nobel were invented [3].

Mining industry is a part of primary sector of the economy (this sector also includes agriculture, forestry and fishing). The primary sector is usually less important in industrial countries, but goods supplied by mining are widely used in developing and even in developed countries. Mineral resources are the beginning for everything. Basically, all things around us are a result of use of mineral resources. The extraction and processing of minerals is a valuable part of development and civilization growth [4].

1.1 Principles of Hard Rock Excavation

Based on information from *International Organizing Committee for the World Mining Congresses*, total mineral production on year of 2014 was around 17.5 billion tons and this number increases with years. This amount consists of several types of commodities: 1.6 billion tons of iron and ferro-alloy metals, over 90 million tons of non-ferrous metals, 30 thousand tons of precious metals, nearly 800 million tons of industrial minerals and 15 billion tons of mineral fuels [5].

For mineral extraction, mechanical and drill-blast methods are widely used. Usually, mechanical excavation methods are applied for nonabrasive rock with uniaxial compressive strength (UCS) lower or about 150 MPa and in very abrasive rock about 70 MPa [6]. Drill-blast methods can be used in rocks with UCS around 100-200 MPa and higher. However, in the last decades, there is a trend to develop mining equipment for hard rock excavation utilizing mechanical methods. That could be seen in some popular types of excavators: tunnel and raise boring machines, roadheaders, longwall drum shearers and continuous

miners; but also in new unconventional techniques: projectile impact, high-pressure water jet cutting technology, laser drilling and microwave inducting [3].

1.1.1 Basics of Mechanical Rock Excavation

Various factors affects the mechanical rock excavation process. They might be divided into two main groups: physical and mechanical properties of rock as well as cutting tool parameters and cutting parameters.

Physical and mechanical properties of rock

Young's modulus

Young's modulus E (elastic modulus) is the measure of the stiffness of rock [7].

Porosity

Porosity can be described as the measure of voids in the rock [8].

Density

Density describes the value of mass per volume of a substance [8].

Uniaxial compressive strength

USC is the maximum axial compressive stress that the rock sample can withstand before failure and it is the most common way to determine the strength, widely used in mining and related industries. The equation for calculation of UCS is presented below [8].

$$UCS = \frac{F_{fail}}{A_{UCS}} \ [MPa] \tag{1.1-1}$$

where F_{fail} – maximum force on the sample before failure $[N]$;

A_{UCS} – cross-sectional area of the sample $[mm^2]$.

Tensile strength

Tensile strength (the maximum tensile stress experienced by the rock sample at the destruction moment) can be determined with Brazilian Tensile Strength (BTS) test (Indirect Tensile Strength). BTS is calculated as follows [8]

$$\mathrm{BTS} = \frac{2F_{fail}}{\pi d_{\mathrm{BTS}} l_{\mathrm{BTS}}} \; [MPa] \tag{1.1-2}$$

where d_{BTS} – diameter of the sample $[mm]$;

l_{BTS} – length of the sample $[mm]$.

Cerchar Abrasivity Index

The factor, which is influence on cutting tool consumption and operation cost is rock abrasivity (the property of rocks, expressed in the ability to wear the cutting tool during excavation process). One of the ways to evaluate abrasion rate is using the Cerchar Abrasivity Test, introduced in the 1970s in France. The testing principle is based on a steel pin with defined geometry and hardness scratching the surface of a rough rock sample over a distance of 10 mm under static load of 70 N. The Cerchar Abrasivity Index (CAI) is then calculated from the measured diameter of the resulting wear flat on the pin [9]:

$$CAI = 10 \cdot \frac{d_{wear}}{c_{wear}} \tag{1.1-3}$$

where d_{wear} – diameter of wear flat $[mm]$;

c_{wear} – unit correction factor.

The CAI is usually used for TBM and roadheader excavations prediction models as a significant factor.

Table 1.1-1 Summary Cerchar Abrasivity Test [10]

CAI	Abrasivity description	Examples
$\mathbf{0.0 - 0.3}$	Not abrasive	Wood, peat
$\mathbf{0.3 - 0.5}$	Hardly abrasive	Clay-siltstone
$\mathbf{0.5 - 1.0}$	Slightly abrasive	Slate, marble (pure)
$\mathbf{0.1 - 2.0}$	Abrasive	Limestone, marble (containing SiO_2)
$\mathbf{2.0 - 4.0}$	Highly abrasive	Quartz sandstone, basalt
$\mathbf{4.0 - 6.0}$	Extreme abrasive	Quartz, granite, gneiss

In RWTH Aachen University (Germany), experiments for determining of CAI for numerous of materials have been carried out. Results of the research are shown in Table 1.1-1.

Cutting tool parameters

Cutting speed

It is desirable to set the cutting speed respectively low, as it affects the wear rate. If the speed is high, the generated by friction heat leads to undesirable wearing of the cutting tool [11].

Cutting depth

The cutting depth influences the specific energy consumption required for excavation (Figure 1.1-1). The larger the cutting depth, the lower the specific energy consumption. However, with increasing in cutting depth, the cutting forces also increase. Therefore, the maximum cutting depth is limited by the power of the cutting equipment, as well as stability and possible penetration depth of the cutting tool [12].

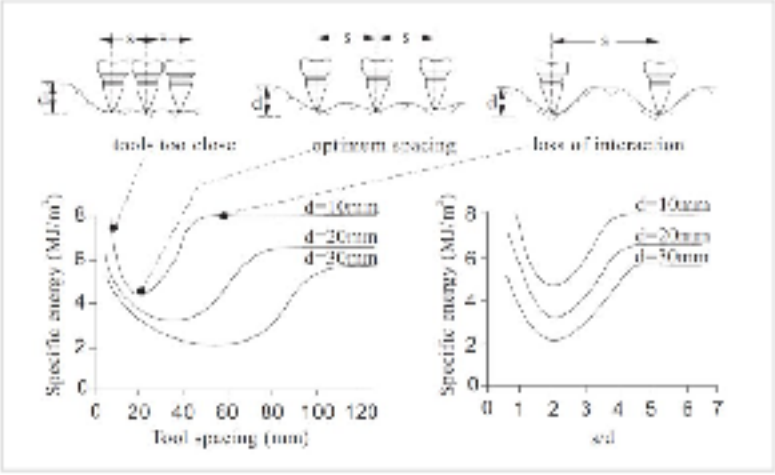

Figure 1.1-1 Tool spacing and its effect on specific energy [12]

Spacing between cuts

The optimum spacing between cuts is the distance, at which crack propagation from two nearby cuts will be superimposed (Figure 1.1-1). If the spacing is too large, ribs are formed, because of absence of crack overlaying. In case of too small spacing, all material between cuts will be excavated, but it will lead to performing of additional cuts in order to excavate the assigned volume. In both cases, it affects in additional time and energy consumption [13].

Angles

In addition, the process of sustainable cutting is limited by the fast wearing of cutting tool, which reflects in increasing of cutting forces. For avoiding undesired wearing and increasing of cutting forces, the cutting tool should be mounted under established parameters. Several studies investigated the effect of cutting tool rotation and geometry on cutting process and predicting of rock cutting force. There are number of empirical formulas for cutting force prediction. Major amount of equations operate such parameters of tool geometry as semi-angle of pick, rake angle and angle of attack [14].

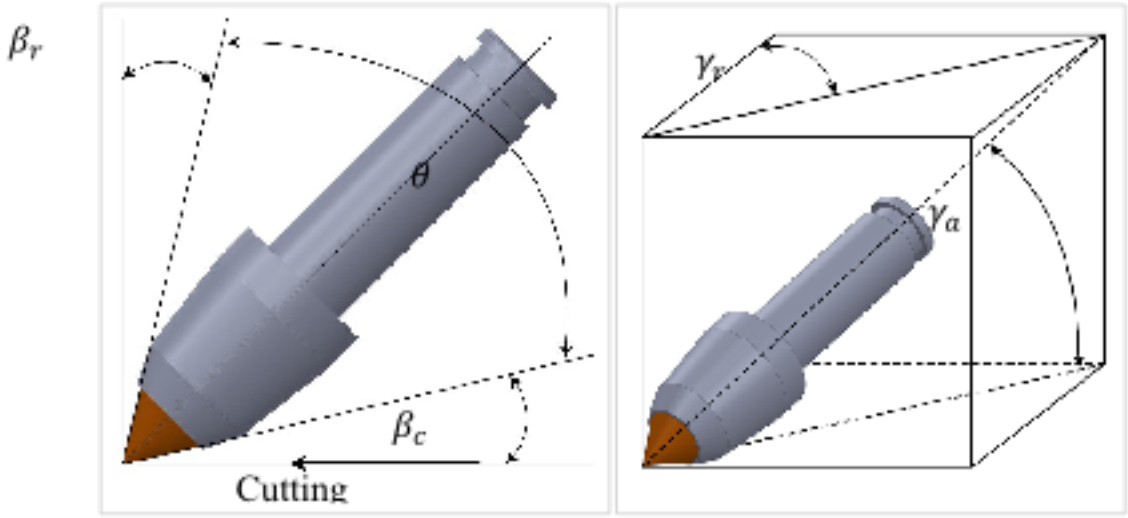

Figure 1.1-2 Cutting geometry of point-attack picks

The angles are defined as follows (Figure 1.1-2):

- θ – pick angle;
- γ_a – attack angle;
- γ_r – rotation angle;
- β_c – clearance angle;
- β_r – rake angle.

Rake angle α_r

It is the angle between the tool face and the plane normal to the surface of the cut and pressing through the tool cutting edge. Rake angle has pronounced effects on cutting process. The parameter generally has an optimum value. Deviation from the optimum has negative impact. A larger angle causes accreting of tool wearing, while a smaller angle can lead to higher cutting forces and heat generating [15].

Clearance angle β

That is an angle between the lower surface of the pick and a plane parallel to the cutting direction. Numerous studies show that the clearance angle has pronounced negative effect on cutting forces if the angle has a value around 5° or lower. To meet the kinematic requirements, the clearance angle is considered to be around 7.5° [11].

Attack angle γ

Angle of attack is noticeable parameter affecting the performance of point attack picks. This is an angle between cutting path and tool axis. This angle provides the proper contact between the cutting tool and rock. Correct positioning of the attack angle will depend on the pick cone angle. Studies say that with increasing cone angle, the angle of attack should also increase and vice versa [11]. Moreover, the increase in cutting force and the decrease in normal force observes after increasing of attack angle [16].

1.1.2 Conventional Methods of Hard Rock Excavation

At present, the two of the most economical methods of excavation are mechanical excavation and drill and blast methods [8].

Drill and blast method

Exploitation of majority of hard rock deposits typically considers preliminary disintegration of rock mass. In the rock UCS around 100-200 MPa and higher, the blasting is generally necessary to break large volumes of rock. The technique is carried out under conditions that all workers, equipment, machinery, buildings and environment will not be damaged. Annually, USA and Australia use more than 3 million tons of explosives for rock breaking in mining, which is around 75 % of the countries demand [17] [18].

Drilling and blasting is the most common and widespread method of hard rock excavation but it has a number of restrictions. There are a lot of resources and investigations made within this study.

Blasting is the process of material fracturing by the use of a certain amount of explosive so that a predetermined volume of material is broken [19].

The process of drilling and blasting technique requires very strict safety compliance. Many preliminary operations should be performed before blasting. The basic of them are:

- choosing suitable drilling bit and drilling technique;
- determining type, diameter and length of blast holes;
- choosing type and amount of explosive;
- determining method of initiation;
- performing drilling;
- charging process of blast holes;
- initiation of safety restrictions;
- blasting; and
- ventilation (in terms of underground environment).

In mining, two types of explosives are used: primary and secondary. They differ in the possibility to impact, produce heat, friction etc. Normally, secondary explosives cannot be initiated without primary explosive. Often, the secondary explosive is presented by emulsion (e.g. ANFO) and delivered to the blast holes in the tank [19].

There are three main factors of blasting that affect the environment – air shock waves, ground vibration and fly rocks (Figure 1.1-3).

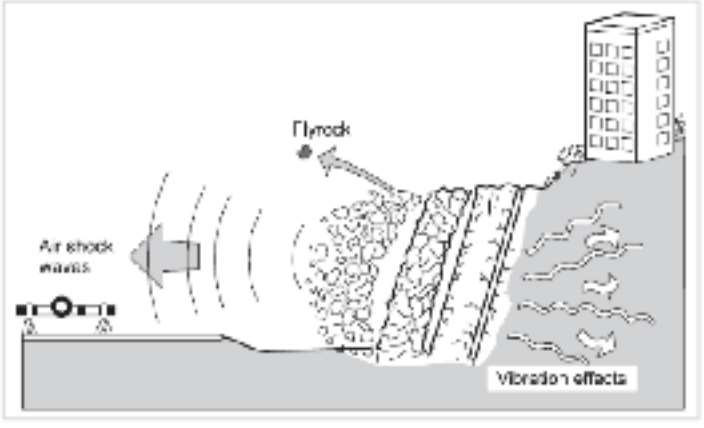

Figure 1.1-3 Three factors that affect environment in blasting [20]

Mechanical excavation methods

Tunnel boring machines

Tunnel boring machine (TBM) performs mechanized destruction of rocks, shipment of broken material and support setting. Either shielded or open-type tunneling boring machines are applied for hard rocks. All types of hard rock TBMs excavate rock use disc cutters mounted in the cutter head. The rock is excavated by cutting discs, developing compressive stress fractures causing it to chip them away from the rock in the tunnel face.

Excavated rock is transported through the cutter head to the belt conveyor, creating continuous process of excavation [8].

Figure 1.1-4 Tunnel boring machine

In today's urban underground construction, the highest priority belongs to various TBMs: mechanized and automated systems for the construction of tunnels with various shapes and cross-sectional dimensions in different geological conditions. It has turned out that such method as TBM machinery excavation has a number of advantages over the other mining methods. Therefore, annually 500 TBMs are produced in the world.

The use of these machines has the advantage over the drilling and blasting method as its impact on the surrounding soil is negligible, and smoother walls of the future tunnel are a result. Transportation process of a TBM to its operational location, mobility during excavation and high initial cost are among their disadvantages [8].

Roadheader

Roadheaders are the partial-face machines (can excavate only a portion of the face at once), developed in late 1940s. Typical appearance of modern roadheader can be seen in Figure 1.1-5. As the major advantages of roadheaders over other mechanical excavation techniques are their mobility, flexibility, and selective mining ability. Such advantages provide roadheaders worldwide use in underground mining, tunneling and even surface mining operations [21].

The main component of a roadheader is a boom movable in any directions. A cutterhead with cutting tools is attached to a boom and excavates a face. The material, excavated by cutterhead, drops on a so-called loading apron. Using continuous loading system (e.g. star wheel, gathering arm), the loading apron gathers and loads the material on

the chain conveyor located in the central part of the loading apron. From the chain conveyor, through the body of the roadheader, the muck is passed to the tail conveyor. The tail conveyor carries the material to the transportation system (e.g. rail cars, trucks, etc.) [21].

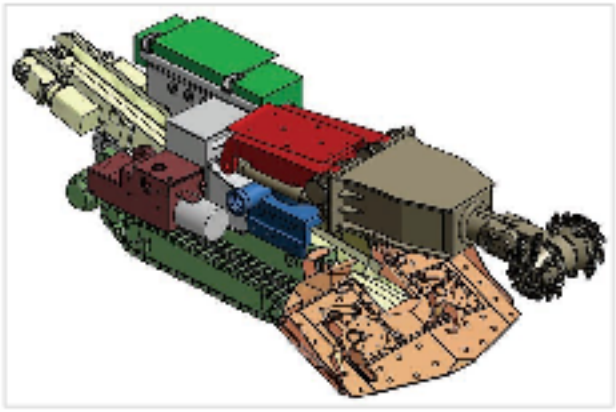

Figure 1.1-5 Typical roadheader [21]

As the roadheader is a partial-face machine, the excavation is performed selectively. This leads to decreasing in ore dilution factor and positively effects on processing of ore. In addition, such kind of boom and cutterhead eases the access to the face and the process of inspecting and changing of cutting tool.

During mining operations it is very important to be mobile and have the possibility to relocate excavation equipment to another face frequently. It can be fulfilled with roadheaders, as they are mainly crawler mounted and high mobile machines. They are mainly smaller and lighter in comparison with other underground excavators, which benefits in lower capital expenses. The roadheaders have modular structure and, as an advantage, can be assembled or dissembled in a couple of days. Roadheaders can create excavations of any shape, and it is very important in the context of underground mining (mostly, underground mining excavation requires non-circular cross-section of opening). Additionally, it is easy to adapt the roadheaders to mining designs. Their operating angles are up to 15°. If bracing jacks are used their operating angles increase up to 25° [8].

The roadheaders can excavate only in rocks with UCS 100-120 MPa. This number can increase up to 160 MPa if the rock highly fractured, jointed or foliated. Another limitation is a level of water flow. It should be dry or with very low water flow. Roadheaders cannot operate in abrasive rock, as it can cause high wear rate and the uneconomical cutting tools consumption [8].

1.1.3 Emerging Technologies of Mechanical Hard Rock Excavation

There are a various number of unique technologies of hard rock excavation, which locate on different stages of development. Such technologies are described below.

Undercutting disc cutter technology

The undercutting disc technology was developed in Australia for cutting the rock by producing tensile stresses rather than compressive stresses like in typical cutting discs (Figure 1.1-6). The disc attacks rock in undercutting manner, similar to the cutting action of a drag bit. It allows reducing cutting forces by 2.5 times. The disadvantage of the technology is considered the potentially dangerous bending stresses. The side forces acting on this type of cutting action limits area of applicability [22].

The prototype of the machine with such technique has been manufactured and tested by companies Wirth and Sandvik Voest Alpine, the basic application area of it is narrow vein mining [8].

Figure 1.1-6 Conventional (left) versus undercutting (right) disc [22]

Continuous mining machine (CMM) Mobile Tunnel Miner (MTM)

German and Canadian companies developed concept of continuous mining machine for excavation hard rock based on the undercutting disc technology. It was created prototype, modified Atlas Copco mini full facer. The final prototype design had four arms with 560 mm undercutting discs at the ends (Figure 1.1-7) [22].

The motion of the arms can be programmed, which allows creation of the tunnel excavation of any form. The machine was designed for excavation of rocks with mean forces around 250 kN and peak forces near to 1 MN. The provided total power was 700 kW. CMM weighted 150 t and had possibility to excavate tunnel with diameter equals 4.25 m [22].

Figure 1.1-7 Wirth Continuous Mining Machine [22]

First tests of CMM had been successful. Unfortunately, the machine was broken on rocks with UCS around 250 MPa [22].

Tunnel Boring Extender (TBE)

In 2003, Wirth Group presented the machine using undercutting fragmentation method to create 14.4 m diameter tunnels. TBE 500/1440 H-HST (Figure 1.1-8) combines three elements: reaming technique, undercutting disc technology and the ability to bore not round sections tunnels [23].

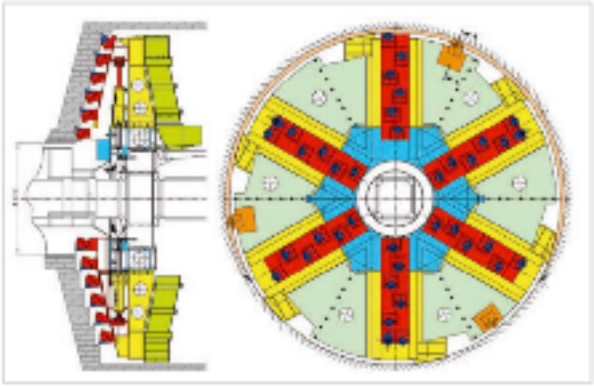

Figure 1.1-8 Tunnel Boring Extender [23]

For a reaming tunnel-boring project, the conventional TBM is driven a smaller diameter excavation in the center. Afterwards, proper diameter is bored. It is conducted with bracing the TBE in the pilot gallery and reaming with six boring arms to the final diameter. The aspect of this procedure is the undercutting discs arranged on slides in the arms. The slides are driven radially outwards during rotation of the head. During the cutter rotation they are spirally moved to the outside [23].

Variable tunnel shapes may be obtained while changing radial displacement of the cutting discs. The company claims that such machine requires less power than conventional

TBM with equivalent parameters and weighs in two times less than the TBM. Despite all information, the feasibility of using this technique in hard rock has not been demonstrated [8].

Alpine Reef Miner ARM 1100

Another example of using undercutting discs is ARM 1100 (Figure 1.1-9). The Alpine Reef Miner is a disc-mining machine, designed for mining narrow reefs of hard rocks [22].

Referring to Voest Alpine [24], the ARM is featured with undercutting disc principle for efficient energy utilization; gripper system for transferring the high cutting forces while weight of the machine is low and fully remote controlling. It is suitable for low height ore bodies mining.

Figure 1.1-9 The ARM 1100 [24]

The machine was tested in the platinum mines in South Africa. Mines, where ARMs were implemented, have typical UCS value equal to 40-120 MPa and 150-200 MPa; the rocks are high abrasive [22].

During the tests, the machines cut the rock successfully but the cutter costs were very high. In addition, the cutting process produced high level of dust. These factors caused taking out of the ARMs from the mines and returning to conventional brill-and-blast. To be competitive in this situation, the operation costs should be reduced to around 80 % of current ones [22].

Activated/oscillating disc cutting

Activated or oscillating disc cutting technology is a method of hard rock cutting which uses a disc cutter, which oscillates in a plane orthogonal to the disc axis while it attacks the rock in an undercutting manner [22]. Such technique can lead to fatigue cracking of rock that causes weakening.

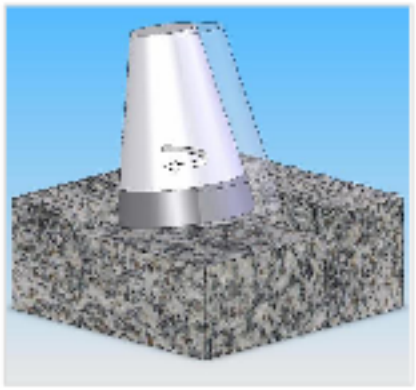

Figure 1.1-10 Activated/oscillating disc cutting [22]

Laboratory tests showed that using of oscillating disc cutters can reduce cutting force by 3.75 times comparing to conventional discs and by 1.5 times comparing to undercutting discs [22].

This technique was tested in mining operational conditions. During the operations, two main problems arose: short lifetime of cutters and repeating failures of oscillating mechanism. The further implementations of oscillating disc-cutting technology are investigated [22].

Minidiscs

In terms of any disc cutting, the contact area of the disc with the rock is directly proportional to the force requirements of the cutting disc to achieve a given depth. That shows the following: smaller disc needs less force for penetrating the same depth in the rock.

In 1990s, the minidisc cutter has been tested under different rock conditions. These tests have shown that minidiscs have many advantages: high cutting efficiency and penetration rate, low cutting force requirement, low maintenance, initial and replacement costs, longer lifetime, etc. On the other hand, weaknesses of minidiscs and the mounting system such as bearing and sealing assembly, the cutter retaining system and insufficient amount of wear material cannot permit the discs to become popular [22].

ICUTROC technology

The introduction of roadheaders with low cutting speed (1.4 m/s instead common 3 m/s) allows excavation of hard rocks and high abrasive rocks. However, new theoretically expected results required the alteration of entire machine system, which initialized of the EU project ICUTROC [25].

The project integrated machine and pick manufactures as well as universities and mining industry representatives. This gave strong theoretical and practical background in creating the hard rock oriented roadheader. New pick qualities, new pick cooling system and cutter head with improved tool quality were developed. The stiffness and the structural strength of machinery had been improved for resisting high loads during cutting of hard rock.

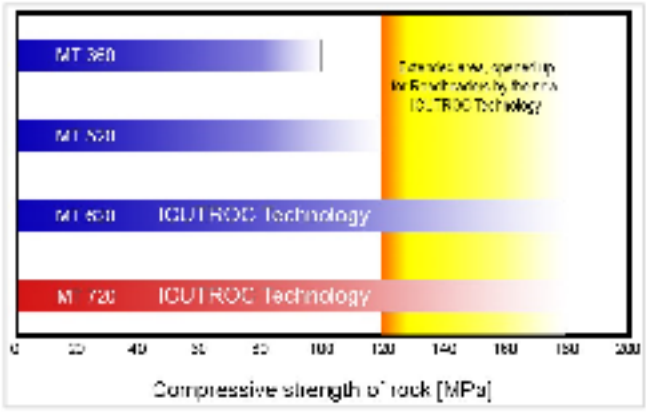

Figure 1.1-11 Comparison of roadheader models by compressive strength of rock [26]

Tests show a decrease of pick wear by 60 %, which allowed reducing the pick consumption by 75 % during cutting of rocks with compressive strength in range of 90-200 MPa. Afterwards, the roadheaders with ICUTROC system were used during tunnel construction and mining operation in Italy, Greece, Germany, Russia and Canada [25] [27].

Projectile impact

Percussion devises are presented as energy conversion elements of power pulse systems, power by primary sources of energy (e.g. electric, pneumatic, hydraulic explosion, etc.) [3].

The need of high-energy projectile impact for performing different technological operations has led to development of significant number of percussion devises. It was the launching for production numerous number of executive bodies for various purposes. Some of the implementations have been used in the mining, metallurgical, construction and road facilities industries.

One of the main factors influencing the volume and application field of machines with projectile impact is the tensile strength of the mined rocks. There was considered that the

index of rock breaking performance depends on the compressive strength and percussion energy.

Many companies manufacture machines with projectile impact. Some of them are mass-produced and operate in various industries; others are made in the form of concept for scientific research and testing of design solutions. At present, a fairly large range of machines with the executive bodies of projectile impact corresponding to a wide area of application has been formed [8].

Regardless of the large amount of machines, they are based on the same fundamental scheme. The scheme includes following functional units: a moving mechanism, a percussion device to the tool, a boom-arm, electro-hydraulic drive and control system.

The executive bodies of the machines use hydraulic or hydro-pneumatic percussion device. Hammers differ in the principle of hydro-kinematic scheme, energy value and the frequency of strikes.

However, the question of the rational combination of energy and impact frequency to the power of the percussion is still controversial. Most researchers agree on the fact that the performance of the percussion machinery depends on the frequency of strikes, in case when the strike energy ensures the exceeding threshold of strength of the rock. Excessive impact energy affects the process of overgrinding rocks. The action of additional static load on the tool allows increasing the efficiency of destruction of rocks by two times.

The analysis of results of machineries with percussion mechanisms during excavation allows to distinguish their advantages over conventional machines: excavation of rocks with higher strength, reduce in energy consumption, less amount of fines, decreasing level of dust, more cost-effective, increasing of excavation speed, more safety, etc.

A pick assisted by high-pressure water jet

Hydromechanical method of rock fracturing based on rock breaking via a conical pick assisted by a high-pressure water jet.

The method consists in the fact that the jet of water, oriented one way or another with respect to the machine tool, provides reducing its loading of the interaction with the rock.

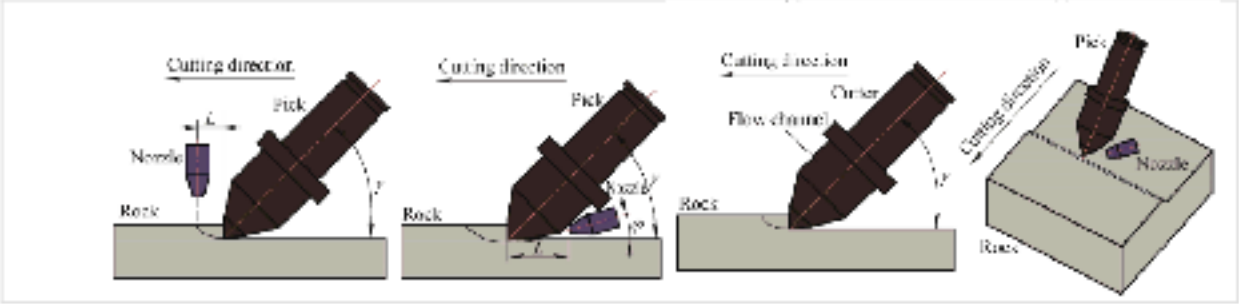

Figure 1.1-12 Model of rock breaking via a pick assisted by water jet [28]

From the viewpoint of the efficiency of destruction of rocks, working bodies of the TBMs are the most interesting. They use high-pressure water jet in combination with a cutting tool. Thus, for example, Wirth GmbH tested TBI-260 with executive body diameter of 2.6 m, equipped with disc roller cutters and water jets of high pressure. The excavation of sandstones was tested. Jet nozzle produced forward cracks in the rock massif, breaking the continuity and reducing its strength. As a high-pressure water source, it was used four pressure intensifier with a pressure of 300-400 MPa, the water consumption of 120 liters per minute and the power of 250 kW. Test results showed that by using a high pressure water jet, cutting force is reduced for more than 50 % and the rate of production increased by 2 times. It was excavated 84.5 m and noted almost complete absence of dust, improving performance of tunneling equipment, reducing overgrinding of the rock mass and the elimination of the danger of sparks under friction picks with rock massif. The use of such a working body allowed reducing the sinking cost by 30-50 % [28].

Companies Robbins and Flow Research designed and tested roadheader with hydromechanical executive body. On the boom-mounted cutting head, 35 sapphire nozzles with diameter of 0.25 mm were located. The pressure of water exceeded 420 MPa. In tests carried out using granite with UCS equals to 235 MPa, the penetration rate increased by 1.5-2 times compared to mechanical destruction [28].

In general, the tests of hydromechanical executive bodies of tunneling machines and the experience of their operation have established the effectiveness and availability of hydro-mechanical method of destruction and highlight the following key benefits [28]:

- extension of the range of applications of tunneling machines to harder rocks (with UCS up to 160-235 MPa);
- reduction in cutting force by 40-60%;

- reduction in torque and power on executive body in 1,3-2,2 times;
- 1.5-3 times increase in penetration rate without increase in executive body power;
- 2-6 times reduction in cutting tool consumption;
- up to 2 times increase in machine productivity without increase in mass and dimensions;
- 70-85 % dust reduction and 90-100 % sparking reduction;
- vibration reduction;
- 30-50 % decrease in tunneling costs.

However, the widespread implementation of hydromechanical method of rock destruction faces serious technical problems.

Effective use of the hydromechanical method should involve water jets which initial pressure is at least 80-100 MPa (the required value of the initial pressure tends to its increase, a number of authors suggests minimum 200-400 MPa) and a flow rate of 6.3 l/min per cutting tool. Consequently, selective roadheader must be equipped with high-pressure water source (pump) with a working pressure of at least 100 MPa. Power of the pump can be equal to the power of the executive body, and often exceeds it.

The high velocity of the water at the outlet of the jet-forming device causes its considerable abrasive wear, the nozzle resistance decreases rapidly with the increase of the initial pressure. At a pressure of 70-80 MPa, a carbide nozzle can be used during about 200 hours and, at a pressure of 350 MPa, – just 4.3 hours. The resistance of sapphire and diamond nozzles is by 4-5 times higher, but due to the difficult processing of sapphire and diamond nozzles, they have imperfect shape. The presence of the abrasive particles in the water highly increase wearing of the nozzles, so the strict requirements of the water treatment system is presented. Filtration system should have filters with openings no more than 0.5 microns. It is associated with the use of bulky equipment, the size of which is much larger of the pump unit.

Laser drilling

During the recent decade, intense research has been conducted into application of high-energy laser beams for rock disintegration. Military equipment conversion is

concerned as primarily source for prototypes. In such studies, laser energy is used for the process of melting, thermal spallation or evaporation of rock [29].

Destruction mechanism of laser beam depends on the pulse energy density. At low density, absorbed optical radiation causes heating of rock and its destruction by melting.

At the bottomhole, laser radiation generates significant temperature gradient of 1100 °C on the surface and 75 °C at a depth of 2.2 mm beneath it. Arisen discontinuous stresses lead to rock peeling and thermal cracking in the same way as it happens in the thermal destruction [29].

Under the influence of a powerful laser beam, the destruction is close to electrical breakdown of dielectric. At starting, there is a narrow channel breakdown, where the shock wave is generated. The rock goes into a vapor condition with rapid release of gases. Depending on the optical properties of rock (absorption or ray propagation), the blasted canal ends with a cavity expansion.

Generally, a laser-drilling tool has no mechanical contact with the rock and its durability is not particularly limited. Structurally, the drilling tool (laser) is mounted on the end of the drill string, and power is supplied from the generator located in the tube. Rotation is carried out by flow of washing liquid.

The following types of lasers have been identified for their use in rock drilling [29]:

- Hydrogen fluoride and deuterium fluoride lasers. The operation length of wave is 2.6-4.2 micrometers. MIRACL or Mid-Infrared Advanced Chemical Laser was used for reservoir rocks test.
- Carbon dioxide laser. It operates at 10.6 micrometers wavelength and with 1 MW power. The laser can be operated in continuous or pulsed wave mode. Nevertheless, in terms of long length of wave, attenuation occurs through fiber optics.
- Carbon monoxide laser. Operation wavelength is 5-6 micrometers and power is 200 kW. The laser operates in continuous and pulsed wave mode.
- Chemical oxygen iodine laser. This laser has operating wavelength of 1.315 micrometers. This type of lasers was used by militaries for missile destroying. Such technique has high precision and range that can be implemented successfully for rock drilling.

- Other types.

Major part of researches of laser drilling is focusing on usage of laser as a vaporizer of the rock. With such techniques, the advantages over rotary drilling can be visible. The advantages include increasing rate of penetration, provision of temporary casing, increased bit life, decreasing in dependencies on bit design and rotary speed, accurate and precise drilling, uniform diameter of bore hole, etc.

As the main disadvantage of laser cutting, high power consumption is considered.

Microwave irradiation

Another method for rock destruction consists in using of microwave irradiation. This method will be described and investigated further in this work.

1.2 Microwave Irradiation of Hard Rock

Microwave irradiation has a great potential for use in mining. Microwaves can be used during defrosting of frozen soils; rock softening and crushing, ore decomposition; extraction of metals from waste and sludge; for grinding, leaching, magnetic separation, and high temperature drying [30].

This chapter describes the basics of microwave irradiation and application of its in mining.

1.2.1 Basics of Microwave Energy Irradiation

Microwave energy is a form of electromagnetic energy transmitted by high-frequency waves. Electromagnetic waves consist of an electric and a magnetic wave moving perpendicular to each other (Figure 1.2-1). The speed of the electromagnetic waves equal to speed of light and the length of the waves λ is in inverse ratio to its frequency [31]:

$$\lambda = \frac{c}{f_{em}} \quad [m] \tag{1.2-1}$$

where c – speed of light $[m/s]$;

f_{em} – frequency $[Hz]$.

The wavelength of microwaves range from 1 mm to 1 m – with respective frequencies from 300 GHz to 300 MHz. The microwave heating process refers to a family of electrical

heating technology, which also includes, for example, induction, resistance heating and infrared heating. In all cases, specific features of the electromagnetic energy are used [32].

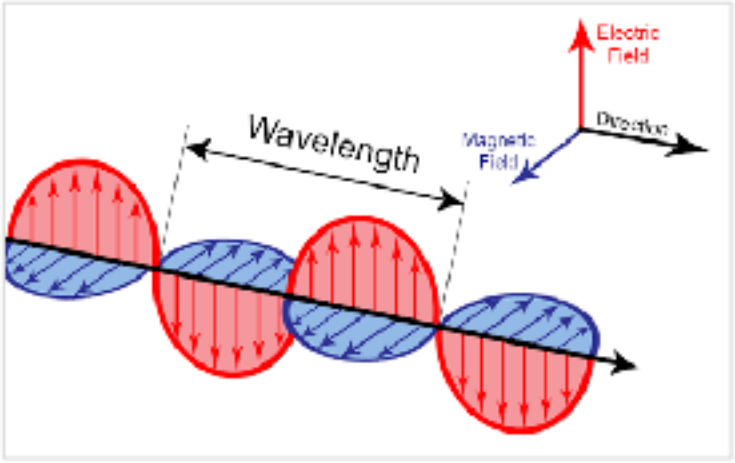

Figure 1.2-1 Electromagnetic waves

As well as electromagnetic waves, microwaves decay while penetration into a dielectric material. The rate of the decay depends on the physical and electrical properties of the material, as well as frequency of the waves [33]. Materials with ability to absorb microwave energy is dielectrics.

Microwave treatment of a rock produces the amount of heat, which depends on exposure time, power level and chemical composition of the rock. Different minerals can absorb or be transparent to microwaves [34] [35].

The dielectric constant, also known as relative permittivity, describes the dielectric properties of solid and it is dimensionless ratio of the permittivity of a substance to the permittivity of free space [36] [37]:

$$\varepsilon_r = \frac{\varepsilon}{\varepsilon_0} = \frac{\varepsilon' - i\varepsilon''}{\varepsilon_0} = \varepsilon_r' - i\varepsilon_r'' \qquad (1.2\text{-}2)$$

where ε_r – relative complex permittivity;

ε – complex permittivity;

$\varepsilon_0 = 8.854 \cdot 10^{-12}\ [F/m]$ – permittivity of free space;

ε' – real of relative complex permittivity;

ε'' – imaginary of relative complex permittivity;

$i = \sqrt{-1}$ – complex number;

ε_r' – real part of relative complex permittivity;

ε_r'' – imaginary part of relative complex permittivity.

The real and imaginary part of relative complex permittivity depend on frequency and temperature. Selected dielectric constants can be seen in Table 1.2-1.

Table 1.2-1 Relative permittivity of selected minerals (rocks) [38] [39]

Mineral (rock)	Relative permittivity
Biotite	$4.7 - 9.3$
Chlorite	9.0
Muscovite	$6.2 - 8.0$
Plagioclase feldspar	$5.4 - 7.1$
Quartz	$4.2 - 5.9$
Granite (dry)	$4.8 - 18.9$

While propagation of microwaves into rock, the loss can be observed. The dielectric loss can be parameterized in terms of either the loss angle δ_e or the corresponding loss tangent $\tan\delta_e$. The dielectric loss tangent $\tan\delta_e$ can be found from the equation bellow [36].

$$\tan\delta_e = \frac{\varepsilon_r''}{\varepsilon_r'} \tag{1.2-3}$$

Materials can be divided into two groups by loss factor:

- Low loss ($\tan\delta_e \ll 1$);
- High loss ($\tan\delta_e \gg 1$).

It was defined, that the penetration depth d_p of microwaves is the depth at with the power has been weakened to $1/e$ (around 37 %) of the power at the surface. For materials with such dielectric properties (low loss/high loss), the penetration depth is calculated as follows [40].

Low loss $$d_p = \frac{\lambda\varepsilon^{0.5}}{2\pi\varepsilon_r''} \tag{1.2-4}$$

High loss $$d_p = \frac{\lambda}{2\pi\varepsilon_r''^{0.5}} \tag{1.2-5}$$

The different minerals consistent in the rock leads to differential volumetric expansion under microwave irradiation. This creates stress along grain boundaries, which

causes cracks and weaken the rock (reducing in UCS, tensile strength, etc.) [33] [41] [42] [43] [44].

1.2.2 Application of Microwave Energy in Mining Industry

There is little experience with the use of microwave energy in mining industry, however, there are several applications where microwaves are used and the number of perspective studies.

Thawing of soils

The method of microwave thawing of soils is an innovative method of construction under the conditions of permafrost, allowing a warming soil for piling, construction of communications and oil pipelines, road construction and maintenance [45].

So far, the thawing of frozen soil was carried out with the help of thermal methods, characterizing by intensive labor- and energy-intensive consumption. Therefore, they are used only in those cases when other effective methods are unacceptable. It is applied near the existing underground utilities and cables; if it is necessary, thawing of the frozen ground in case of emergency and repair work.

Disadvantages of common methods are high consumption of fuel, steam, water and electricity, the complexity of assembling and disassembling as well as warmth-keeping and high cost.

High-tech alternative to the above methods for thawing soils is a technique based on the use of microwave energy to create fast, reliable and environmentally friendly way of heating. This technology has higher penetration level, less energy (fuel) consumption and reduced duration of treating.

Under the leadership of N. Ryabets, there were carried out extensive studies of the dielectric properties of frozen ground in the range of microwaves, theoretical and experimental research of thawing of frozen soils under the effect of microwaves [45]. 915 and 430 MHz frequencies were analyzed. The studies have shown that, at 430 MHz generator frequency, thawing depth is 0.8 m at power flux density of 10 W/cm^2, and irradiation time was equal to 10 min (rock is sand and sandy loam, light humidity $10-15\,\%$ with an initial temperature of $-5\,°C$). At the same time, the required costs of

microwave energy is $30-35$ kWh/m^3. At a frequency of 915 MHz and power flux density $23\,W/cm^2$ (exposure time 3-5 min), thawing depth was 0.25-0.35 m. Thus, radiation with longer wavelength has proved higher efficiency for soil thawing. From this study, in 1985, facilities were constructed, based on magnetrons M93 and M116. Using of it allowed from two to three times reduce in the cost of work and reduces the duration of elimination of accidents.

Another study has described the working body for extending a well diameter in permafrost rock. It uses the magnetron M81 having frequency of 2.45 GHz and power of 5 kW, which was directed to the well walls, for irradiation of frosted rocks [46].

Mineral processing

Microwave drying of minerals and coal

The drying of minerals with microwaves was studied in Institute of Geotechnics of Slovak Academy of Science. The study confirmed that microwave energy very sufficiently and fast dries minerals, such as magnetite, galena, siderite and quartz. The quality of drying depends on permittivity and their grain [47].

In addition, it was studied the drying of coal in microwave furnace. The advantage of drying with microwaves over classical method is the velocity of drying, which in case of microwaves in 10 times higher [47]. This is because microwave-drying process has different mechanism, the drying runs from the middle of the mineral to the surface. The water is pressured out from the coal to the surface and can be taken by airflow [30].

Gold extraction from the tailings

More effective dressing and extraction of minerals can be performed with implementation of microwaves in the processing of the rocks. The microwave energy implementation allows more effective extraction of gold from the tailings of old mines. A usual method with the use of cyanides solutions does not extract gold, as it is concluded in other minerals (pyrite and arsenopyrite). Furthermore the current technology is highly energy demanding and not environmentally friendly. Therefore, it is necessary to use microwaves for destruction of sulfide sells. The shell absorbs microwave energy, as a result rapidly heated and cracked; this allows solutions access the metal [48].

The method was tested in Canada. The results shown lower decomposition temperature, 420 ºC comparing to 550 ºC for formal heating. The percentage of extraction of gold increases with microwave facility power. At power 5-6 kW, it was observed complete extraction of gold (98 %). Feasibility study says that cost per ton can be reduced by 45 % if the microwave heating is implemented [48] [49] [50].

Microwave treatment of coal

The process of desulphurization of coal with microwaves was tested. The coal was treated with microwaves for further magnetic separation.

Magnetic separation depends on the difference in the magnetic moment associated with coal and mineral particles. The microwave irradiation boosts the magnetic sensibility of minerals and makes it more open to separation process [30].

The study of L. Turčániová (Institute of Geotechnics, Slovak Academy of Sciences) says that it is possible to remove up to 80 % of total Sulphur content in the coal [51]. As the advantage of the desulphurization with microwaves was highlighted extremely short time for desulphurization after microwave irradiation.

Microwave-assisted leaching

Leaching of refractory gold ores

Microwave destruction technology is energetically favorable for the rocks, containing a small amount of ore minerals when one mineral is heated without waste rock heating [52].

The possible area of application of microwave technology is the preparation of refractory ores for hydrometallurgical extraction of gold. The degree of extraction of gold from refractory ores during leaching of the ore without pretreatment is quite low. To increase the extraction, various methods of pretreatment material can be used: firing, high pressure and biochemical oxidation. These methods are quite expensive and long lasting.

The main reason why the microwave energy can be successfully used in the extraction of gold leaching is the fact that the gold-bearing minerals are usually excellent absorbers of microwaves and the ore-bearing material is transparent.

It was demonstrated that microwave irradiation techniques can be applied efficiently and efficiently to the refractory gold ores leaching [52].

Microwave leaching of electronic wastes

In Prague, the study of microwave-assisted leaching of electronic wastes was performed and the leaching kinetics at different temperatures was studied. An electronic scrap (Cu 64.65 %, Al 4.54 %, Zn 0.53 %, Pb 0.16 %) with the leaching agents (2 M HCl and 2 M H_2SO_4) were used [30].

The results shown insignificant dissolution of Cu, but the recovery of Pb and Al show some positive results with dependencies on temperature and duration. Pb was fully recovered after 60 minutes heating at 80 °C (conventional leaching shows 65 %). The dissolution of Al was 91 % (60 minutes, 60 °C), comparing to 83 % for conventional methods [30].

Boulders destruction

In 1965, researches were carried out on destruction of boulders on "Rovnoe", "Akademicheskoe", "Sokolovskoe" and "Golovinskoe" open pits (former USSR). It was used high frequency microwave facility – "Electra". The practice has shown effectiveness of using microwaves for fragmentation of boulders. The performance of 15 m^3/h has been achieved during boulders fragmentation of volume up to 7.5 m^3 [53].

Microwave heating for fracture of kimberlite

In Russia (2006-2008), studies of kimberlite fracturing with microwave energy were executed. It was determined that destruction of kimberlite under microwave heating occurs for two reasons: rapid water evaporation contained in rock, when the saturation pressure will exceed rock strength; prompt polar expansion of minerals [48].

Study says that kimberlite is a porous rock with water content level at 7 %. At 150 °C the vapor pressure achieve 500 kPa, it gives the water pressure to be the main cause of kimberlite fracture. Dielectric behavior with different water content as well as microwave penetration were measured. Experiments confirm that for high productivity (60 % of chips is under 3 mm in diameter), the temperature should be under 200 °C and the temperature grows equals 40 °C/sec [54].

The productivity of the method was estimated as 0.1 tons per hour (microwave facility power 5 kW) and 1 ton per hour (microwave facility power 50 kW) [54].

Experimental method of rock softening

Employees of Institute of Geotechnical Mechanics (Dnipro, Ukraine) have invented an original method of destruction of rocks by irradiating with two microwave generators [55].

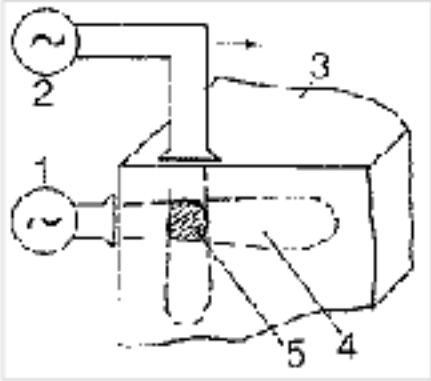

Figure 1.2-2 Softening the rock by the influence of two microwave generators [55]

At first, the rock irradiated with lower power flux density ($150 - 300\,W/cm^2$) from the generator (1) until creating heat trace, and then irradiating with higher power flux density ($300 - 5000\,W/cm^2$) from the generator (2) in the perpendicular direction (Figure 1.2-2). The first phase of the irradiation creates in the rock (3) heated zone (4) with an increased value of the fictional component of the dielectric constant. For radiation generator (2), this area is strongly absorbing, while the unheated rock is transparent. As a result, the power produced by generator (2) is absorbed mainly in the zone of intersection of irradiations (5). Rapid heating of zone (5) causes thermal expansion, phase changes, gas phase formation, etc. It leads to the destruction of the rock. Moving the generator (2) on the surface of the heat along the trace (4), can be created a channel of broken rocks can be created [55].

On the stage of concept, it exists significant number of microwave-assisted machineries. However, they are not cost effective in the context of technical and economic progress.

1.3 Formulating the Research Problem

Based on the above, the objective of this work is to analyze the reduction in cutting resistance of granite specimen irradiated by microwave irradiation with different irradiation times.

For the implementation of this objective, the following should be done:

- determination of dependencies of cutting forces, wearing, energy consumption, particle distribution on spacing between cuts;
- determination of dependencies of cutting forces, wearing, energy consumption, particle distribution on distance from initial surface;
- determination of dependencies of cutting forces, wearing, energy consumption, particle distribution on duration of treatment of sample with microwaves;
- development of regression model of dependency of cutting forces on duration of treatment of sample with microwaves, spacing between cuts and distance from initial surface.

2. RESEARCH METHODS

Investigation of the influence of the microwave irradiation on the reduction of cutting resistance of granite was set as a task in the current study. This chapter explains research methods applied to process test results and obtain regression models.

2.1 Analysis of the Cutting Forces

The basic principle of the rock destruction is in overcoming the bonding between the particles to disintegrate the rock. Inducing stresses that surpass the rock strength in the rock formation is the basis of mechanical rock cutting; by this, the crack propagation and chip formation are caused [22].

During cutting of rock, three-dimensional forces act on the cutting tool (Figure 2.1-1). These forces are as follows

- Cutting force F_x;
- Normal force F_z;
- Side force F_y.

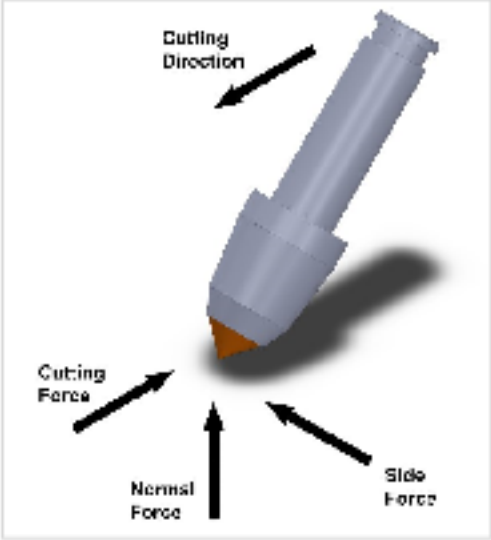

Figure 2.1-1 Forces acting on the cutting tool while cutting

Cutting force occurs parallel to cutting direction, it is mainly responsible for the actual rock fragmentation. The normal force is directed perpendicular to cutting path and hold the pick in the rock. The side force acts perpendicular to the cutting path and keeps the pick in the cutting line [56] [13]. The total force F_{Total} might be determined as follows:

$$F_{Total} = \sqrt{F_x^2 + F_y^2 + F_z^2} \qquad (2.1\text{-}1)$$

In this study, mean forces and maximum forces (or peak forces) are of the highest interest, as they are used for determining parameters of excavation equipment. Mean forces and maximum forces should be evaluated and analyzed. The procedure will be described further in this chapter.

2.1.1 Peak Force Analysis

As a possible method of analysis, it was decided to use the method of maximums for analyzing data out. In this method as amplitudes of forces, it is chosen to take differences between peaks σ_{maxi} of the force-time diagram (Figure 2.1-2) and the mean value σ_μ. In addition, only peaks, which are higher than mean value, should be taken into account.

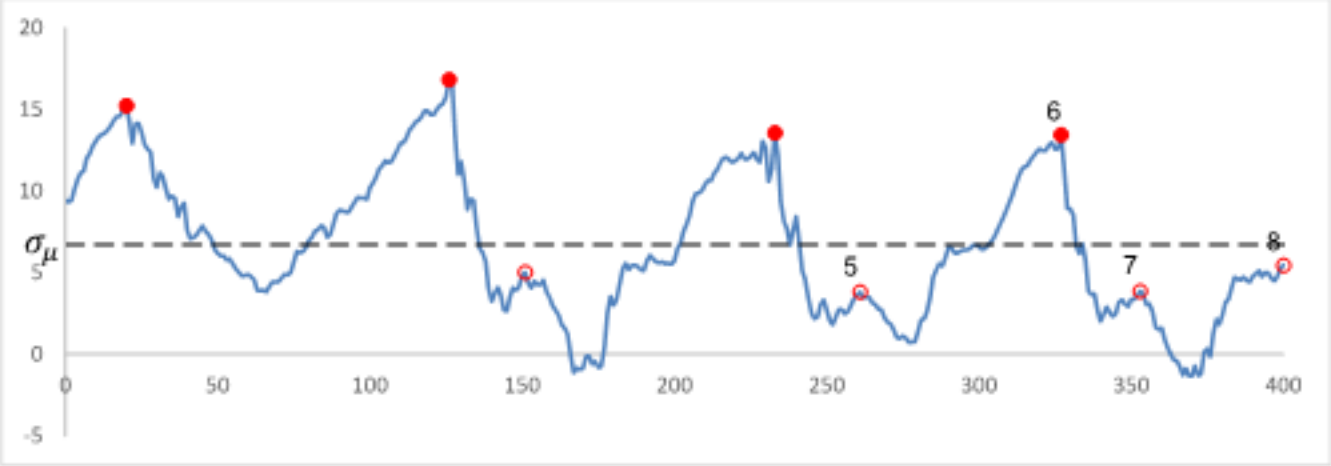

Figure 2.1-2 Example of the force-time diagram

In this way, the peaks (3), (5), (7) and (8) are excluded from evaluation, as they lay lower than σ_μ. Next step is to find the amplitudes of stresses σ_{ai} equal to σ_{maxi} and σ_μ difference. If these amplitudes are arranged in ascending order, it could be taken as the variation series. The variation series is important for the determining of the distribution function.

In the method of maximums, it is assumed that distribution of minimums and distribution of maximums are symmetric with respect to σ_μ.

2.1.2 Verification of the Peak Force Analysis

Probability theory is the branch of mathematics analyzing patterns of random phenomena such as random events and variables, stochastic processes, their properties and operations.

The approaches, described in Chapter 2.1.1, should be applied to the force-time diagram of the cutting forces. The data points for F_{max}, exctracted by the peak analysis will follow a random variable distribution. From the view of the distribution density histogram of experimental data, the form of a distribution law is assumed.

If the histogram has a clear peak and symmetry with respect to this peak, it could be checked using the hypothesis of a normal distribution. The procedure for checking the normal distribution hypothesis is shown below.

If it is not symmetrical, other hypotheses shall have to be checked for.

At first, it is necessary to base a hypothesis of affiliation on the Gaussian distribution.

Use of Pearson's test involves checking of the hypothesis such as, at the significant level $\alpha = 0.05$ the random variables distribution F_{max} does not conflict with the Gaussian distribution.

For the force F_{max} it is necessary to calculate mean μ, variance σ^2 and the range of $F_{max_{max}} - F_{max_{min}}$.

$$\mu = \frac{\sum_{i=1}^{n} F_{maxi}}{n} \tag{2.1-2}$$

$$\sigma^2 = \frac{\sum_{i=1}^{n} (F_{maxi} - \mu)^2}{n-1} \tag{2.1-3}$$

Depending on the number of random variables N, the amount of intervals should be chosen. For this purpose, Sturges rule will be used [57]:

$$k = 3.3 \log N + 1 \tag{2.1-4}$$

Next step is to select borders of intervals. The random variable can be divided into intervals in many ways, but it is preferable to do so according to asymptotic optimal grouping for the Gaussian distribution [58]:

$$t_i = \frac{x_i - \mu}{\sigma} \rightarrow x_i = \sigma t_i - \mu \qquad (2.1\text{-}5)$$

Such dividing is preferable because of the increasing possibility of criteria to differ similar hypothesizes.

Table 2.1-1 Optimal border points of intervals for checking the Gaussian distribution with Pearson's chi-squared test [58]

k	t_1	t_2	t_3	t_4	t_5	t_6	t_7	t_8	t_9	A
3	-1.111	1.111	–	–	–	–	–	–	–	0.407
4	-1.383	0.000	1.383	–	–	–	–	–	–	0.553
5	-1.696	-0.689	0.689	1.696	–	–	–	–	–	0.683
6	-1.882	-0.997	0.000	0.997	1.882	–	–	–	–	0.756
7	-2.060	-1.265	-0.492	0.492	1.265	2.060	–	–	–	0.810
8	-2.195	-1.455	-0.786	0.000	0.786	1.455	2.195	–	–	0.847
9	-2.319	-1.622	-1.022	-0.383	0.383	1.022	1.622	2.319	–	0.875
10	-2.423	-1.758	-1.205	-0.650	0.000	0.650	1.205	1.758	2.423	0.896

In case an interval has a low number of values, less than 5, it shall be deemed as insufficient. Such intervals should be merged.

The perfect Gaussian distribution for calculated mean and variance can be calculated by formula [58]:

$$f(x) = \frac{1}{\sqrt{2\sigma^2\pi}} e^{-\frac{(x-\mu)^2}{2\sigma^2}} \qquad (2.1\text{-}6)$$

The next step is calculate the frequency of occurrence of randoms in the interval n_i and determine probability deriving P_i [58]

$$P_i = \int_{x_i}^{x_{i+1}} f(x)dx \qquad (2.1\text{-}7)$$

When it is considered that this is a composite hypothesis, the number of degrees of freedom equals

$$r = k - m - 1 \qquad (2.1\text{-}8)$$

where m_{es} – number of estimated parameters.

The critical value of Pearson's chi-squared is then calculated as follows [58]

$$S_{\chi^2} = N \sum_{i=1}^{k} \frac{\left(\frac{n_i}{N} - P_i\right)^2}{P_i} \qquad (2.1\text{-}9)$$

The result of the equation (2.1-9) should be compared with the chi-squared distribution table. It should be smaller.

Calculate $P\{S > S'\}$ [58]

$$P\{S > S'\} = \frac{1}{2^{\frac{r}{2}} \cdot \Gamma\left(\frac{r}{2}\right)} \cdot \int_{S_{\chi^2}}^{\infty} s^{\frac{r}{2}-1} e^{-\frac{s}{2}} ds > \alpha \qquad (2.1\text{-}10)$$

If the equation (2.1-10) is true, then the considerable random variable obeys normal distribution.

2.2 Investigated Parameters

During the cutting process multiple numbers of parameters are tracked, measured and processed, described as follows.

Energy consumption evaluation

For this study, specific energy consumption of cutting process will be evaluated. The specific energy consumption equals the amount of energy to be consumed for a cubic meter of rock [8].

To determine the specific energy E_{sp} in laboratory test, the following equation can be used:

$$E_{sp} = \frac{l_{1c} \cdot \sum \overline{F_x}}{3600 \cdot V_{cut}} \quad \left[\frac{kWh}{m^3}\right] \qquad (2.2\text{-}1)$$

where l_{1c} – length of cut $[m]$;

$\overline{F_x}$ – mean cutting force of one cut $[kN]$;

V_{cut} – volume of cut material by $\sum \overline{F_x}$ $[m^3]$.

Another form of energy consumption that could be evaluated is energy consumed by the microwave facility during the irradiation process

$$E_{mic} = \frac{\sum E_{P_i}}{3600} \quad [kWh] \qquad (2.2\text{-}2)$$

where E_{P_i} – energy spent for irradiation, per second $[kJ/sec]$.

Wearing

About 80 % of all failures of excavation machines are caused by wear of parts. Especially intense abrasion exposes the working bodies of excavation equipment [59].

Some general effects of tool wear include increased cutting forces, increased cutting temperatures and poor surface finish. In addition, it may lead to tool breakage and causes change in tool geometry.

Excavation performance and wear rate are the main themes of many studies. However, wearing should be taken into account and processed during experimental analysis. Thus, the wear is a question of material consumption as well as the important indicator of rock excavation (Figure 2.2-1).

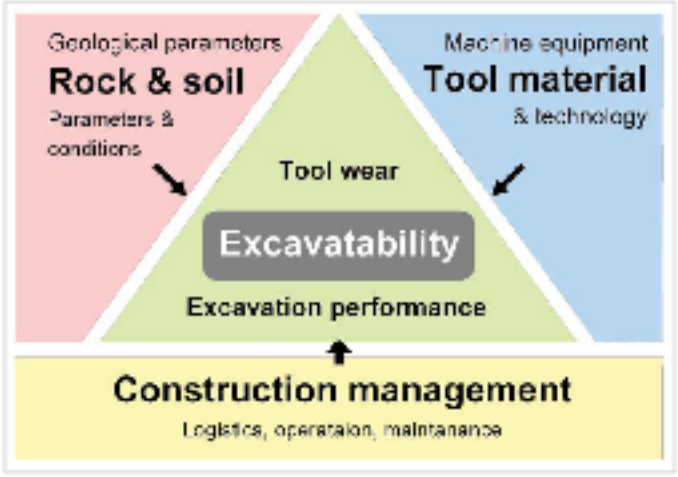

Figure 2.2-1 Parameters influencing tool wear and excavation performance [9]

Tool wear takes place in processes involving friction of surfaces, high pressures and temperatures. Therefore, there are the two main causes of wearing in the current research: abrasion and diffusion.

The abrasiveness of rock is a factor with considerable influence on the tool wearing. Since in this work such a hard rock as granite is used, it is understood that granite is an extremely abrasive rock ($CAI = 4.0 - 6.0$; Table 1.1-1) and wearing of the cutting tool will thus be significantly high.

Another factor controlling the wear rate is cutting speed. A high cutting speed results in the increase of the tool temperature, increasing the wear rate in turn.

At high temperatures in the cutting zone, diffusion takes place that is mutual dissolution of friction bodies. As a result, changes in chemical composition and mechanical properties of the surface layers of the tool accelerate the wear [60].

Also, forces that appeared during the cutting process, play a significant role in the wear rate. This impact acts in two directions. Increase in the forces results in the increase of the wear rate. On the other hand, when the cutting tool is worn, the forces increase significantly [11].

In this study, an unusual method for wear rate evaluation will be applied. This is due to the experiment's conditions. The major procedure is to determine difference in weight of the cutting tool before and after cutting process relatively to the cutting way:

$$W = \frac{m_i - m_{i+1}}{l_{cl}} \quad \left[\frac{g}{m}\right] \tag{2.2-3}$$

where m_i – mass of a pick before cutting layer $[g]$;

m_{i+1} – mass of a pick after cutting layer $[g]$;

l_{cl} – cut length on a layer $[m]$.

Particle size distribution

The particle size plays a major role in the case of health safety. Many particles are easily inhaled and can be deposited in the respiratory tract depending on their size, density, shape, charge and surface properties as well as on the breathing pattern of the individual. Numerous studies and organizations, e.g. Occupational Safety and Health Administration (OSHA), point that the size of particles that are respirable (i.e. can reach the deep part of the lungs) is less than 10 μm. However, the size of particles that can be inhaled is reaching 100 μm [61] [62]. Unfortunately, there was no possibility to determine particle size under 63 microns during this research.

In addition, more grinding means creating a larger surface area, which in turn requires higher energy consumption. Less grinded material indicates a better use of energy, which should cause less energy consumption or a bigger volume of cut material in comparison to over ground material.

2.3 Procedure of Establishing a Regression Model

The procedure of the development of the regression model $y = f(x_1, x_2, x_3)$ is described below [63] [64].

First of all, a table with initial data should be created. It should include variable parameters (x_1, x_2, x_3) and experimental values y.

Next step is creating the multiple regression equation. Research shows that most experimental results can be described as a complete cubic polynomial. Polynomial regression of three-factorial design is:

$$y = b_0 + b_1x_1 + b_2x_2 + b_3x_3 + b_{12}x_1x_2 + b_{13}x_1x_3 + b_{23}x_2x_3 + b_{123}x_1x_2x_3 + b_{11}x_1^2 + b_{22}x_2^2 + b_{33}x_3^2 + b_{111}x_1^3 + b_{222}x_2^3 + b_{333}x_3^3. \quad (2.3\text{-}1)$$

For the determination of the full equation, a method of multiple regression analysis will be used.

There are two different methods to perform regression modelling. The first is the taking of the full polynomial and analyzing the importance of the equation members as their numbers decrease. The second starts from a simple equation with a minimum number of members, increasing the number of explanatory variables by gradual addition and calculating the importance.

The regression equation in such case becomes

$$y = b_0 + b_1x_1 + b_2x_2 + b_3x_3 \quad (2.3\text{-}2)$$

The coefficients b_i are determined by the system of equations, based on Gaussian elimination

$$\begin{cases} nb_0 + b_1\sum x_1 + b_2\sum x_2 + b_3\sum x_3 = \sum y \\ b_0\sum x_1 + b_1\sum x_1^2 + b_2\sum x_1x_2 + b_3\sum x_1x_3 = \sum yx_1 \\ b_0\sum x_2 + b_1\sum x_1x_2 + b_2\sum x_2^2 + b_3\sum x_2x_3 = \sum yx_2 \\ b_0\sum x_3 + b_1\sum x_1x_3 + b_2\sum x_2x_3 + b_3\sum x_3^2 = \sum yx_3 \end{cases} \quad (2.3\text{-}3)$$

Such system of equations can be written in matrix form as follows

$$\begin{pmatrix} n & \sum x_1 & \sum x_2 & \sum x_3 \\ \sum x_1 & \sum x_1^2 & \sum x_1 x_2 & \sum x_1 x_3 \\ \sum x_2 & \sum x_1 x_2 & \sum x_2^2 & \sum x_2 x_3 \\ \sum x_3 & \sum x_1 x_3 & \sum x_2 x_3 & \sum x_3^2 \end{pmatrix} \cdot \begin{pmatrix} b_0 \\ b_1 \\ b_2 \\ b_3 \end{pmatrix} = \begin{pmatrix} \sum y \\ \sum y x_1 \\ \sum y x_2 \\ \sum y x_3 \end{pmatrix} \quad (2.3\text{-}4)$$

Calculated coefficients b_i have to be included in the equation (2.3-2):

$$y = \cdots + \cdots x_1 + \cdots x_2 + \cdots x_3 \quad (2.3\text{-}5)$$

Determining residual variance of regression:

$$S_{res}^2 = \frac{\sum_{g=1}^{n} \left(Y_{gi} - y_i\right)^2}{n - (k+1)} \quad (2.3\text{-}6)$$

where y_i – calculated value of the parameter by equation (2.3-5);

Y_{gi} – experimental value;

$(k+1)$ – the number of coefficients in the equation (2.3-5);

n – sample size.

Add the next member of polynomial to the equation:

$$y = b_0 + b_1 x_1 + b_2 x_2 + b_3 x_3 + b_{12} x_1 x_2 \quad (2.3\text{-}7)$$

For the new equation, the whole process should be repeated. After that, the statistical significance of the variance difference between polynomials can be estimated

$$\frac{S_{res_j}^2}{S_{res_{j+1}}^2} > F_{1-p} \quad (2.3\text{-}8)$$

where F_{1-p} – F distribution table value, $m_1 = n - (k+1),\ m_2 = \infty$;

(bigger S_{res}^2 value has to be the numerator).

If condition (2.3-8) is fulfilled, then the member is added to polynomial, when it is false, the member has to be skipped. All members of equation (2.1-2) have to be processed and checked.

Determining correlation coefficient

$$R = \sqrt{1 - \frac{\sum_{g=1}^{n}\left(Y_{gi} - y_i\right)^2}{\sum_{g=1}^{n}\left(Y_{gi} - Y_g\right)^2}} \tag{2.3-9}$$

where Y_g – mean experimental value.

As a result, the equation that describes the experimental output with highest accuracy should be received.

3. EXPERIMENTAL STUDY OF THE CUTTING PROCESS

The purpose of the current experiments is to determine the effect of the microwave irradiation duration, spacing between cuts and distance from irradiated surface of a granite block on the cutting force, wearing and specific energy consumption.

3.1 Equipment

In this study, laboratory equipment was used. This equipment is listed and described in the current chapter.

The testing rig

Cutting tests were carried out using the testing rig HXS 1000-50. The rig was developed for the determination of cutting forces and volumes using various cutting tools during operation with blocks (samples) under experimental field conditions.

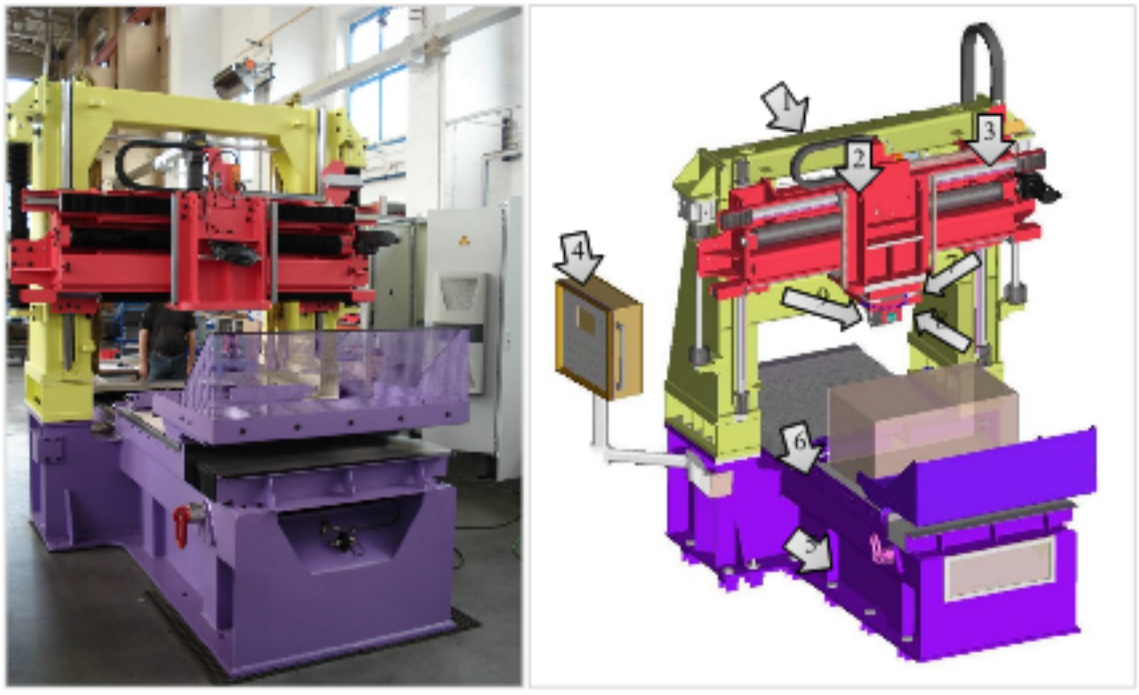

Figure 3.1-1 Photo (left) and 3D model (right) of the testing rig [65]

The machine was produced by ASW-GmbH Naumburg for conducting cutting tests at TU Bergakademie Freiberg. General view of the testing rig is given in Figure 3.1-1 and basic technical data are in Table 3.1-1 [66].

It consists of a base frame (5), a movable work table (6), where the test block is located, fixed 2-cross beam-portal (1), traverse (2), work bridge (3), tool holder (9), a load cell (7), laser scanner (8) and control panel (4).

Table 3.1-1 Technical data of the testing rig [66]

Nominal capacity		60 kW
Cutting speed	x-axis y-axis z-axis	1,750 mm/s 7 mm/s 16 mm/s
Cutting depth (max.)		50 mm
Acceleration (max.)		10 m/s^2
Permissible forces	x-axis y-axis z-axis	50 kN 30 kN 50 kN
Max. dimensions of a sample	length width height	600 mm 1,000 mm 500 mm
Weight of the sample (max.)		1,300 kg
Angle of attack		15° … 90°
Angle of rotation		−90° … 90°

The cutting parameters are set up using a control panel. The movement of the tool in the Y-axis is executed by moving the traverse. In the Z-axis, the movement is realized by adjusting the work bridge to the needed height. The cutting movement is performed by moving of the work table in the X-direction.

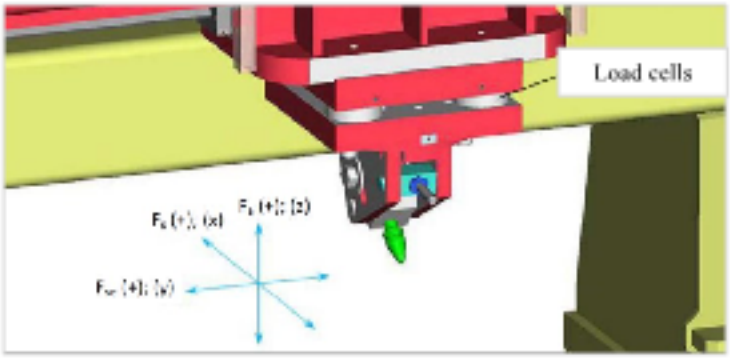

Figure 3.1-2 Force components of the HSX-1000-50 [65]

The cutting-force measuring system used in the machine, can measure forces in the range from -50 to +50 kN (±30 kN in Y-direction). The error of the measurement is equal to 0.5 % (0.25 kN). This is an acceptable error in case of hard rock cutting.

The proving ring

Before commencement of the tests, calibration of force sensors was carried out. For the calibration of the testing rig HXS 1000-50, the proving ring M11721, with maximum load 30 kN, was used (Figure 3.1-3).

The proving ring consists of two main elements, the ring itself (1) and the diameter-measuring system (2). Forces are applied to the ring through the external bosses (3) for attachment. The resulting change in diameter, referred to as the deflection of the ring, is measured with a micrometer screw and the vibrating reed mounted diametrically within the ring. The micrometer screw and the vibrating reed are attached to the internal bosses of the ring [67].

Figure 3.1-3 The proving ring M11721

The procedure of calibration is:

1) mount the proving ring centrally on the testing rig machine according to the mode of loading (for compression, the proving ring is placed centrally between the two loading platens, the cutting tool and the sample surface);
2) connect the PC and set the minimum load for the load cells;
3) record readings of the proving ring and the load cells;
4) shift the cutting tool in the direction of the sample surface by 0.01 mm;
5) record the proving ring and the load cells readings again;
6) repeat steps 4-5 till force reaches maximum safe load;
7) repeat whole procedure for the three coordinates XYZ.

The proving ring is provided with recalculation data table (Annex G). The results of the proving ring and the testing rig were compared. The results from this procedure are shown in Annex G.

It can be seen that there is no significant deviation between test results and pattern diagram. The error is in the established range ($0.5\ \% = 250\ N$).

Cutting tools

In this study, cutting tools such as point-attack bit BG35K-19.5589, made by company BETEK were used. The cutting tools were modified for suitability with the testing rig. The final model of the bit can be found in the Annex A. The tools are made of steel and tungsten carbide. Tungsten carbide is used for wear-resistance of the tip and steel for the tool shank. Such tools have prevalence as tool for selective cut heading machines and drum shearer-loaders. Eight cutting tools were used for the cutting tests. Each cutting tool was used in the unique conditions. During the experiments, the bit was rotated by 45 degrees to provide uniform wearing of the tungsten bit.

Miscellaneous

For the collecting data, computer DEWE 5000 was used (Figure 3.1-4). This computer features special hardware and preinstalled software DEWESoft (Figure 3.1-4) – the use of which provides the possibility to determine precise values of force acting in X, Y and Z directions – video streaming and scanning sample surface. The camera, FASTCAM SA3 made by Photron USA was used with the computer. In using the camera for recording, records with up to 120,000 frames per second rate can be obtained.

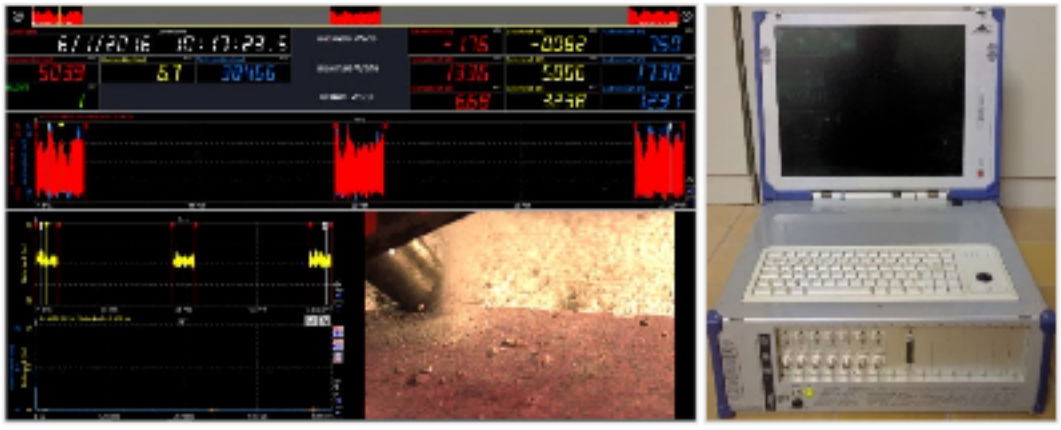

Figure 3.1-4 Software and PC

The laser unit can scan the surface of the specimen determining distance from the unit to the surface of the sample with a precision of ≤70 μm. With the use of such technology, coordinates of the surface can be mapped out, the cutting track investigated and the cut volume calculated [66].

Sieve shaker and test sieves

After cutting tests, the material was analyzed on particle size distribution. The sieve shaker and the set of sieves were used for this purpose (Figure 3.1-5). The sieve shaker is a machine with a vibrating engine, designed for sorting of crushed (bulk) materials by sieving it through sieves.

The vibratory sieve shaker Retsch VE 1000 is used in current research with the set of sieves. Retsch VE 1000 is a throw-action sieve shaker, also known as vibratory sieve shaker. An electromagnetic drive sets a spring-mass system in motion and transfers the oscillations to the sieve stack. The probe is exposed to a movement in three dimensions and is distributed uniformly across the whole area of the sieve [68].

Figure 3.1-5 The sieve shaker, sieves and the lab scale

The sieve shaker has number of installations such as duration of shaking, amplitude of shaking and pause interval. Adjustment of these parameters serves to optimize the sieving process for different types of material. Amplitude and sieving time are set digitally and are continuously observed by an integrated control-unit. Therefore, sieving results are reproducible and precise.

Current sieve shaker can carry out wet and dry sieving. Most sieving analyses are carried out on dry materials, as in this study. Wet sieving only takes place if material is already wet or a sample consists of very fine particles tending to agglomerate.

The set of sieves used in the study is presented by 0.063 mm, 0.125 mm, 0.25 mm, 0.5 mm, 1 mm, 2 mm, 4 mm, 8 mm, 10 mm, 12.5 mm and 16 mm. Additionally, rubber balls were added to the sieves with passing size 0.063 mm and 0.125 mm to increase passage of materials and prevent adhering.

For determining the weight of total mass and particles within range size, the screens are measured before and after the sieving on the lab scale produced by Sartorius. The lab scale has an accuracy of 0.01 gram.

The results of the sieving and weighting are noted down in the Excel table for further analysis and calculations.

3.2 Specimen

Three granite blocks by Montanuniversität Leoben, Austria were taken for the study. Chemical composition was tested by the company Baustoffprüfstelle Wismar GmbH.

Initially, all blocks had 500×500×300 mm dimensions. The blocks have a granular texture with some xenomorphic crystals. The main components are quartz, plagioclase feldspar, biotite, muscovite and chlorite as well as apatite, epidote, sphene and xenotime. Also, compressive strength of the samples equals 202.7 MPa. More information concerning physical and chemical properties of specimens can be found in Annex D.

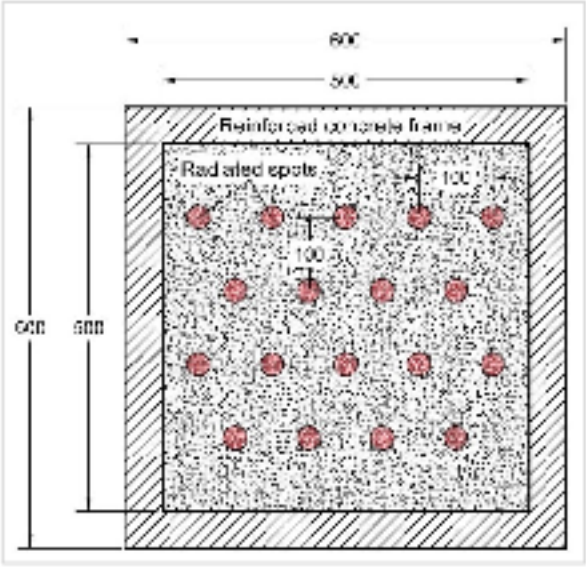

Figure 3.2-1 Model of irradiated blocks

Afterwards, blocks were exposed to microwave irradiation, which took place at Montanuniversität Leoben, Austria. The experiments were performed with continuous

power of 25 kW and radiation time 30 and 45 seconds. Before and during the irradiation, temperature of specimens was measured. The temperature increased from 220 °C to 3000 °C, after 30 seconds, and 5000 °C, after 45 seconds. The irradiation process leads to forming of cracks up to 15 cm length [69].

For preventing destruction of irradiated blocks, they were inserted into reinforced concreate frame (Figure 3.2-1). After that, specimens were processed during another investigation.

As a result, blocks used in the study have sizes equal approximately to 500×500×276 mm for the non-irradiated sample and 600×600×350 mm for the samples after 30 and 45 seconds irradiation (length × width × height respectively).

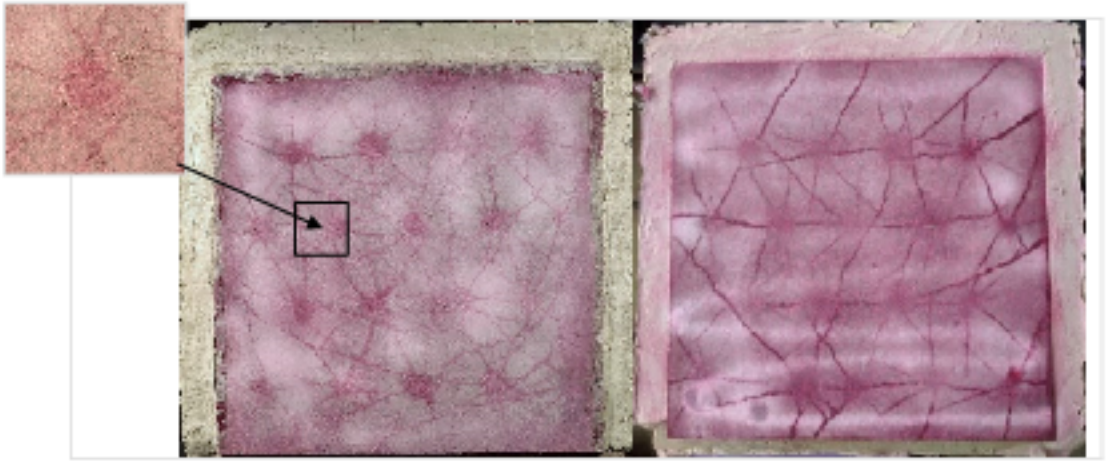

Figure 3.2-2 Photos of 45 and 30 seconds irradiated blocks respectively

Figure 3.2-2 demonstrates the state of samples with 30 and 45 seconds treating before current study.

3.3 Conditions of the Experimental Study

Preparation of experimental research was carried out as follows. The specimen was installed and properly fastened to the movable table of the testing rig (Figure 3.3-1). Calibration of the sensors has been made according to the instructions (Chapter 3.1), results of it can be found in Annex G.

Next step is preparation of the surface of the block for cutting process: measuring basic points (x-, y-, z-coordinates of the block borders) for determining cutting area and setting of the particle collectors. For microwave treated samples, mounting and setting of the camera was needed. After preparation of the working area, process of the testing rig

setup was started: i.e. cutting depth, cutting speed, spacing between cuts, number of cuts, cut length, cut area and the angle of attack.

Figure 3.3-1 Complete mounting of the sample

Angle of attack

The importance of an angle of attack and other dependent angles are described in Chapter 1.1. For current experiments, the decision was made to set an angle of attack equal to 45°.

Cutting depth

During the stage of experiment design, it was decided to establish the cutting depth at 4 mm. This decision was informed by previous research, made in this study, experiments made on the rig and the rig capabilities.

Cutting speed

The cutting speed was set up at $0.1\ m/s$. Such speed is relatively low. It was considered that on a high speed, the wearing of the pick could increase due to heating. A high speed during the cutting process could also result in high forces that would cause rig vibration and tamper with results obtained.

Spacing between cuts

During the stage of experiment design, it was considered to make the current parameter a variable. In order to obtain valuable results from the cutting tests, distances of 8 mm and 12 mm were chosen.

Cutting length and cut area

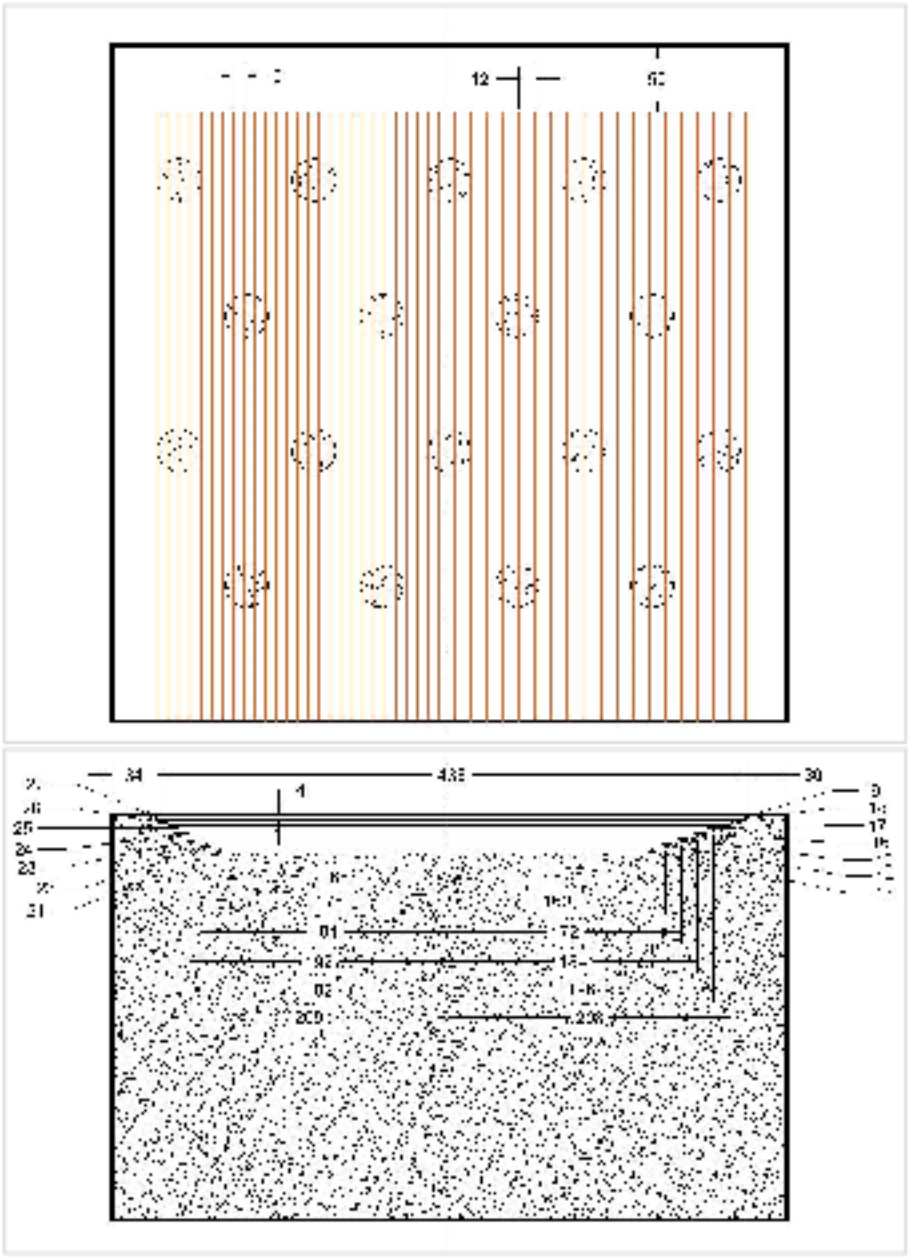

Figure 3.3-2 Cutting zones

The cutting process demands high force influence on the sample, which can cause the cracking or chipping of big parts of the sample, especially near the edges. For this reason reinforced framing was made as well as designation of a safe zone on the edges of the blocks. For the irradiated blocks with reinforced frame, the safe zone was 50-70 mm towards the back of the block and around 30-50 mm on the left and right sides (the width of the concrete frame was not taken into account). The untreated sample had bigger safe zones, due to the lack of a reinforced frame and the damage incurred during previous experiments and leveling. The safe zones in the untreated sample are equal to 90 mm at the back and 70 mm and 100 mm at the sides. Additionally, tilted upside-down 30 seconds irradiated sample was

used as the untreated block. The safe zone was 70 mm from the back and around 70 mm from sides.

Number of cuts

Each block was figuratively divided in two equal parts along the x-axis. This was made to create equal conditions for the cutting process with different spacing between cuts. Since the area for cutting was considered to be the same and space between cuts was different, the number of cuts in each section ranged from 10 to 25.

The cutting tests were carried out without leveling of the surface. This means that after cutting a layer, the next layer was cut in the quarry manner (the number of cuts on the next layer was decreased by one from each side) because of the cutting tool shape and importance of the safe zone. Cutting of the next layer began directly under the second cut of the first layer. The data result from first cuts were not considered in further calculations, as it is a blocked cut and, as such, has a different mean, maximum and vector direction of the force.

After each three cuts made by the testing rig the cutting tool was rotated. This was to allow even wearing of the pick as well as a smooth shape of the pick. In addition, during this operation timeouts were provided during which the tool cooled down and the speed of the wearing was decreased.

Scanning

Scanning of the surface was an important part of the experiments. When a layer was cut and new surface cleaned, laser scanning of the new surface was made. For this, the machine was switched to another mode. In this mode, after inserting two basic points (highest and lowest) on the specimen, the rig starts measuring the distance from the laser to the surface, finding the optimal distance. When measuring is finished, the mode needed to be switched again. In the new mode, edge points of the cutting area should be keyed in. After this, the laser scans the surface on the optimal distance, perpendicularly to the cutting direction by constantly shifting 2 mm further until the whole cut area is measured.

Particle size analysis

The data was collected using the computer, described in 3.1. The PC required connecting and setting up before experiments. The high-speed camera was installed for shooting the cracking and chipping of the sample during the process.

After the cutting of the layer, the chipped material was collected in bags. The collected material was used afterwards in the sieve analysis. The process of sieving analysis required a number of manipulations. First of all, weighing of the set of sieves on the lab scale was performed and results were listed in an Excel table. Next, mounting of the chosen sieves with material onto the sieve shaker was done. The sieving machine was then set up. The settings for the shaker were as follows:

- duration time of 5 minutes;
- amplitude of 1.2 mm;
- interval of 10 seconds.

On finishing the sieving process, each sieve was weighed again and the data inserted in the Excel table.

3.4 Processing and Analysis of Results of the Experimental Study

As a result of the cutting tests the force-time diagrams for the X, Y and Z directions were obtained. The forces were subjected to further analysis. Also, the wear rate, particle size distribution and energy consumption have been analyzed. The description of these results is represented in this section.

3.4.1 Description of the Cutting Process

Loud noise, considerable vibration levels and formation of a small dust cloud in front of the pick accompanied the cutting process of granite. Scattering of particles during cutting was directed sideways with respect to cutting direction. The cutting tool was heated by the cutting process, but temperature was within possibility to hold the tool with hands without discomfort.

Cutting tests with 45 seconds treated block were stopped after cutting of 4 layers caused by failure of the sample (Figure 3.4-1).

Figure 3.4-1 Failure of the sample

An analysis of the 45 seconds block preliminary to cutting showed that cracks achieved lengths up to 100 mm, which is visualized by a pink penetration fluid.

Figure 3.4-2 Pieces, created as a result of failure of the sample

The pieces, formed as a result of the failure, have considerable size. The biggest piece has dimensions around 150×230×220 mm and weight of 11.3 kg (Figure 3.4-2).

3.4.2 Cutting Forces

After the finish of the experiments, it is possible to apply the approach of the analysis of the experimental data, described in Chapter 2.1.1, to the obtained data.

The result of the cutting process exported in Excel (as the data arrays), the output has more than 43,000 rows for each cut. Now, it is possible to apply the analysis to the data array of cutting forces.

In MS Excel the formula described in Chapter 2.1.1 was used to determine the peaks of a force-time diagram, taking into account values exceeding a mean value.

The data obtained by the approach should be statistically processed. The output was built in ascending order and can be found in Annex B.

From the distribution (Figure 3.4-3), it can be assumed that it is a Gaussian distribution. As the next step of the processing should be the process of confirmation of the obeying current random variable to the Gaussian distribution.

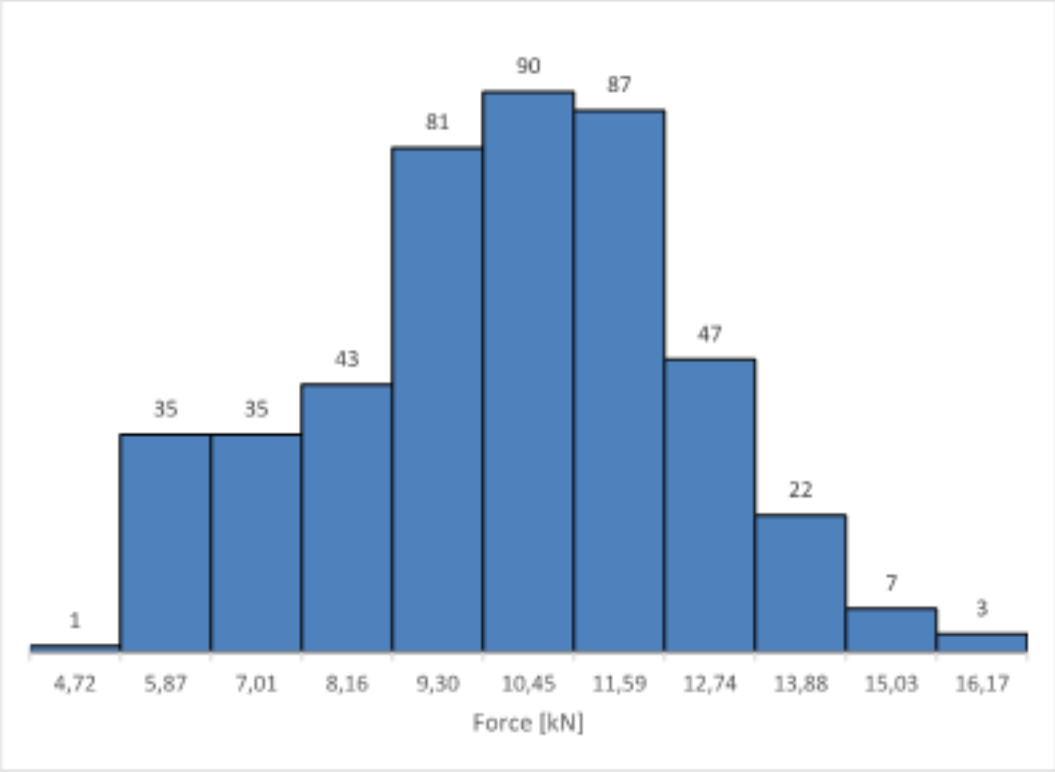

Figure 3.4-3 Distribution of the random variables of the peaks, represented in Annex B

Using Pearson's chi-squared test it will be checked for the hypothesis that at significance level $\alpha = 0.05$ obtained random variables distribution is not contrary to the Gaussian distribution.

At first, it is needed to calculate mean and variance of the random variable using the formulas (2.1-2) and (2.1-3):

$$\mu = 9.547 \qquad \sigma^2 = 5.221$$

As written in Chapter 2.1.2, next is choosing the amount of intervals with formula (2.1-4), the number of random variables equals to $N = 452$, then

$$k = 9.76 \approx 10$$

Next step is choosing the borders of intervals following the formula (2.1-5) and Table 2.1-1. Calculated intervals are in the Table 3.4-1.

Table 3.4-1 Calculated intervals

	1	2	3	4	5	6	7	8	9	10
x_i	$-\infty$	4.011	5.530	6.794	8.062	9.547	11.031	12.299	13.563	15.082
x_{i+1}	4.011	5.529	6.794	8.062	9.547	11.031	12.299	13.563	15.082	∞

Then it is required to calculate frequency of belonging random to the interval n_i and determine probability deriving by formula (2.1-7)

Table 3.4-2 Belonging of the random variable to the intervals

	1	2	3	4	5	6	7	8	9	10
n_i	0	24	38	48	108	118	67	34	11	4

In current situation intervals 1 and 2, as well as 9 and 10, should be merged.

Table 3.4-3 Merged random variable distribution belonging

	1-2	3	4	5	6	7	8	9-10
n_i	24	38	48	108	118	67	34	15

The number of degree of freedom calculated by equation (2.1-8) equals 5.

Then probability deriving for intervals was calculated

Table 3.4-4 Probability deriving for the intervals

	1-2	3	4	5	6	7	8	9-10
$P_i[f(x)]$	0.04	0.08	0.14	0.24	0.24	0.14	0.08	0.04
$P_i$exp	0.05	0.08	0.11	0.24	0.26	0.15	0.08	0.03

Using the formula (2.1-9) the critical value of Pearson's chi-squared 8.31<18.31 was determined, which means that condition is fulfilled. In addition, it was calculated $P\{S > S'\}$ by equation (2.1-10) which is equal to $0.14 > 0.05$. All requirements are fulfilled; the random variables meet normal distribution.

Figure 3.4-4 shows convergence of the frequency polygon and histogram of the distribution. As the data meet Gaussian distribution, further processing can be completed. The results of processing forces can be found in Annex H.

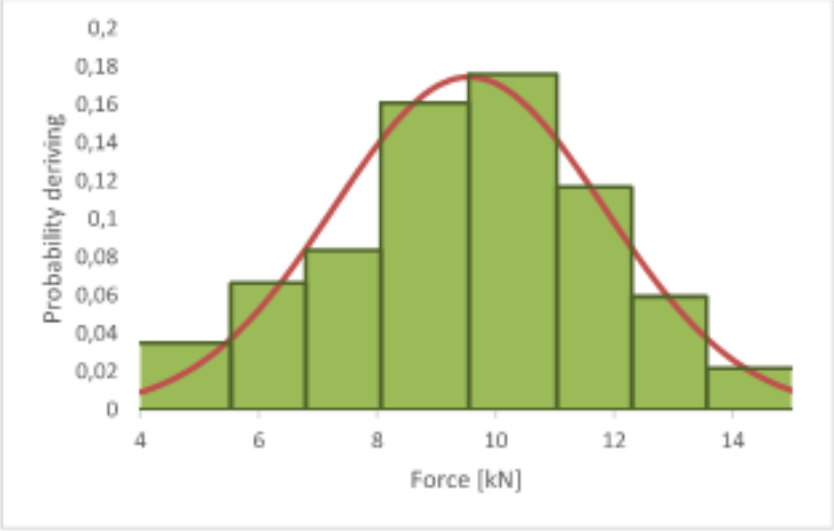

Figure 3.4-4 Proven normal distribution of the peaks

The analysis of experimental results based on investigating of influence of spacing between cuts, distance from initial surface and irradiation duration on cutting forces.

Further, it is shown the diagrams of forces, which are means for cut layers, in Figure 3.4-5, Figure 3.4-6 and Figure 3.4-7. The forces presented with different colors and line properties are explained in the Table below.

Table 3.4-5 Legend to the forces diagrams

45 second irradiated block, mean forces;
45 second irradiated block, maximum forces;
30 second irradiated block, mean forces;
30 second irradiated block, maximum forces;
non-irradiated block, mean forces;
non-irradiated block, maximum forces.

Cutting forces

Influence of spacing

According to Figure 3.4-5 the dependency of the forces on the spacing is low in terms of values under study. The forces of cutting process with spacing between cuts of 8 mm are 13 % lower compared with that of 12 mm.

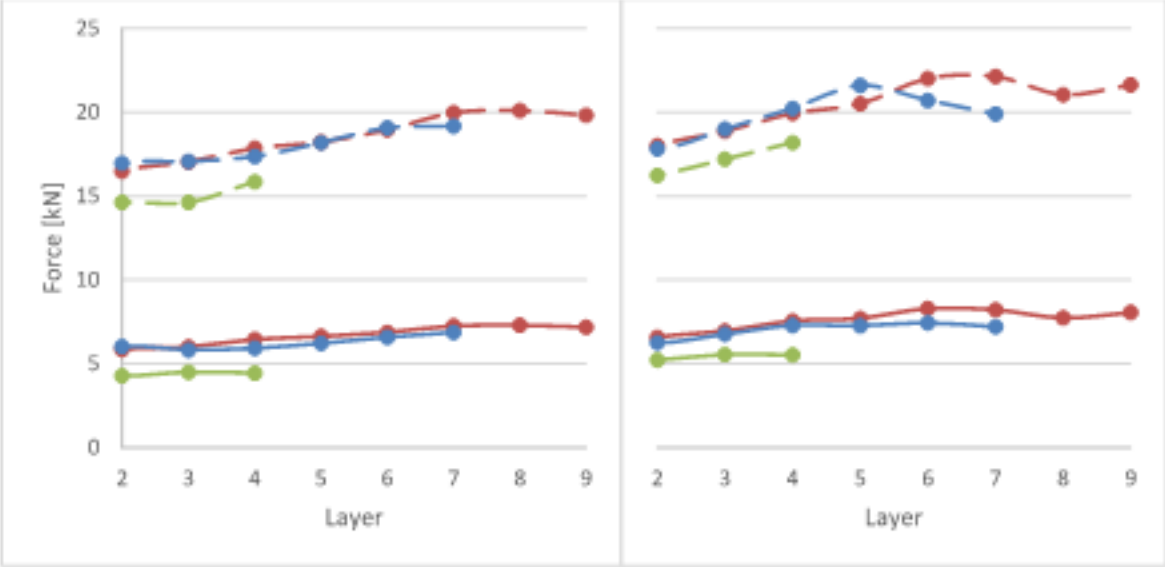

The legend is in Table 3.4-5

Figure 3.4-5 Cutting forces $\boldsymbol{F_x}$, with spacing 8 mm (left) and 12 mm (right)

Influence of distance from initial surface

The influence of distance from initial surface is shown in Figure 3.4-5. It is seen that while penetrating deeper in a sample the forces slightly increase. The growth for each subsequent layer is around 3 %. This increase is also caused by decreasing of cracking of the sample and wearing of the individual picks, since all samples show a similar increase of the forces with increasing depth, a decreasing influence of the radiation seems unlikely. However, it must be said, that a reliable quantification of the penetration depth of the radiation in the 45 seconds irradiated block cannot be done as the preliminary failure.

Influence of duration of treatment

Graphs in Figure 3.4-5 show the effect of microwave irradiation on the cutting forces. As it is demonstrated, 45 seconds treated sample in average required on 22 % lower forces in comparison to non-irradiated sample. However, during cutting of 30 seconds irradiated sample observed slightly higher forces for cutting in comparison to untreated block.

Side forces

As it is seen from Figure 3.4-6, side forces are much lower than cutting and normal forces, less than 11.5 kN maximum. This means, with such conditions and for current study, they have less influence on cutting process.

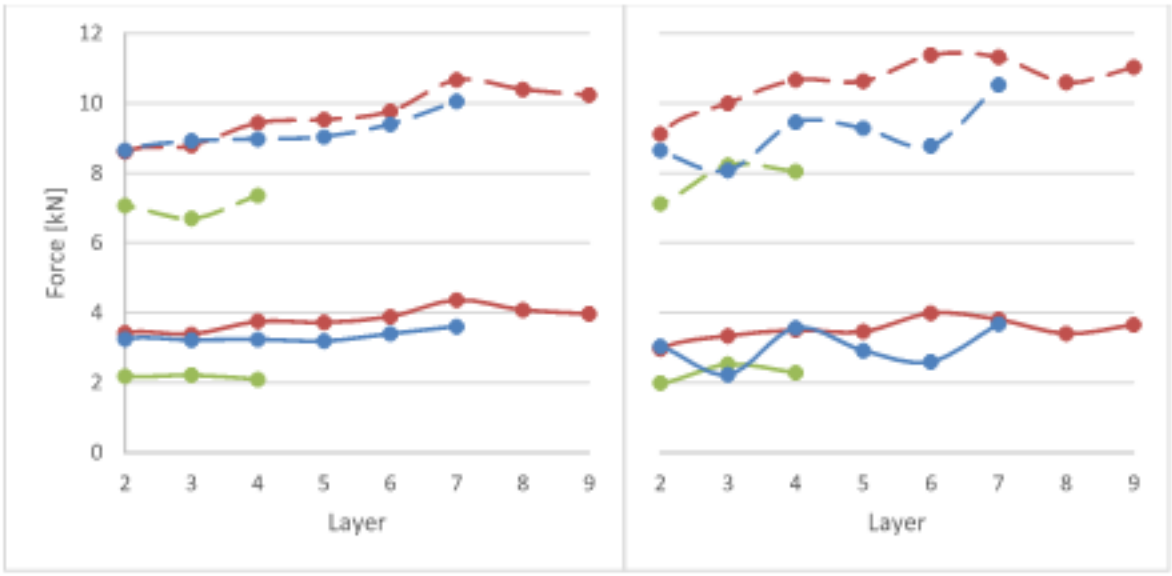

The legend is in Table 3.4-5

Figure 3.4-6 Side forces F_y, with spacing 8 mm (left) and 12 mm (right)

Normal forces

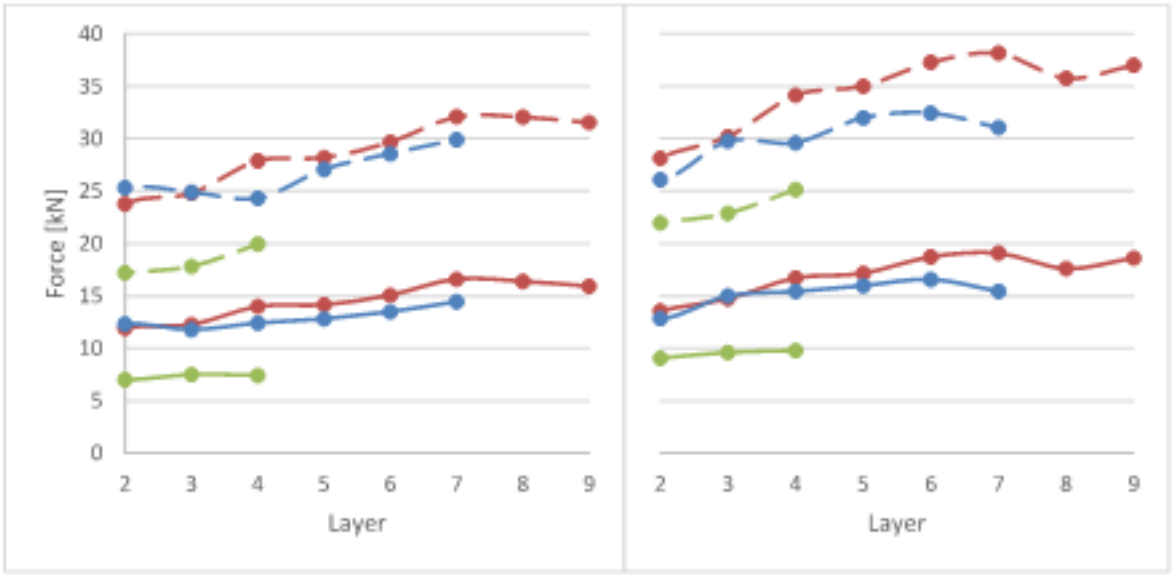

The legend is in Table 3.4-5

Figure 3.4-7 Normal forces F_z, with spacing 8 mm (left) and 12 mm (right)

Normal forces in average repeat the behavior of cutting forces. The only difference is that they operate in the range up to 40 kN. The according diagrams can be seen in Figure 3.4-7.

Total forces

The same, as for normal forces, could be seen for total forces. The behavior of total forces mainly repeats the behavior of cutting forces.

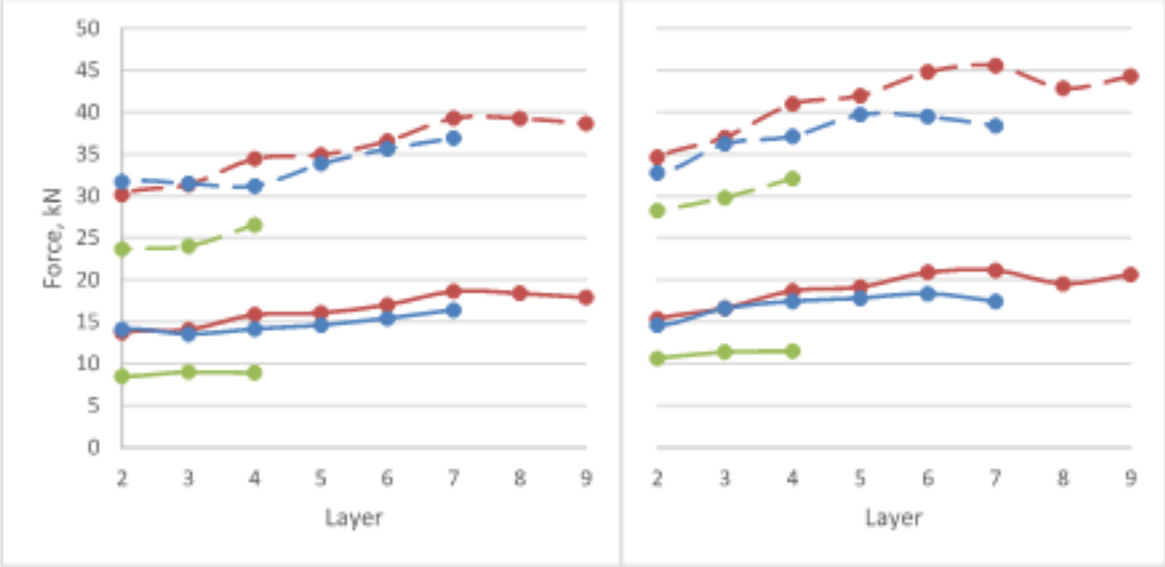

The legend is in Table 3.4-5

Figure 3.4-8 Total forces, with spacing 8 mm (left) and 12 mm (right)

The total force, for cutting 45 seconds irradiated sample with spacing 8 mm, achieved where 9.03 kN and 26.58 kN as mean and maximum respectively. At the same time, the total force, for cutting the same sample with spacing 12 mm, reached 11.5 kN and 32.12 kN.

Up to 18.65 kN and 39.31 kN were seen during cutting of 30 seconds treated block with space between cuts 8mm as total forces. During cutting of this sample with spacing 12 mm, the total forces achieved 21.15 kN and 45.58 kN.

The untreated sample showed total forces up to 16.42 kN and 36.95 kN for 8 mm spacing, as well as 18.37 kN and 39.75 kN for 12 mm spacing.

3.4.3 Specific Energy

In this study, the energy consumption is based on the cutting force F_x. This is due to the fact that normal force F_z and side force F_y are not performing by the rig.

The calculation of the specific energy consumption was carried out utilizing Formula (2.2-1).

Influence of spacing

In average, the specific energy consumption of cutting process with spacing between cuts of 8 mm was 20 % higher than cutting process with spacing of 12 mm between cuts (Figure 3.4-9).

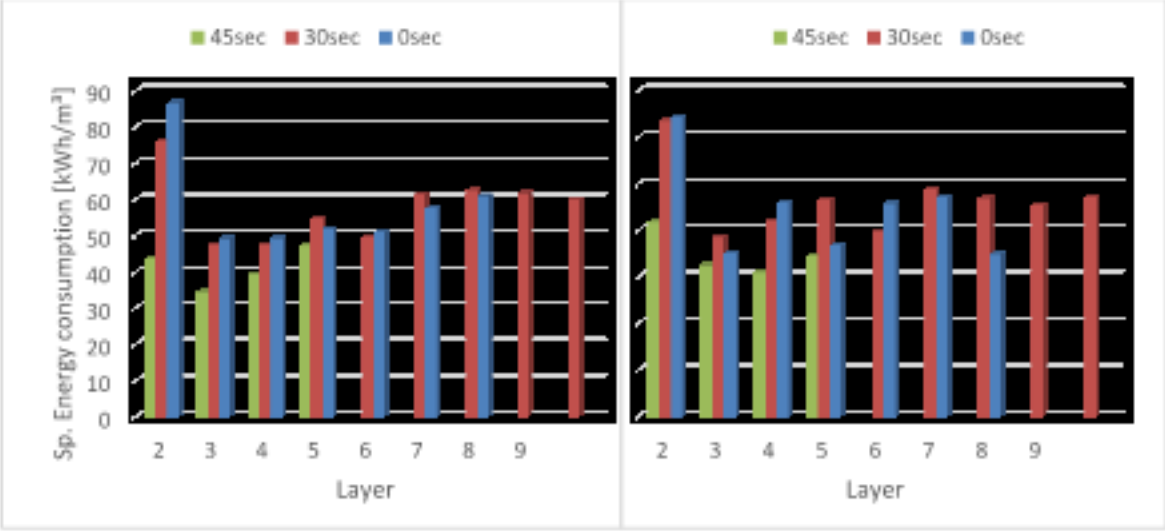

Figure 3.4-9 Specific energy consumption of cutting process with spacing between cuts 8 mm (left) and 12 mm (right)

Influence of distance from initial surface

Depending on the distance from the initial surface and duration of microwave irradiation, the specific energy consumption varies between 30 and 60 kWh/m^3. As seen in Figure 3.4-9, the specific energy increases during cutting process after increasing depth with respect to initial surface.

Influence of duration of treatment

From the diagrams (Figure 3.4-9) is seen that the specific energy needed for cutting of 45 seconds threated block is the lowest. Comparing specific energy consumption of cutting process with spacing 8 mm shows (layers compared respectively):

- the specific energy consumption of 45 seconds treated block is lower by 29.8 %, 20.3 % and 9.4 % that for untreated block;
- the 45 seconds treated block demands on 27.01 %, 17.05 % and 13.99 % less energy than 30 seconds treated sample for excavation the same volume;
- the difference between specific energy consumption of 30 seconds treated block and untreated block is insignificant (in the range of 2.8-13.2 %).

For the 12 mm spacing, these numbers are as follows:

- the untreated block demands on 7.4 %, 32.8 % and 6.3 % more energy, comparing to 45 seconds treated block;

- the specific energy spent for cutting the 30 seconds treated block is higher by 15.46 %, 26.40 % and 26.16 % than 45 seconds treated block;
- che blocks with 30 seconds treatment duration and untreated did not show significant difference in specific energy consumption, except layers 4th and 7th, for which the specific energy of untreated block exceeds 26.84 % and 34.10 % respectively.

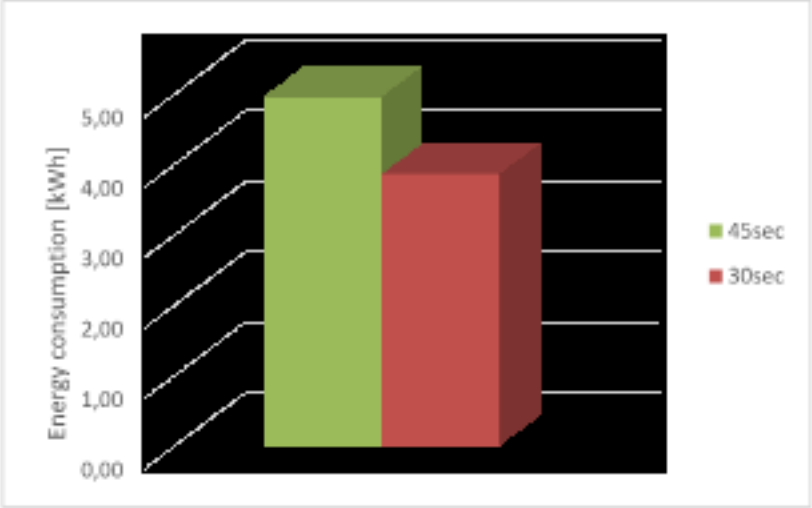

Figure 3.4-10 Energy consumption of microwave irradiation process

From the data, gathered during microwave irradiation, it was calculated the energy consumption spent on microwave treatment. The calculation was made with Formula (2.2-2).

Taking into account the energy consumed by irradiation process, it could be seen in the Figure 3.4-10 that 45 and second irradiation duration process demands 4.96 kWh which is on 22 % more than for 30 second (3.86 kWh).

3.4.4 Wearing

For collecting data concerning tool wearing, during the cutting process were used multiple number of cutting tools. Each tool was involved only in the process with the same cutting parameters, such as cutting speed, cutting depth, spacing between cuts and the duration of microwave irradiation.

The tools were weighed after each cut layer on the high accuracy weight scale, with precision 0.001 g. Every measurement was repeated 3 times for avoiding statistical error. The collected data is shown in the Annex D. To determine wearing, the equation (2.2-3) was used. Results of calculation and cut distance per layer can be found in the Annex D.

Influence of spacing

Looking in the Figure 3.4-11, it can be seen that for the block treated with microwaves for 45 seconds, the wear rate, during cutting with spacing 8 mm, was around 0.011 g/m, while, during cutting with spacing 12 mm, the ware rate was in range 0.016-0.019 g/m.

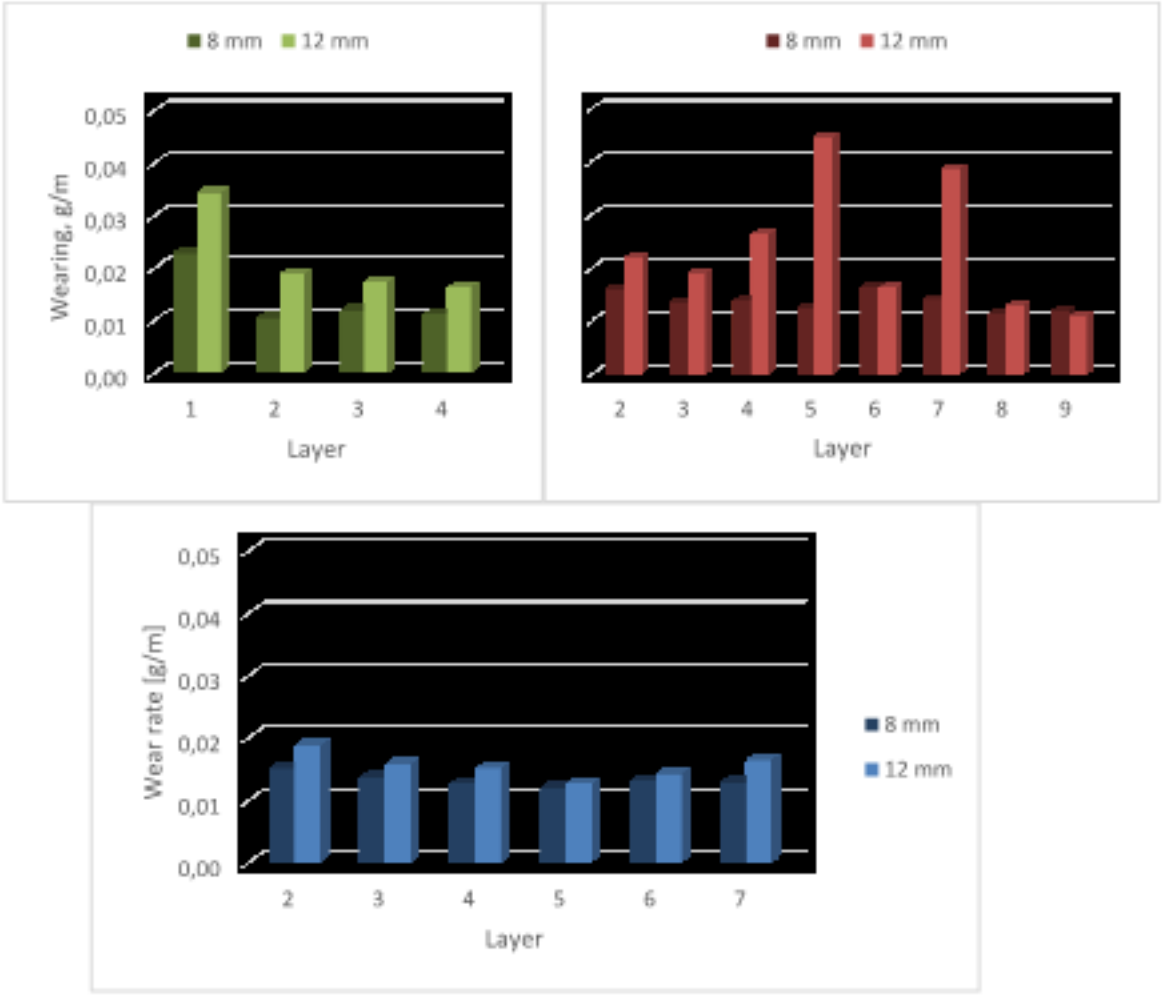

Figure 3.4-11 Wear rate of cutting tool comparing 8 mm and 12 mm, for spacing 45 sec (top left), 30 sec (top right) and 0 sec (bottom)

30 seconds irradiated block showed wear rate of 0.011-0.017 g/m for cutting with spacing between cuts 8 mm and 0.011-0.045 g/m for 12 mm. The wear rate, during cutting the untreated sample with 8 mm between cuts, was 0.012-0.015 g/m, while during cutting with 12 mm spacing – it was 0.012-0.019 g/m.

In addition, it should be mentioned that influence of spacing between cuts on wear rate during cutting of irradiated blocks higher than during cutting of non-irradiated block. The difference between 8 mm and 12 mm cutting is around 15 % for non-irradiated block, in average 30 % for 30 seconds treated block and more than 35 % for 45 seconds treated block.

Influence of distance from initial surface

Concerning the influence of distance from initial surface on wearing, it is cannot be clearly identified. As seen from Figure 3.4-11, there is no significant changing in ware rate with each subsequent layer and Figure 3.4-12 describes wear rate as almost linear function. Exception is cut layers 5 and 7 of 30 seconds irradiation block, which hardly can be statistically explained without additional investigations of the sample homogeneity.

Influence of duration of treatment

Results show that wear rate of untreated block and 45 seconds treated block have no major difference comparing to other blocks.

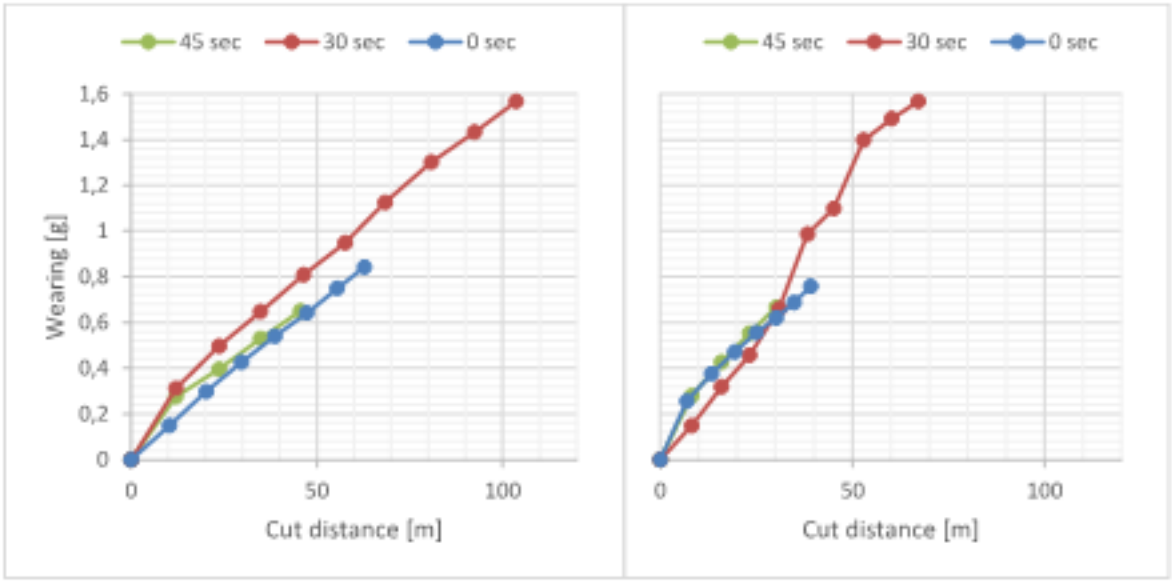

Figure 3.4-12 Wearing, distance between 8 mm (left) and 12 mm (right)

From Figure 3.4-12, it is seen that after cutting 40 m of the non-irradiated granite with spacing between cuts equals to 8 mm, the tool was worn by 0.56 g, when 45 seconds treated block was worn by 0.6 g and 30 seconds threated block – by 0.72 g. At the same time, the cutting of 30 m of the non-irradiated granite, with spacing between cuts equals to 8 mm, worn the tool by 0.62 g, 45 seconds threated block – by around 0.66 g and 30 seconds treated – by 0.62 g.

3.4.5 Particle Distribution

The experiments included the process of analysis of particle size distribution. The table of results of the sieving analysis are presented in Annex E.

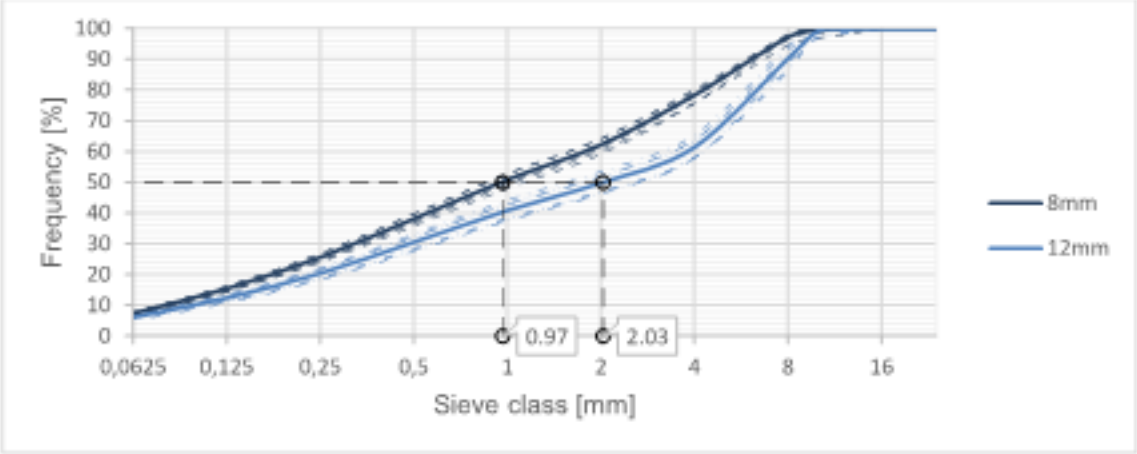

Figure 3.4-13 Cumulative frequency curve of the sieving analysis for untreated block

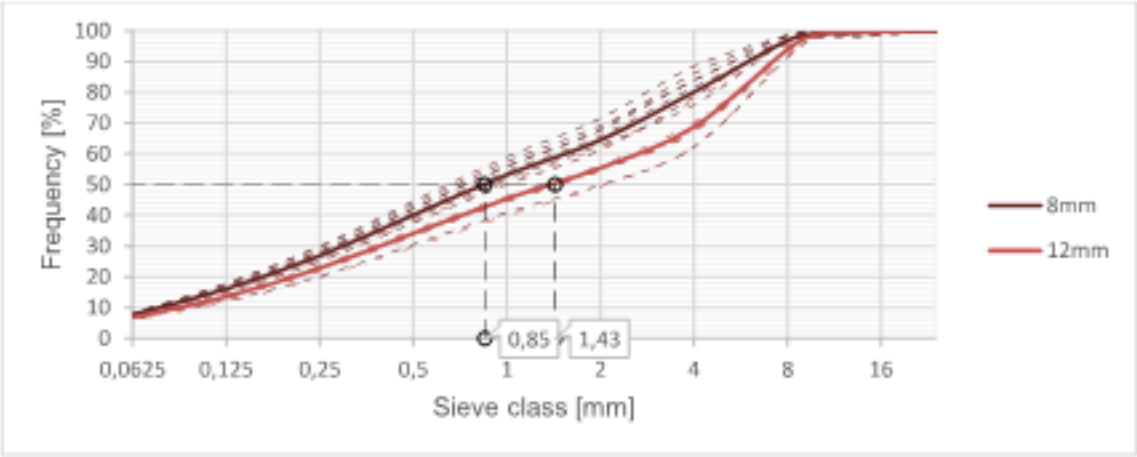

Figure 3.4-14 Cumulative frequency curve of the sieving analysis for 30 seconds treated block

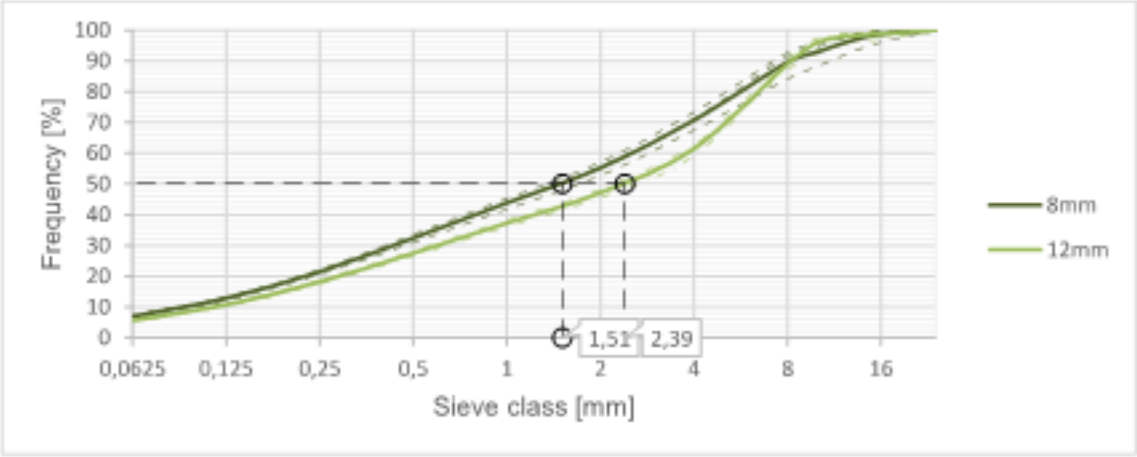

Figure 3.4-15 Cumulative frequency curve of the sieving analysis for 45 seconds treated block

Influence of spacing

In Figure 3.4-13, Figure 3.4-14 and Figure 3.4-15 present a comparison of particle distribution curves with different spacing between cuts. As seen, the difference in particle

size under 100 μm is under 3 %. But with passing 50 % of material, it is clear that 12 mm spacing cutting process creates less fines, which is positively affects cutting conditions, further processing and transportation.

Influence of distance from initial surface

The variance of particle size distribution with respect to layer can be found in Figure 3.4-13, Figure 3.4-14 and Figure 3.4-15 as dotted lines. The deviations of sieving results (over 1 mm particle size) for different layers of 45 second irradiated block are 43.84 ± 1.77 % (8 mm spacing) and 37.34 ± 1.08 % (12 mm spacing). These results for 30 seconds treated block are 53.28 ± 5.73 % and 45.48 ± 2.98 %. Moreover, the deviations for untreated sample are 50.86 ± 1.9 % and 40.86 ± 2.98 %.

Influence of duration of treatment

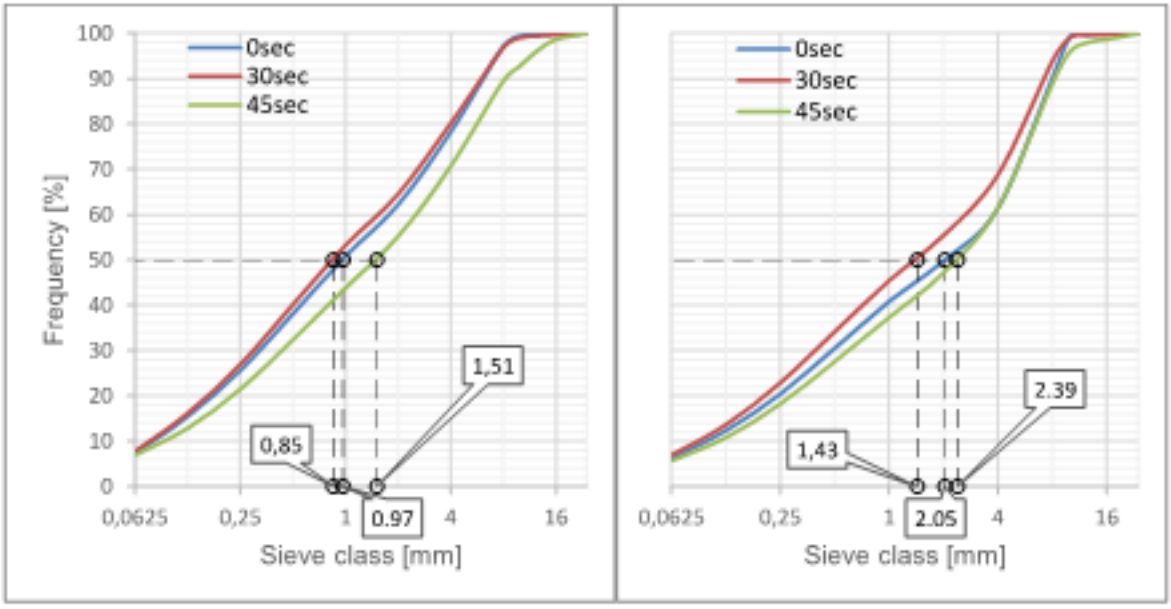

Figure 3.4-16 Cumulative frequency curves, 8 mm (left) and 12 mm (right)

The influence of duration of irradiation by microwaves can be seen in Figure 3.4-16. 45 seconds irradiated block has bigger grain size with respect to other samples, it consists of 50 % particles with diameter higher than 1.51 mm (2.39 mm), when non-irradiated and 30 seconds irradiated samples have 0.85 mm (1.43 mm) and 0.97 mm (2.05 mm) respectively. In this case, microwave treating has positive effect, as the cutting process after irradiation during 45 seconds creates the smaller volume of fine particles.

4. DEVELOPMENT OF REGRESSION MODELS AND FORCE MAPPING

In chapter below, presented are the results of development of regression models for numerous of factors investigated in the current study. The procedure for development is given in Chapter 2.3.

4.1 Regression Models of Forces

Initial data for development of regression model are given in Annex C. The regression models and the resulted equations describe dependency of an appropriate force F on duration of irradiation T, spacing between cuts S, and distance from initial surface D.

Using the method of multiple regression analysis, the determination of the full regression equation is accomplished.

In this study, it was chosen to start regression analysis from simple equation and afterwards increase the number of explanatory variables until highest regression coefficient will be found. As the simple equation, formula (2.3-2) was chosen.

The system of equation (2.3-4) for $F_{x_{mean}}$ takes the form

$$\begin{pmatrix} 34 & 750 & 340 & 640 \\ 340 & 26550 & 7500 & 13800 \\ 340 & 7500 & 3536 & 6400 \\ 640 & 13800 & 6400 & 14464 \end{pmatrix} \cdot \begin{pmatrix} b_0 \\ b_1 \\ b_2 \\ b_3 \end{pmatrix} = \begin{pmatrix} 223.96 \\ 4771.2 \\ 2270.36 \\ 4412.28 \end{pmatrix}$$

After solving the system of linear equations and determination of coefficients b_i, the formula (2.3-2) has a view

$$F_{x_{mean}} = 3.147157421 - 0.014377651 \cdot T + 0.226176471 \cdot S + 0.079437322 \cdot D$$

Table 4.1-1 Regression model for mean values of cutting forces

Step	Regression equation	S^2_{res}	$\frac{S^2_{res_l}}{S^2_{res_{(l+1)}}}$	$F_{(1-p)}$	R
1	$y = \cdots + \cdots x_1 + \cdots x_2 + \cdots x_3$	0.36			0.84
2	$y = \cdots + \cdots x_1 + \cdots x_2 + \cdots x_3 + \cdots x_1x_2$	0.37	1.03	1.46	0.84
3	$y = \cdots + \cdots x_1 + \cdots x_2 + \cdots x_3 + \cdots x_1x_3$	0.31	1.15	1.46	0.86
4	$y = \cdots + \cdots x_1 + \cdots x_2 + \cdots x_3 + \cdots x_2x_3$	0.37	1.03	1.46	0.84
5	$y = \cdots + \cdots x_1 + \cdots x_2 + \cdots x_3 + \cdots x_1x_2x_3$	0.32	1.12	1.46	0.86
6	$y = \cdots + \cdots x_1 + \cdots x_2 + \cdots x_3 + \cdots x_1^2$	0.06	5.99	1.46	0.98
7	$y = \cdots + \cdots x_1 + \cdots x_2 + \cdots x_3 + \cdots x_1^2 + \cdots x_2^2$	0.06	1.04	1.46	0.98
8	$y = \cdots + \cdots x_1 + \cdots x_2 + \cdots x_3 + \cdots x_1^2 + \cdots x_3^2$	0.05	1.17	1.46	0.98
9	$y = \cdots + \cdots x_2 + \cdots x_3 + \cdots x_1^2$	0.27	4.50	1.46	0.88

Next step is calculation of the residual variance of regression (2.3-6) and correlation coefficient (2.3-9). The residual variance equals 0.36 and correlation coefficient equals 0.84. The results are written in Table 4.1-1.

Further, should be added next explanatory variable from the equation (2.3-1). For such equation the system of equations is

$$\begin{pmatrix} 34 & 750 & 340 & 640 & 13800 \\ 750 & 26550 & 7500 & 13800 & 462600 \\ 340 & 7500 & 3536 & 6400 & 138000 \\ 640 & 13800 & 6400 & 14464 & 314400 \\ 7500 & 265500 & 78000 & 138000 & 2761200 \end{pmatrix} \cdot \begin{pmatrix} b_0 \\ b_1 \\ b_2 \\ b_3 \\ b_{12} \end{pmatrix} = \begin{pmatrix} 223.96 \\ 4771.2 \\ 2270.36 \\ 4412.28 \\ 48440.4 \end{pmatrix}$$

The resulted equation is

$$F_{x_{mean}} = 3.422017365 - 0.026837969 \cdot T + 0.198690476 \cdot S + 0.079437322 \cdot D + 0.001246032 \cdot T \cdot S$$

The residual variance equals 0.37 and correlation coefficient equals 0.84. Now, it is needed to determine statistical significance of variance difference between polynomials by equation (2.3-8). The result is 1.03, which is lower $F_{(1-p)} = 1.46$. The explanatory variable x_{12} should be skipped, as it is not significant.

The procedure should be repeated. In this case, the system looks like

$$\begin{pmatrix} 34 & 750 & 340 & 640 & 13800 \\ 750 & 26550 & 7500 & 13800 & 462600 \\ 340 & 7500 & 3536 & 6400 & 138000 \\ 640 & 13800 & 6400 & 14464 & 314400 \\ 13800 & 462600 & 138000 & 314400 & 10058400 \end{pmatrix} \cdot \begin{pmatrix} b_0 \\ b_1 \\ b_2 \\ b_3 \\ b_{13} \end{pmatrix} = \begin{pmatrix} 223.96 \\ 4771.2 \\ 2270.36 \\ 4412.28 \\ 93877.2 \end{pmatrix}$$

The resulted equation is

$$F_{x_{mean}} = 3.960296762 - 0.04599853 \cdot T + 0.226176471 \cdot S + 0.032212273 \cdot D + 0.001905286 \cdot T \cdot D$$

The residual variance is 0.31 and correlation coefficient is 0.86. The statistical significance, in this case, should be calculated as residual variance of first equation divided by residual variance of current. It equals 1.15, which is less than 1.46 (F distribution table value). This variable does not improve the regression.

The explanatory variable x_{13} is skipped. The new system of equation is

$$\begin{pmatrix} 34 & 750 & 340 & 640 & 13800 \\ 750 & 26550 & 7500 & 13800 & 462600 \\ 340 & 7500 & 3536 & 6400 & 138000 \\ 640 & 13800 & 6400 & 14464 & 314400 \\ 6400 & 138000 & 66560 & 144640 & 1504256 \end{pmatrix} \cdot \begin{pmatrix} b_0 \\ b_1 \\ b_2 \\ b_3 \\ b_{23} \end{pmatrix} = \begin{pmatrix} 223.96 \\ 4771.2 \\ 2270.36 \\ 4412.28 \\ 44695.04 \end{pmatrix}$$

The resulted equation will be

$$F_{x_{mean}} = 3.01530842 - 0.014377651 \cdot T + 0.239361371 \cdot S + 0.0864418 \cdot D - 0.000700448 \cdot S \cdot D$$

The residual variance and correlation coefficient for such equation equal 0.37 and 0.84. The regression model is not improved. The variable can be skipped.

The same process is repeated with adding x_{123}. The system of equations will have a view

$$\begin{pmatrix} 34 & 750 & 340 & 640 & 13800 \\ 750 & 26550 & 7500 & 13800 & 462600 \\ 340 & 7500 & 3536 & 6400 & 138000 \\ 640 & 13800 & 6400 & 14464 & 314400 \\ 138000 & 4626000 & 1435200 & 3144000 & 10460736 \end{pmatrix} \cdot \begin{pmatrix} b_0 \\ b_1 \\ b_2 \\ b_3 \\ b_{123} \end{pmatrix} = \begin{pmatrix} 223.96 \\ 4771.2 \\ 2270.36 \\ 4412.28 \\ 951904.8 \end{pmatrix}$$

The equation for such system looks like

$$F_{x_{mean}} = 4.384653945 - 0.039043064 \cdot T + 0.165854586 \cdot S + 0.0426001 \cdot D + 0.000148619 \cdot T \cdot S \cdot D$$

The residual variance is 0.32 and correlation coefficient is 0.86. The regression model is not improved. The variable can be skipped.

The new system of equation is

$$\begin{pmatrix} 34 & 750 & 340 & 640 & 13800 \\ 750 & 26550 & 7500 & 13800 & 462600 \\ 340 & 7500 & 3536 & 6400 & 138000 \\ 640 & 13800 & 6400 & 14464 & 314400 \\ 26550 & 978750 & 265500 & 462600 & 37563750 \end{pmatrix} \cdot \begin{pmatrix} b_0 \\ b_1 \\ b_2 \\ b_3 \\ b_{23} \end{pmatrix} = \begin{pmatrix} 223.96 \\ 4771.2 \\ 2270.36 \\ 4412.28 \\ 163075.5 \end{pmatrix}$$

The equation for such system has a form

$$F_{x_{mean}} = 3.470653993 - 0.095667514 \cdot T + 0.226176471 \cdot S + 0.05046748 \cdot D - 0.00282456 \cdot T^2$$

The residual variance is 0.06 and correlation coefficient is 0.98. The statistical significance of variance difference between polynomials is 5.99. All requirements are fulfilled and explanatory variable is accepted.

The process was repeated further, but the importance of other explanatory variables was not proved. The final equation of regression model of mean cutting forces is

$$F_{x_{mean}} = 3.470653993 + 0.095667514 \cdot T + 0.226176471 \cdot S + 0.05046748 \cdot D - 0.00282456 \cdot T^2 \quad (4.1\text{-}1)$$

The visualization of the regression model (4.1-1) for mean cutting forces $F_{x_{mean}}$ is shown in Figure 4.1-1.

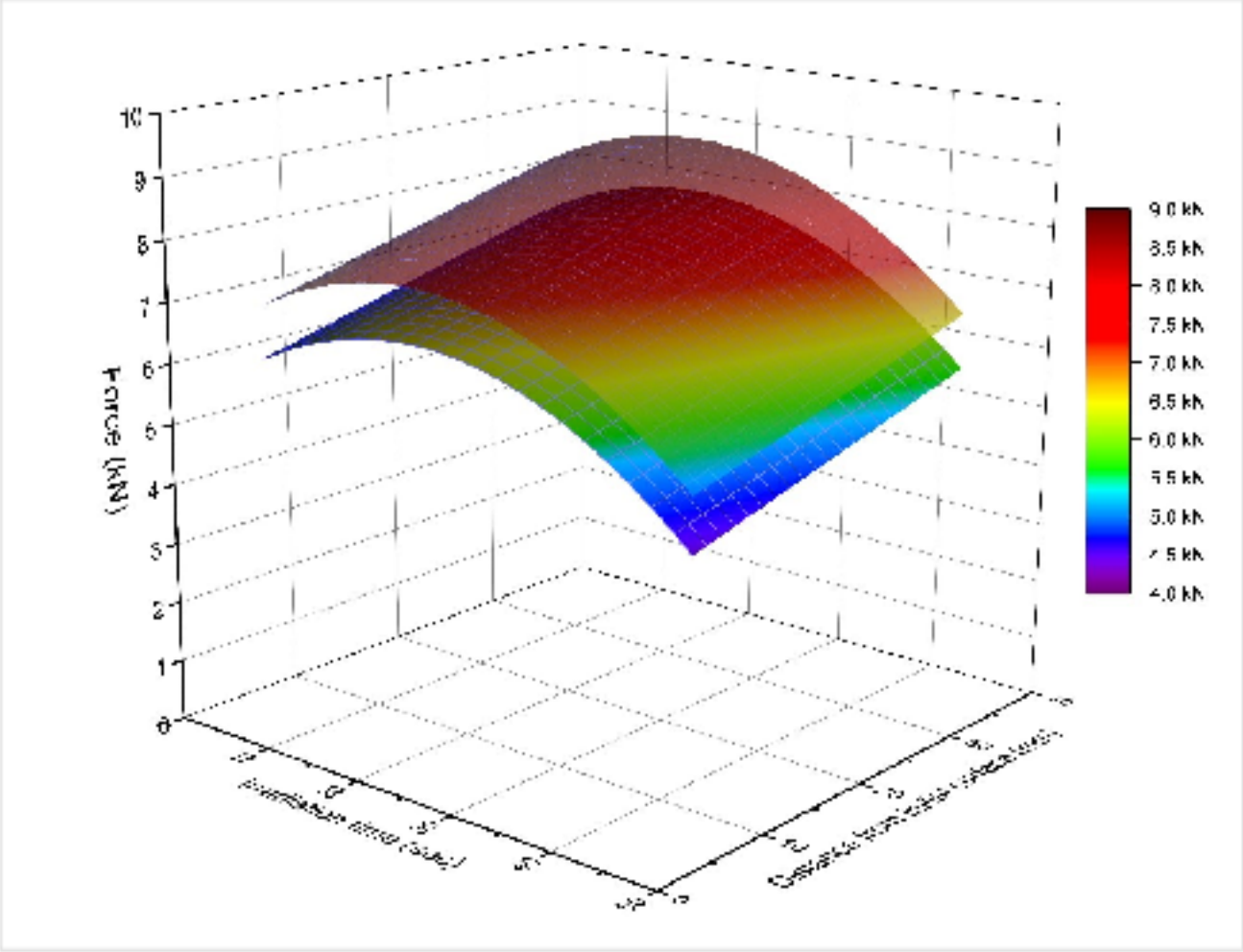

Figure 4.1-1 Response function of mean cutting forces $F_{x_{mean}}$ on irradiation time and distance from initial surface with spacing 8 mm (lower) and 12 mm (upper)

The same procedure was implemented for determination of $F_{x_{max}}$, $F_{y_{mean}}$, $F_{y_{max}}$, $F_{z_{mean}}$ and $F_{z_{max}}$.

The equation of regression model of maximum cutting forces is

$$F_{x_{max}} = 11.573862984 + 0.097032916 \cdot T + 0.494558824 \cdot S + 0.133780488 \cdot D - 0.003142205 \cdot T^2$$

Mean side forces regression model equation is

$$F_{y_{mean}} = 3.344489479 + 0.078016994 \cdot T - 0.059117647 \cdot S + 0.022825203 \cdot D - 0.002132336 \cdot T^2$$

The equation of regression model of the mean normal forces looks like

$$F_{z_{mean}} = 5.307086322 + 0.321586213 \cdot T + 0.595147059 \cdot S + 0.155172764 \cdot D - 0.009474243 \cdot T^2$$

In the same way, the equation of regression model of maximum side forces was determined

$$F_{y_{max}} = 6.602914873 + 0.131420958 \cdot T + 0.136911765 \cdot S + 0.065813008 \cdot D - 0.003580608 \cdot T^2$$

The maximum normal forces equation of regression model is

$$F_{z_{max}} = 11.065932568 + 0.457940041 \cdot T + 1.200882353 \cdot S + 0.298069106 \cdot D - 0.013046364 \cdot T^2$$

The visual interpretation of regression models of $F_{x_{max}}$, $F_{y_{mean}}$, $F_{y_{max}}$, $F_{z_{mean}}$ and $F_{z_{max}}$ are presented in Annex H. In the Annex H also presented comparison of regression models mean and maximum forces with same spacing.

Important fact, that the regression models are applicable only within established boundaries of variable factors.

It can be seen that each equation of regression models has the same polynomials, but with different coefficients. The regression models are square dependent on microwave treatment duration. The linear dependency of regression models on distance from initial surface has been established. In addition, there is linear dependency of regression models on space between cuts, as it is only two spacing have been used.

At the same time, the signs before coefficients are repeating, except the coefficient at S (spacing between cuts) of the regression model of mean side force $F_{y_{mean}}$. This situation has an explanation. It can be explained by the fact that with decreasing of spacing, the

equilibrating side force (directed in opposite direction) decreases. However, it is not repeated in maximum side forces.

4.2 Force Mapping

To illustrate the assistance of microwave treatment in rock breaking, force mapping was implemented. This procedure allows visualizing an acting force in 3D environment.

For creating force maps, the data, collected by DEWE 5000, was used. The procedure includes implementation of moving averaging gridding. This function is used to estimate the value of a surface at a specific grid node. It works as calculation of an average of the known values of the surface at nearby control points. In fact, it projects nearby known values to the grid node location. Afterwards, a complex approximation is made by averaging the values, typically weighting the closest points more heavily than distant points.

The resulted force maps have the X and Y coordinates from the data as an X-axis and Y-axis respectively. Z-axis is presented by forces F_x, F_y, F_z and F_{Total} for second layer and averaged 2-4 layers for each block. The force mapping of average cutting force F_x can be seen in Figure 4.2-1, all other maps of forces is presented in Annex I.

On the Figure 4.2-1 (and all other maps of forces), with red dots are presented the places of irradiation with microwaves. The irradiation is presented in a checkerboard pattern with space between dots equals 100 mm.

As a dotted line is visualized the boundary between 8 mm and 12 mm spacing. On graphs, forces with spacing 8 mm lie in upper part of a graph respectively to boundary.

The color scale is mutual for set of maps.

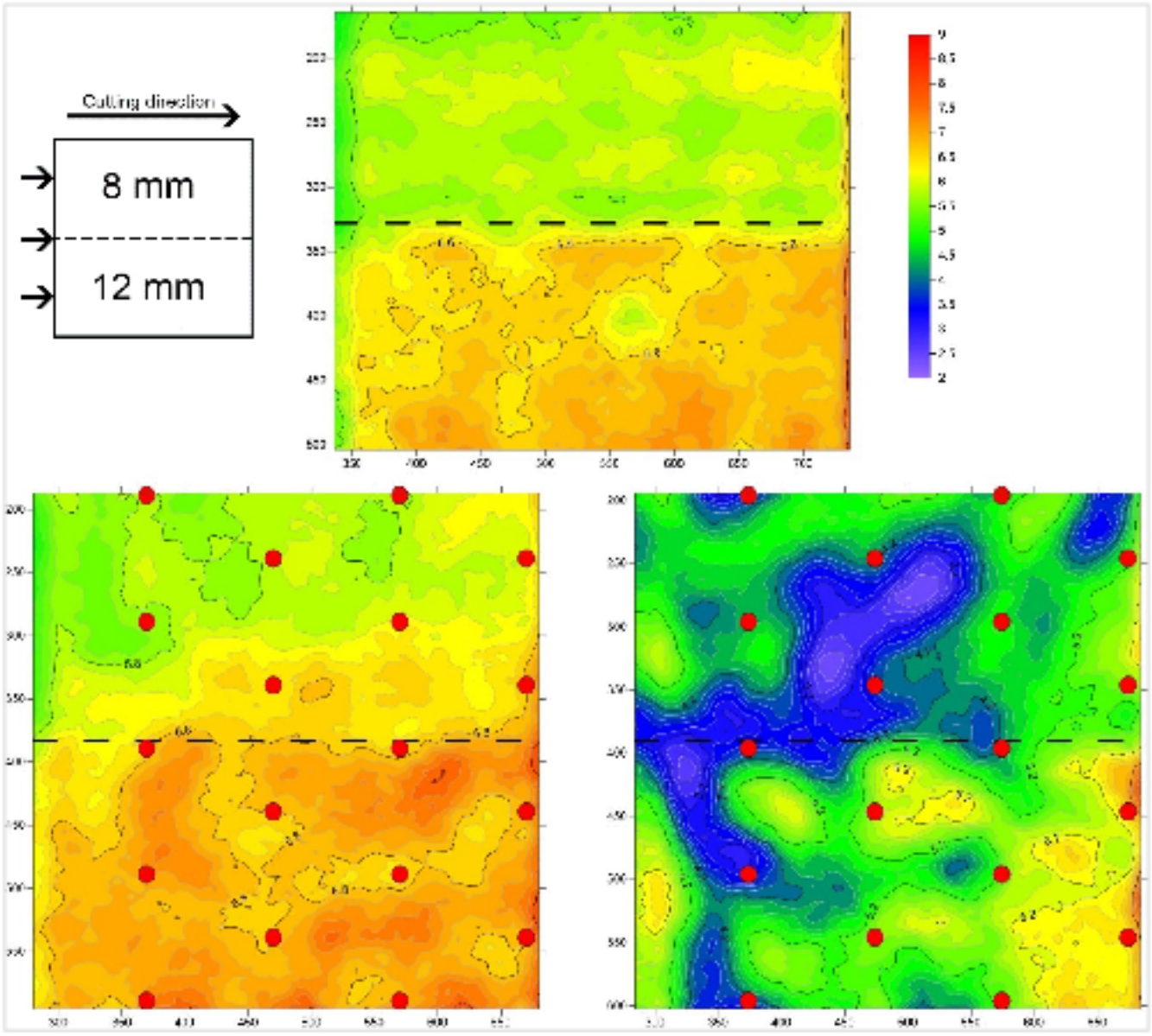

Figure 4.2-1 Set of force mapping of average cutting force $\boldsymbol{F_x}$ of three layers (2- 4) for untreated sample (upper), 30 seconds irradiated sample (lower left) and 45 seconds irradiated sample (lower right)

It can be seen that for all maps of forces the 8 mm spacing shows lower loads and peaks that 12 mm. However, in force mapping of side forcesF_y, it is opposite (Figure Annex I-1, Figure Annex I-5). This fact is supporting the assumption made in Chapter 4.1, that decreasing of spacing in experimented range can increase side forces, generated during cutting.

All sets of force mapping have consistent pattern, such as the lowest loads are presented in 45 seconds irradiated sample and the highest loads in 30 seconds irradiated sample.

CONCLUSION

The thesis that describes researches made with high power microwave irradiation as a promising solution in hard rock excavation. The solution consists of using microwave energy for reducing cutting resistance of granite. Additionally, the study shows dependencies of forces, wearing, energy consumption and particle size distribution on spacing between cuts, time of irradiation with microwaves and distance from the initial surface.

Minerals of the granite have different dielectric properties. It leads to heating of some parts of the specimen, which causes its cracking. This fact has positive effects in cutting force reduction. In the study, the cutting force has been reduced by 22 % after 45 seconds microwave irradiation. This means, that specific energy consumption was also reduced; analysis shows reduction by 20-40 % (for different cutting conditions) for 45 seconds treated sample. However, 30 seconds exposure time did not show any positive effect on forces and specific energy consumption. The difference in wear rate with respect to microwave irradiation is not clearly visible. The dependency between particle size distribution and microwave irradiation is noticeable only for 45 seconds exposure time, the analysis shows the smaller volume of fine particles.

The study included analysis of two positions of spacing between cuts, such as 8 mm and 12 mm. The analysis shows that with spacing 8 mm cutting forces smaller for around 13 % and wearing of the tool is slower. However, increasing of spacing to 12 mm positively effects on specific energy consumption and particle distribution. The results show reduction in specific energy consumption by 20 % and the material is less overgrinded for spacing 12 mm.

Regression models describing dependences of mean and peak cutting forces on irradiation time, distance from the initial top surface of the sample and spacing were obtained. Force maps characterizing force distribution within the cut face were created.

In total, microwave energy assistance for cutting of granite has shown good results in case of its treatment during 45 seconds. The further investigations to be carried out are suggested.

Future work

According to this work, the future research could be recommended for increasing of knowledge in the field of microwave assisted mechanical excavation:

1. Determination of optimum microwave irradiation duration and power.
2. Crack propagation analysis and their influence on the forces.
3. Separately determine the wear and microwave irradiation influences on cutting forces.
4. Determination of the optimum distance between spots.
5. Further investigations on the depth of influence of the microwave irradiation.

BIBLIOGRAPHY

[1] J. Osepchuk, "A History of Microwave Heating Applications," *IEEE Transactions on Microwave Theory and Techniques,* vol. 32, no. 9, pp. 1200-1224, 1984.

[2] W. Maurer, Novel Drilling Techniques, London: Pergamon Press, 1968.

[3] P. Darling, SME Mining Engineering Handbook, Third Edition, SME, 2011.

[4] Z. Kenessey, "The Primary, Secondary, Tertiary and Quaternary Sectors of the EconomyA," *Review of Income and Wealth,* vol. 33, no. 4, pp. 359-385, 1987.

[5] C. Reichl, M. Schatz and G. Zsak, "World Mining Data," Federal Ministry of Science, Research and Economy, Vienna, 2016.

[6] H. Kargl, "Technical Development of Hard Rock Cutting," Montanuniversität Leoben, Leoben, 2016.

[7] J. Hudson and J. Harrison, Engineering Rock Mechanics: An Introduction to the Principles, London: Elsevier, 2000.

[8] N. Bilgin, H. Copur and C. Balci, Mechanical Excavation in Mining and Civil Industries, Boca Raton: CRC Press, 2013.

[9] H. Käsling and K. Thuro, "Determining Abrasivity of Rock and Soil in the Laboratory," in *Geologically Active – Williams et al. (eds)*, London, Taylor & Francis Group, 2010, pp. 1973-1980.

[10] RWTH Aachen University - Institute of Mining Engineering, "Hard rock analysis: Abrasivity determination using Cerchar Abrasivity Index (CAI)," [Online]. Available: http://mre.rwth-aachen.de/en/wp-content/uploads/sites/3/2016/08/Abrasivity-determination-Cerchar-Abrasivity-Index.pdf. [Accessed 1 December 2016].

[11] R. Fowell, O. Hekimoglu and S. Altinoluk, "Drag Tools Employed on Shearer Drums and Roadheaders," 20 May 2016. [Online]. Available: https://www.researchgate.net/publication/265191783_DRAG_TOOLS_EMPLOYED_ON_SHEARER_DRUMS_AND_ROADHEADERS. [Accessed 5 December 2016].

[12] H. Speight, "Observations on Drag Tool Excavation and the Consequent Performance of Roadheaders in Strong Rock," *The AusIMM Proceedings,* no. 1, pp. 17-32, 1997.

[13] B. Grafe, "Potential des Hinterschneidens mit Rundschaftmeißeln zur Steigerung der Schneideffizienz," TU-Freiberg, Freiberg, 2014.

[14] R. Goktan and N. Gunes, "A Semi-Empirical Approach to Cutting Force Prediction for Point-Attack Picks," *The Journal of The South African Institute of Mining and Metallurgy,* no. 105, pp. 257-264, 2005.

[15] M. Günay, E. Aslan, I. Korkut and U. Seker, "Investigation of the Effect of Rake Angle on Main Cutting Force," *International Journal of Machine Tools & Manufacture,* pp. 953-959, 15 January 2004.

[16] S. Singh, T. Alam and S. Chattopadhyaya, "A Review on the Excavator Tool Bits Wear," *National Conference on Machines and Mechanisms,* vol. 16, pp. 823-829, 2013.

[17] D. Kramer, "Explosives," *USGS Mineral Resources Program,* pp. 1-4.

[18] "A Global Strategic Business Report," Global Industry Analysts, 14 Januany 2015. [Online]. Available: http://www.strategyr.com/pressMCP-2749.asp. [Accessed 08 December 2016].

[19] M. Phifer and P. Hem, "Blasting," 17 November 2016. [Online]. Available: http://technology.infomine.com/reviews/Blasting/welcome.asp?view=full. [Accessed 5 December 2016].

[20] Sandvik Tamrock Corp., "Rock Excavation Handbook," [Online]. Available: http://www.metal.ntua.gr/uploads/3290/254/Excavation_Engineering_Handbook_Tamrock.pdf. [Accessed 22 November 2016].

[21] D. Jasiulek and K. Stankiewicz, "An Adaptive Control System of Roadheader with Intelligent Modelling of Mechanical Features of Mined Rock," *Journal of KONES Powertrain and Transport,* vol. 18, no. 2, pp. 197-203, 2011.

[22] A. Ramezanzadeh and M. Hood, "A State-of-the-Art Review of Mechanical Rock Excavation Technologies," *International Journal of Mining & Environmental Issues,* vol. 1, no. 1, 2010.

[23] Wirth Group, "Reaming Tunnel Boring Machine, Undercutting Technique," Wirth Group, 2003.

[24] Voest-Alpine Bergtechnik GmbH, "Alpine Reef Miner ARM 1100," [Online]. Available: http://www.miningandconstruction.sandvik.com/sandvik/9082/Internet/S002630.nsf/Alldocs/Products*5CContinuous*2Dmining*and*tunneling*machines*5CContinuous*reef*miners*2AAlpine*Reef*Miner*ARM*1100/$FILE/ARM_1100.pdf. [Accessed 23 November 2016].

[25] U. Restner and B. Reumueller, "'Metro Montreal" – Successful Operation of a State-of-the-Art Roadheader," EUROCK 2004 & 53rd Geomechanics Colloquium, Salzburg, 2004.

[26] S. Redmond and V. Romero, Rapid Excavation and Tunneling Conference Proceedings, Englewood: Society for Mining, Metallurgy, and Exploration, 2011.

[27] K. Gehring and B. Reumiiller, "Hard Rock Cutting with Roadheaders the ICUTROC Approach," Tunnelling Association of Canada, Richmond, 2003.

[28] L. Songyong, L. Xiaohui, C. Junfeng and L. Mingxing, "Rock Breaking Performance of a Pick Assisted by High-pressure Water Jet under Different Configuration Modes," *Chinese Journal of Mechanical Engineering,* vol. 28, no. 3, pp. 607-617, 2015.

[29] V. Mahto and H. Siddique, "Application of High Power Laser in Oil and Gas Well Drilling: An Overview," National conference on Advances in Lasers and Spectroscopy, Dhanbad, 2012.

[30] M. Lovás, I. Znamenáčková, A. Zubrik, M. Kováčová and S. Dolinská, "The Application of Microwave Energy in Mineral Processing – a Review," *Acta Montanistica Slovaca,* vol. 16, no. 2, pp. 137-148, 2011.

[31] S. Parker, McGraw-Hill Concise Encyclopedia of Physics, 2nd Edition, New York: McGraw-Hill Inc., 1993.

[32] D. Pozar, Microwave Engineering, 4th Edition, New York: John Wiley & Sons, 2012.

[33] F. Hassani, P. Nekoovaght and N. Gharib, "The Influence of Microwave Irradiation on Rocks for Microwave-assisted Underground Excavation," *Journal of Rock Mechanics and Geotechnical Engineering,* vol. 8, no. 1, pp. 1-15, 2016.

[34] T. Chen, J. Dutrizac, K. Haque, W. Wyslouzil and S. Kashyap, "The Relative Transparency of Minerals to Microwave Radiation," *Canadian Metallurgical Quarterly,* vol. 3, no. 23, pp. 349-351, 1984.

[35] J. Walkiewicz, A. Clark and S. McGill, "Microwave-Assisted Grinding," *IEEE Transactions on Industry Applications,* vol. 27, no. 2, pp. 239-243, 1991.

[36] L. Chen, C. Ong, C. Neo, V. Varadan and V. Varadan, Microwave Electronics: Measurement and Materials Characterization, London: John Wiley & Sons, 2004.

[37] R. Meisels, M. Toifl, P. Hartlieb, F. Kuchar and T. Antretter, "Microwave Propagation and Absorption and Its Thermo-mechanical Consequences in Heterogeneous Rocks," *International Journal of Mineral Processing,* vol. 135, pp. 40-51, 2015.

[38] W. Telford, L. Geldart and R. Sheriff, Applied Geophysics, 2nd Edition, Cambridge: Cambridge University Press, 2012.

[39] J. Schön, Physical Properties of Rocks : Fundamentals and Principles of Petrophysics, Amsterdam: Elsevier, 20015.

[40] J. Santamarina, "Rock Excavation with Microwaves: A Literature Review," *Foundation Engineering: Current Principles and Practices,* vol. 1, pp. 459-473, 1989.

[41] S. Kingman and N. Rowson, "Microwave Treatment of Minerals - A Review," *Minerals Engineering,* vol. 11, no. 11, pp. 1081-1087, 1998.

[42] S. Kingman, G. Corfield and N. Rowson, "Effects of Microwave Radiation Upon the Mineralogy and Magnetic Processing of a Massive Norwegian Ilmenite Ore," *Magnetic and Electrical Separation,* vol. 3, no. 9, pp. 141-148, 1999.

[43] D. Whittles, S. Kingman and D. Reddish, "Application of Numerical Modelling for Prediction of the Influence of Power Density on Microwave-Assisted Breakage," *International Journal of Mineral Processing,* vol. 1, no. 68, pp. 71-91, 2003.

[44] M. Toifl, R. Meisels, P. Hartlieb, F. Kuchar and T. Antretter, "3D Numerical Study on Microwave Induced Stresses in Inhomogeneous Hard Rocks," *Minerals Engineering,* vol. 90, pp. 29-42, 2016.

[45] N. Rjabets, «Fundamentals of Softening and Thawing Permafrost with Microwave Energy (Rus.),» YANC SO RAN, Yakutsk, 1991.

[46] Y. Misnik, «Electrothermomechanical Action Machinery (Rus.),» Kolyma, 1973.

[47] I. Florek and M. Lovás, "The Influence of the Complex Electric Permittivity and Grain Size on Microwave Drying of the Grained Materials," *Fizykochemiczne Problemy Mineralurgii,* vol. 29, pp. 127-133, 1995.

[48] S. Grundas, Advances in Induction and Microwave Heating of Mineral and Organic Materials, InTech, 2011.

[49] K. Haque, "Microwave Irradiation Pretreatment of a Refractory Gold Concentrate," *Symposium on Gold Metallurgy,* pp. 327-339, 1987.

[50] G. Murray, "Microwave to Slash Refractory Gold Costs," *Mining Magazine,* vol. 178, no. 4, pp. 276-278, 1998.

[51] L. Turčániováa, Y. Soongb, M. Lovása, A. Mockovčiakováa, A. Oriňakc, M. Justinovác, I. Znamenáčkováa, M. Bežovskáa and S. Marchantd, "The Effect of Microwave Radiation on the Triboelectrostatic Separation of Coal," *Fuel,* vol. 83, no. 14-15, pp. 2075-2079, 2004.

[52] J. Chen, Z. Zhang, S. Guo, Z. Zhang, J. Peng, C. Srinivasakannan, X. Li, Y. Zhuang and Z. Xu, "Leaching of Refractory Gold Ores by Microwave Irradiation:

Comparison with Conventional Leaching," *Metallurgist,* vol. 57, no. 7, pp. 647-653, 2013.

[53] A. Obraztsov и V. Semenov, «High-Frequency Methods of Destruction Oversize (Rus.),» *Destruction of Oversize by Industrial Frequency Currents,* № 1, pp. 43-44, 1969.

[54] A. Didenko и A. Prokopenko, «Kimberlite Fracture by Prompt Microwave-Heating (Rus),» *Microwave and Telecommunication Technology,* т. 18, pp. 805-806, 2008.

[55] A. Moskalev, «The Process of Destruction of Rocks with Electromagnetic Waves (Rus.),» Dnipro, 1977.

[56] S. Yasar, M. Capik and A. Yilmaz, "Estimation of Cutter Forces in Small Scale Rock Cutting Test by Multivariate Linear Regression," in *8th Asian Rock Mechanics Symposium*, Sapporo, 2014.

[57] H. Sturges, "The Choice of a Class-Interval," *Journal of the American Statistical Association,* no. 21, pp. 65-66, 1926.

[58] GOSSTANDART, Applied Statistics. Validation Rules of Experimental and Theoretical Distribution Agreement (Rus.), Moscow: IPK, 2002.

[59] N. Dneprov, "Tool wear during excavation works (Rus)," 28 August 2012. [Online]. Available: http://www.t-magazine.ru/pages/iznos. [Accessed 1 December 2016].

[60] S. Tobias and F. Koenigsberger, Advances in Machine Tool Design and Research 1967, Manchester: Permagon Press Ltd., 1967.

[61] Occupational Safety and Health Administration, "Occupational Exposure to Respirable Crystalline Silica - Review of Health Effects Literature and Preliminary Quantitative Risk Assessment," Occupational Safety and Health Administration, 2010.

[62] D. Johnson and J. Vincent, "Sampling and Sizing of Airborne Particles," American Industrial Hygiene Association, Fairfax, 2003.

[63] N. Draper and H. Smith, Applied Regression Analysis, New York: John Wiley & Sons, 1998.

[64] I. Eliseeva, Econometrics (Rus.), Moscow: Finance and Statistics, 2005.

[65] ASW-GmbH, Technische Dokumentation zur Sonderhobelmaschine für Gesteinsproben, Naumburg: ASW-GmbH, 2007.

[66] M. Vorona, W. Gaßner and C. Drebenstedt, Scientific Reports on Resource Issues 2010, Freiberg, Germany: Medienzentrum der TU Bergakademie Freiberg, 2010.

[67] B. Schweber, "The Proving Ring: How Innovation Led to a Simple Tool to Verify Weight," 19 May 2015. [Online]. Available: http://insights.globalspec.com/article/987/the-proving-ring-how-innovation-led-to-a-simple-tool-to-verify-weight. [Accessed 06 December 2016].

[68] Retsch GmbH, "The Basic Principles of Sieve Analysis," 2004. [Online]. Available: http://www.ninolab.se/fileadmin/Ninolab/pdf/retsch/documents/af_sieving_basics_2004_en.pdf. [Accessed 20 November 2016].

[69] L. Chebenko, "Determination of the Influence of Microwaves to the Hard Rock Characteristics and to the Cutting Process," TU Bergakademie Freiberg, Freiberg, 2015.

[70] A. Kobzar, Applied Mathematical Statistics (Rus.), Moscow: PHISMATHLIT, 2006.

[71] V. Shashkov, «Applied Regression Analysis (Rus.),» GOU VPO OGU, Orenburg, 2003.

[72] D. Rahmankulov, S. Shavshukova, I. Vykhareva и R. Chanyshev, «Experience of the Use of Microwave Energy in Mining (Rus.),» *Bashkir Chemical Journal,* т. 15, № 2, pp. 114-118, 2008.

[73] P. Hartlieb, "Investigations on the Effects of Microwaves on Hard Rock," Montanuniversität Leoben, Leoben, 2013.

[74] J. Walkiewicz, G. Kazonich and S. McGill, "Microwave Heating Characteristics of Selected Minerals and Compounds," *Minerals and Metallurgical Processing,* vol. 1, no. 5, pp. 39-42, 1988.

[75] E. Wahlstrom, Tunneling in Rock, London: Elsevier, 1973.

LIST OF FIGURES

LIST OF TABLES

LIST OF ABBREVIATIONS

UCS	Uniaxial Compressive Strength;
E	Young's modulus;
F_{fail}	maximum force on the sample before failure $[N]$;
A_{UCS}	cross-sectional area of the sample $[mm^2]$;
BTS	Brazilian Tensile Strength;
d_{BTS}	diameter of the sample $[mm]$;
l_{BTS}	length of the sample $[mm]$;
CAI	Cerchar Abrasivity Index;
d_{wear}	diameter of wear flat $[mm]$;
c_{wear}	unit correction factor;
θ	pick angle;
γ_a	attack angle;
γ_r	rotation angle;
β_c	clearance angle;
β_r	rake angle;
ANFO	Ammonium nitrate and fuel oil;
TBM	Tunnel Boring Machine;
CMM	Continuous Mining Machine;
MTM	Mobile Tunnel Miner;
TBE	Tunnel Boring Extender;
ARM	Alpine Reef Miner;
TBM	Tunnel Boring Machine;
λ	length of the waves $[m]$;
c	speed of light $[m/s]$;
f_{em}	frequency $[Hz]$;
ε_r	relative complex permittivity;
ε	complex permittivity;
ε_0	permittivity of free space;

ε'	real of relative complex permittivity;
ε''	imaginary of relative complex permittivity;
i	complex number;
ε_r'	real part of relative complex permittivity;
ε_r''	imaginary part of relative complex permittivity;
δ_e	the loss angle;
$\tan \delta_e$	loss tangent;
d_p	penetration depth;
F_x	cutting force $[kN]$;
F_z	normal force $[kN]$;
F_y	side force $[kN]$;
F_{Total}	total force $[kN]$;
σ_{maxi}	peaks of a force-time diagram;
σ_μ	a mean of a force-time diagram;
σ_{ai}	amplitudes of stresses;
F_{max}	maximum forces $[kN]$;
α	level of significance;
μ	mean;
σ^2	variance;
N	the number of random variables;
k	amount of intervals;
P_i	probability deriving;
r	number of degrees of freedom;
m_{es}	number of estimated parameters;
S_{χ^2}	the critical value of Pearson's chi-squared;
E_{sp}	specific energy consumption $[kWh/m^3]$;
l_{1c}	length of cut $[m]$;
$\overline{F_x}$	mean cutting force of one cut $[kN]$;
V_{cut}	volume of cut material by $\sum \overline{F_x}$ $[m^3]$;

E_{mic}	energy consumption of microwave irradiation process $[kWh]$;
E_{P_i}	energy, spent for irradiation, per second $[kJ/sec]$;
W	wear rate $[g/m]$;
m_i	mass of a pick before cutting layer $[g]$;
m_{i+1}	mass of a pick after cutting layer $[g]$;
l_{cl}	cut length on a layer $[m]$;
OSHA	Occupational Safety and Health Administration;
S_{res}^2	residual variance;
y_i	calculated value of the parameter by equation;
Y_{gi}	experimental value;
F_{1-p}	F distribution table value;
R	correlation coefficient;
Y_g	mean experimental value;
T	duration of irradiation;
S	spacing between cuts;
D	distance from initial surface.

ANNEX TABLE OF CONTENTS

ANNEX A THE MODEL OF CUTTING TOOL

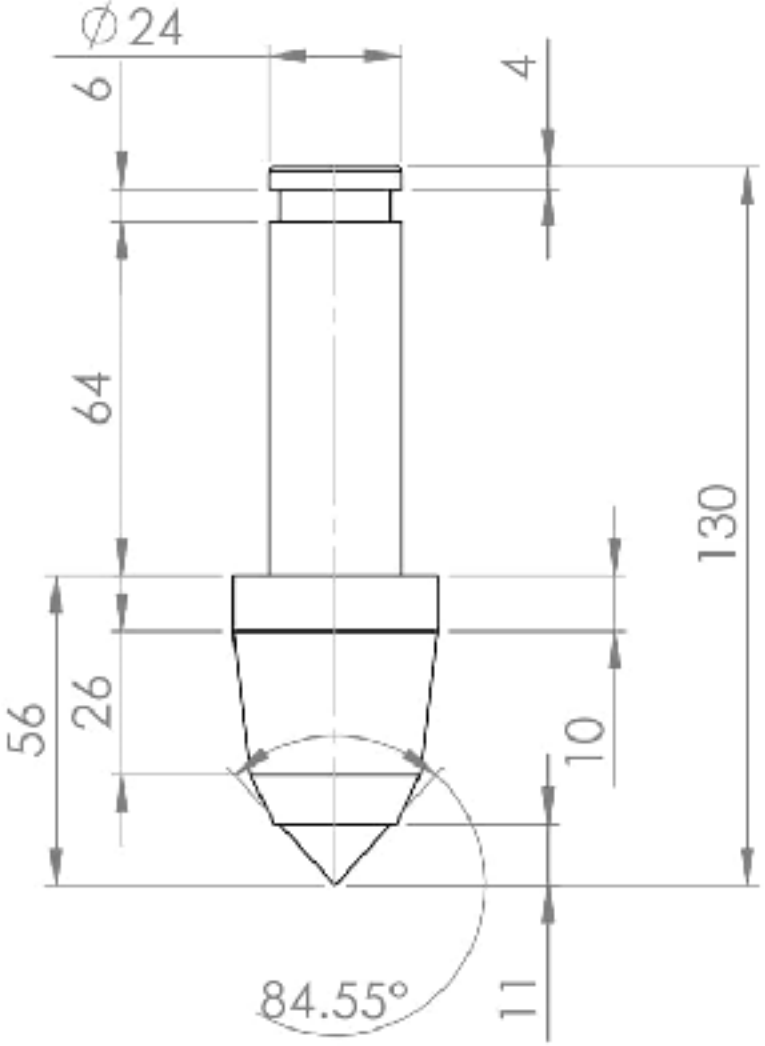

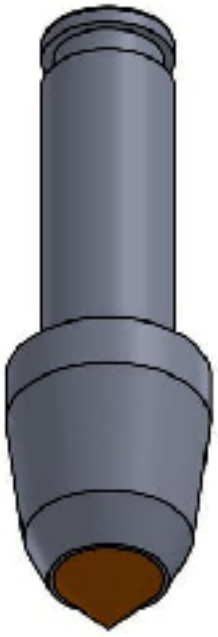

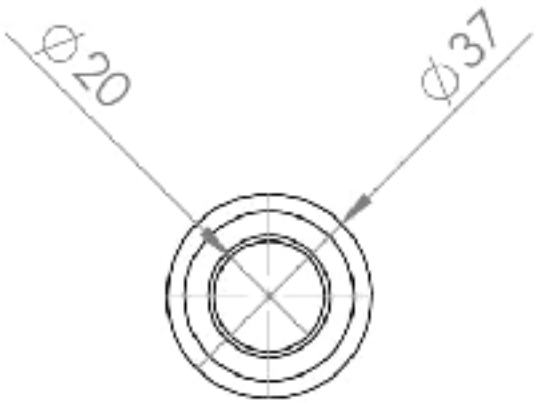

ANNEX B DATA FOR DISTRIBUTION

1	4.72	**51**	6.40	**101**	7.74	**151**	8.79	**201**	9.35
2	4.73	**52**	6.41	**102**	7.76	**152**	8.81	**202**	9.35
3	4.73	**53**	6.42	**103**	7.80	**153**	8.81	**203**	9.36
4	4.74	**54**	6.47	**104**	7.84	**154**	8.84	**204**	9.39
5	4.75	**55**	6.52	**105**	7.89	**155**	8.84	**205**	9.39
6	4.76	**56**	6.57	**106**	7.90	**156**	8.85	**206**	9.40
7	4.78	**57**	6.65	**107**	7.91	**157**	8.86	**207**	9.42
8	4.85	**58**	6.66	**108**	7.93	**158**	8.88	**208**	9.42
9	4.88	**59**	6.68	**109**	8.00	**159**	8.88	**209**	9.47
10	4.93	**60**	6.71	**110**	8.00	**160**	8.89	**210**	9.48
11	4.94	**61**	6.76	**111**	8.07	**161**	8.89	**211**	9.48
12	4.99	**62**	6.76	**112**	8.13	**162**	8.89	**212**	9.49
13	5.02	**63**	6.82	**113**	8.15	**163**	8.93	**213**	9.50
14	5.11	**64**	6.82	**114**	8.15	**164**	8.93	**214**	9.50
15	5.14	**65**	6.88	**115**	8.16	**165**	8.94	**215**	9.51
16	5.15	**66**	6.90	**116**	8.17	**166**	8.94	**216**	9.52
17	5.18	**67**	6.90	**117**	8.19	**167**	8.95	**217**	9.53
18	5.18	**68**	6.92	**118**	8.22	**168**	8.96	**218**	9.53
19	5.21	**69**	6.98	**119**	8.22	**169**	8.96	**219**	9.55
20	5.22	**70**	7.00	**120**	8.23	**170**	8.97	**220**	9.58
21	5.45	**71**	7.01	**121**	8.25	**171**	8.98	**221**	9.60
22	5.48	**72**	7.02	**122**	8.29	**172**	9.00	**222**	9.60
23	5.49	**73**	7.04	**123**	8.29	**173**	9.01	**223**	9.60
24	5.50	**74**	7.05	**124**	8.30	**174**	9.04	**224**	9.61
25	5.53	**75**	7.07	**125**	8.33	**175**	9.06	**225**	9.62
26	5.55	**76**	7.12	**126**	8.35	**176**	9.08	**226**	9.62
27	5.60	**77**	7.17	**127**	8.38	**177**	9.11	**227**	9.63
28	5.63	**78**	7.20	**128**	8.38	**178**	9.11	**228**	9.64
29	5.66	**79**	7.24	**129**	8.39	**179**	9.13	**229**	9.64
30	5.70	**80**	7.28	**130**	8.39	**180**	9.13	**230**	9.65
31	5.75	**81**	7.29	**131**	8.46	**181**	9.14	**231**	9.67
32	5.77	**82**	7.29	**132**	8.50	**182**	9.14	**232**	9.69
33	5.78	**83**	7.31	**133**	8.56	**183**	9.15	**233**	9.72
34	5.79	**84**	7.31	**134**	8.56	**184**	9.15	**234**	9.72
35	5.81	**85**	7.33	**135**	8.57	**185**	9.16	**235**	9.74
36	5.84	**86**	7.35	**136**	8.57	**186**	9.17	**236**	9.76
37	5.87	**87**	7.41	**137**	8.62	**187**	9.19	**237**	9.81
38	5.89	**88**	7.41	**138**	8.66	**188**	9.19	**238**	9.82
39	5.91	**89**	7.43	**139**	8.67	**189**	9.21	**239**	9.84
40	5.95	**90**	7.46	**140**	8.68	**190**	9.22	**240**	9.84
41	5.95	**91**	7.48	**141**	8.73	**191**	9.26	**241**	9.85
42	6.00	**92**	7.53	**142**	8.73	**192**	9.26	**242**	9.88
43	6.02	**93**	7.56	**143**	8.74	**193**	9.28	**243**	9.89
44	6.03	**94**	7.58	**144**	8.75	**194**	9.29	**244**	9.89
45	6.06	**95**	7.59	**145**	8.76	**195**	9.29	**245**	9.92
46	6.10	**96**	7.64	**146**	8.76	**196**	9.30	**246**	9.92
47	6.20	**97**	7.68	**147**	8.77	**197**	9.32	**247**	9.95
48	6.27	**98**	7.73	**148**	8.77	**198**	9.32	**248**	9.96
49	6.33	**99**	7.74	**149**	8.77	**199**	9.33	**249**	9.97
50	6.34	**100**	7.74	**150**	8.77	**200**	9.34	**250**	9.98

251	9.98	**301**	10.70	**351**	11.21	**401**	12.23	**451**	15.85
252	9.99	**302**	10.70	**352**	11.23	**402**	12.28	**452**	16.17
253	10.00	**303**	10.71	**353**	11.23	**403**	12.30		
254	10.00	**304**	10.74	**354**	11.25	**404**	12.31		
255	10.01	**305**	10.75	**355**	11.26	**405**	12.34		
256	10.02	**306**	10.76	**356**	11.27	**406**	12.34		
257	10.02	**307**	10.79	**357**	11.27	**407**	12.38		
258	10.02	**308**	10.80	**358**	11.27	**408**	12.38		
259	10.03	**309**	10.80	**359**	11.29	**409**	12.39		
260	10.05	**310**	10.81	**360**	11.29	**410**	12.39		
261	10.06	**311**	10.81	**361**	11.33	**411**	12.40		
262	10.06	**312**	10.83	**362**	11.36	**412**	12.41		
263	10.07	**313**	10.83	**363**	11.37	**413**	12.42		
264	10.08	**314**	10.83	**364**	11.39	**414**	12.53		
265	10.08	**315**	10.86	**365**	11.40	**415**	12.56		
266	10.11	**316**	10.86	**366**	11.42	**416**	12.63		
267	10.13	**317**	10.87	**367**	11.43	**417**	12.66		
268	10.15	**318**	10.87	**368**	11.44	**418**	12.68		
269	10.15	**319**	10.88	**369**	11.48	**419**	12.69		
270	10.17	**320**	10.89	**370**	11.50	**420**	12.78		
271	10.19	**321**	10.89	**371**	11.52	**421**	12.78		
272	10.20	**322**	10.90	**372**	11.55	**422**	12.78		
273	10.27	**323**	10.91	**373**	11.62	**423**	12.82		
274	10.28	**324**	10.91	**374**	11.62	**424**	12.97		
275	10.28	**325**	10.92	**375**	11.63	**425**	13.03		
276	10.29	**326**	10.94	**376**	11.66	**426**	13.03		
277	10.31	**327**	10.94	**377**	11.68	**427**	13.14		
278	10.33	**328**	10.94	**378**	11.69	**428**	13.17		
279	10.33	**329**	10.95	**379**	11.70	**429**	13.19		
280	10.34	**330**	10.95	**380**	11.70	**430**	13.24		
281	10.34	**331**	10.96	**381**	11.71	**431**	13.28		
282	10.38	**332**	10.98	**382**	11.71	**432**	13.29		
283	10.40	**333**	10.99	**383**	11.72	**433**	13.30		
284	10.40	**334**	11.01	**384**	11.76	**434**	13.30		
285	10.41	**335**	11.01	**385**	11.79	**435**	13.32		
286	10.47	**336**	11.01	**386**	11.79	**436**	13.38		
287	10.48	**337**	11.04	**387**	11.83	**437**	13.44		
288	10.49	**338**	11.07	**388**	11.84	**438**	13.58		
289	10.50	**339**	11.09	**389**	11.85	**439**	13.63		
290	10.51	**340**	11.09	**390**	11.88	**440**	13.68		
291	10.51	**341**	11.12	**391**	11.88	**441**	13.81		
292	10.52	**342**	11.12	**392**	11.94	**442**	13.92		
293	10.54	**343**	11.13	**393**	11.97	**443**	13.93		
294	10.56	**344**	11.14	**394**	11.97	**444**	13.99		
295	10.58	**345**	11.16	**395**	11.99	**445**	14.22		
296	10.58	**346**	11.17	**396**	12.07	**446**	14.55		
297	10.59	**347**	11.18	**397**	12.12	**447**	14.84		
298	10.64	**348**	11.20	**398**	12.12	**448**	14.93		
299	10.67	**349**	11.20	**399**	12.13	**449**	15.10		
300	10.69	**350**	11.21	**400**	12.20	**450**	15.59		

ANNEX C INITIAL DATA FOR REGRESSION MODELS

Number of experiment	Duration of microwave treatment	Space between cuts	Distance from initial surface	Mean cutting force	Mean side force	Mean normal force	Maximum cutting force	Maximum side force	Maximum normal force
1	0	8	8	6.04	3.25	12.32	16.96	8.66	25.35
2	0	12	8	6.26	3.04	12.84	17.82	8.66	26.09
3	0	8	12	5.83	3.22	11.79	17.08	8.93	24.92
4	0	12	12	6.76	2.23	15.01	19.00	8.08	29.79
5	0	8	16	5.93	3.25	12.43	17.36	8.98	24.32
6	0	12	16	7.30	3.57	15.43	20.23	9.46	29.63
7	0	8	20	6.21	3.19	12.82	18.19	9.04	27.09
8	0	12	20	7.27	2.92	15.99	21.61	9.29	32.01
9	0	8	24	6.58	3.41	13.50	19.08	9.40	28.59
10	0	12	24	7.44	2.60	16.59	20.71	8.79	32.47
11	0	8	28	6.87	3.61	14.46	19.18	10.06	29.93
12	0	12	28	7.20	3.68	15.44	19.91	10.53	31.09
13	30	8	8	5.85	3.42	11.94	16.49	8.61	23.78
14	30	12	8	6.58	2.97	13.59	18.01	9.12	28.16
15	30	8	12	6.01	3.39	12.26	17.05	8.79	24.82
16	30	12	12	6.96	3.35	14.73	18.87	10.00	30.21
17	30	8	16	6.46	3.76	14.00	17.86	9.45	27.91
18	30	12	16	7.56	3.51	16.72	19.94	10.67	34.17
19	30	8	20	6.63	3.73	14.15	18.23	9.53	28.20
20	30	12	20	7.71	3.47	17.17	20.51	10.63	35.03
21	30	8	24	6.88	3.89	15.09	18.96	9.77	29.69
22	30	12	24	8.30	4.00	18.75	22.03	11.39	37.30
23	30	8	28	7.27	4.37	16.61	19.98	10.68	32.11
24	30	12	28	8.23	3.82	19.10	22.14	11.32	38.19
25	30	8	32	7.31	4.09	16.40	20.12	10.40	32.10
26	30	12	32	7.74	3.41	17.62	21.06	10.60	35.80
27	30	8	36	7.18	3.98	15.93	19.83	10.24	31.56
28	30	12	36	8.06	3.67	18.63	21.65	11.04	37.03
29	45	8	8	4.29	2.19	7.01	14.63	7.07	17.20
30	45	12	8	5.22	1.99	9.07	16.24	7.13	21.99
31	45	8	12	4.51	2.22	7.50	14.63	6.70	17.83
32	45	12	12	5.55	2.53	9.62	17.21	8.23	22.89
33	45	8	16	4.44	2.10	7.43	15.87	7.37	19.96
34	45	12	16	5.53	2.29	9.81	18.19	8.05	25.17

ANNEX D WEARING DATA

Measuring [g]

	45sec		30sec		0sec		0sec (additional)	
	8 mm	12 mm	8 mm	12 mm	8 mm	12 mm	8 mm	12 mm
Initial	609.703	609.494	611.887	612.325	614.986	614.749	596.073	612.986
	609.698	609.495	611.875	612.325	614.989	614.753	596.072	612.982
	609.701	609.490	611.881	612.320	614.990	614.743	596.075	612.987
	609.701	**609.493**	**611.881**	**612.323**	**614.988**	**614.748**	**596.073**	**612.985**
Layer 1	609.427	609.214	611.571	612.177	614.788	614.608	595.926	612.730
	609.424	609.215	611.569	612.174	614.780	614.604	595.923	612.728
	609.426	609.210	611.569	612.175	614.786	614.607	595.925	612.732
	609.426	**609.213**	**611.570**	**612.175**	**614.785**	**614.606**	**595.925**	**612.730**
Layer 2	609.309	609.071	611.387	612.008	614.632	614.481	595.774	612.613
	609.307	609.064	611.380	612.002	614.627	614.474	595.777	612.601
	609.298	609.064	611.386	612.006	614.634	614.480	595.776	612.614
	609.305	**609.066**	**611.384**	**612.005**	**614.631**	**614.478**	**595.776**	**612.609**
Layer 3	609.169	608.938	611.236	611.871	614.499	614.374	595.647	612.515
	609.174	608.938	611.229	611.861	614.496	614.378	595.646	612.513
	609.169	608.943	611.235	611.868	614.500	614.373	595.648	612.515
	609.171	**608.940**	**611.233**	**611.867**	**614.498**	**614.375**	**595.647**	**612.514**
Layer 4	609.052	608.827	611.073	611.663	614.383	614.187	595.533	612.429
	609.047	608.825	611.069	611.661	614.377	614.191	595.531	612.429
	609.050	608.829	611.074	611.665	614.381	614.188	595.535	612.432
	609.050	**608.827**	**611.072**	**611.663**	**614.380**	**614.189**	**595.533**	**612.430**
Layer 5			610.932	611.339			595.432	612.366
			610.934	611.333			595.429	612.363
			610.931	611.337			595.433	612.367
	0.000	**0.000**	**610.932**	**611.336**	**0.000**	**0.000**	**595.431**	**612.365**
Layer 6			610.756	611.222			595.325	612.298
			610.753	611.225			595.323	612.299
			610.758	611.227			595.324	612.297
	0.000	**0.000**	**610.756**	**611.225**	**0.000**	**0.000**	**595.324**	**612.298**
Layer 7			610.583	610.927			595.230	612.227
			610.576	610.922			595.229	612.229
			610.579	610.927			595.232	612.226
	0.000	**0.000**	**610.579**	**610.925**	**0.000**	**0.000**	**595.230**	**612.227**
Layer 8			610.450	610.834				
			610.444	610.827				
			610.450	610.833				
	0.000	**0.000**	**610.448**	**610.831**	**0.000**	**0.000**	**0.000**	**0.000**
Layer 9			610.316	610.759				
			610.309	610.752				
			610.317	610.758				
	0.000	**0.000**	**610.314**	**610.756**	**0.000**	**0.000**	**0.000**	**0.000**

Wear rate [g/m]

Layer	45sec		30sec		0sec		0sec (additional)	
	8 mm	12 mm	8 mm	12 mm	8 mm	12 mm	8 mm	12 mm
1	0.27	0.28	0.31	0.15	0.20	0.14	0.15	0.25
2	0.12	0.15	0.19	0.17	0.15	0.13	0.15	0.12
3	0.13	0.13	0.15	0.14	0.13	0.10	0.13	0.09
4	0.12	0.11	0.16	0.20	0.12	0.19	0.11	0.08
5			0.14	0.33			0.10	0.06
6			0.18	0.11			0.11	0.07
7			0.18	0.30			0.09	0.07
8			0.13	0.09				
9			0.13	0.08				

Cut distance [m]

Layer	45sec		30sec		0sec		0sec (additional)	
	8 mm	12 mm	8 mm	12 mm	8 mm	12 mm	8 mm	12 mm
1	12.04	8.17	12.04	8.17	8.61	5.74	10.32	6.88
2	11.61	7.74	11.61	7.74	8.2	5.33	9.89	6.45
3	11.18	7.31	11.18	7.31	7.79	4.92	9.46	6.02
4	10.75	6.88	11.61	7.74	7.38	4.51	9.03	5.59
5			11.18	7.31			8.6	5.16
6			10.75	6.88			8.17	4.73
7			12.47	7.74			7.31	4.3
8			11.61	7.31				
9			11.18	6.88				
Total	**45.58**	**30.1**	**103.63**	**67.08**	**31.98**	**20.5**	**62.78**	**39.13**

ANNEX E SIEVING ANALYSIS DATA

Non-irradiated (additional) block

Sieve class [mm]			8 mm		12 mm	
			Fraction [%]	Cumulative frequency [%]	Fraction [%]	Cumulative frequency [%]
	<	**0.063**	7.51	7.51	6.24	6.24
0.063	–	**0.125**	7.95	15.46	6.13	12.37
0.125	–	**0.25**	10.17	25.63	8.06	20.43
0.25	–	**0.5**	12.51	38.14	10.10	30.54
0.5	–	**1**	12.72	50.86	10.33	40.86
1	–	**2**	11.33	62.19	8.94	49.80
2	–	**4**	16.12	78.31	11.61	61.41
4	–	**8**	18.84	97.15	28.85	90.25
8	–	**10**	2.30	99.45	9.00	99.25
10	–	**12.5**	0.41	99.86	0.51	99.76
12.5	–	**16**	0.38	100.00	0.46	100.00
16	<		0.00	100.00	0.00	100.00

Non-irradiated block

Sieve class [mm]			8 mm		12 mm	
			Fraction [%]	Cumulative frequency [%]	Fraction [%]	Cumulative frequency [%]
	<	**0.063**	7.78	7.78	6.34	6.34
0.063	–	**0.125**	6.68	14.46	5.32	11.66
0.125	–	**0.25**	9.48	23.94	7.52	19.18
0.25	–	**0.5**	11.59	35.53	9.41	28.59
0.5	–	**1**	11.54	47.06	9.69	38.28
1	–	**2**	10.41	57.47	8.75	47.03
2	–	**4**	15.63	73.10	11.04	58.06
4	–	**8**	22.87	95.97	28.65	86.71
8	–	**10**	2.84	98.81	10.86	97.57
10	–	**12.5**	0.85	99.66	1.76	99.33
12.5	–	**16**	0.34	100.00	0.67	100.00
16	<		0.00	100.00	0.00	100.00

30 seconds irradiated block

Sieve class [mm]			8 mm		12 mm	
			Fraction [%]	Cumulative frequency [%]	Fraction [%]	Cumulative frequency [%]
	<	**0.063**	7.85	7.85	7.01	7.01
0.063	–	**0.125**	8.31	16.16	6.63	13.63
0.125	–	**0.25**	10.79	26.95	9.26	22.89
0.25	–	**0.5**	13.22	40.16	11.27	34.17
0.5	–	**1**	13.11	53.28	11.32	45.48
1	–	**2**	11.29	64.56	9.98	55.46
2	–	**4**	15.61	80.17	13.35	68.80
4	–	**8**	16.77	96.94	25.18	93.99
8	–	**10**	2.15	99.09	5.13	99.11
10	–	**12.5**	0.37	99.46	0.55	99.66
12.5	–	**16**	0.22	99.69	0.12	99.78
16	<		0.35	100.00	0.30	100.00

45 seconds irradiated block

Sieve class [mm]			8 mm		12 mm	
			Fraction [%]	Cumulative frequency [%]	Fraction [%]	Cumulative frequency [%]
	<	**0.063**	7.02	7.02	5.72	5.72
0.063	–	**0.125**	5.84	12.86	5.06	10.78
0.125	–	**0.25**	8.66	21.51	7.46	18.24
0.25	–	**0.5**	10.92	32.43	9.32	27.56
0.5	–	**1**	11.41	43.84	9.78	37.34
1	–	**2**	11.38	55.22	9.84	47.18
2	–	**4**	15.54	70.76	14.30	61.48
4	–	**8**	18.82	89.58	27.55	89.03
8	–	**10**	3.33	92.91	6.99	96.02
10	–	**12.5**	3.30	96.21	2.00	98.02
12.5	–	**16**	2.50	98.71	0.71	98.73
16	<		1.31	100.00	1.34	100.00

ANNEX F GRANITE SAMPLE PROPERTIES

Baustoffprüfstelle Wismar GmbH

Anerkannt als Prüf-, Überwachungs- und Zertifizierungsstelle

Lübsche Straße 103, 23966 Wismar; Tel.(ISDN): 03841/75 23 06, 7 56 48; Fax: 03841/75 30 78

Kurzfassung zum Prüfbericht-Nr : 2949/03 vom 05.03.2004

Auftraggeber:	Poechacher Naturstein-Werk GmbH & Co. KG Poechacherstraße 7, A - 4222 St. Georgen an der Gusen
Auftragsgegenstand:	Prüfung von Natursteln
Handelsbezeichnung:	Nauhauser Granit
Herkunft/Abbauort:	Nauhaus-Plöking, A-4119 St. Martin im Mühlkreis

Kennwerte	Prüf-bzw. Produktnorm	Prüfergebnis
Wasseraufnahme[1]	DIN EN 13755:2002-07	0,2 M.-%
Rohdichte[1]	DIN EN 1936:1999-07	2670 kg/m³
Biegefestigkeit[1]	DIN EN 12372:1998-08	18,1 MPa
Druckfestigkeit[1]	DIN EN 1926:1999-05	202,7 MPa
Frostwiderstand einschl. Überprüfung der Leistungsmerkmale Druck- und Biegefestigkeit[1]	DIN EN 12371:2002-01, DIN EN 12372:1998-08, DIN EN 1926:1999-05, DIN EN 1341:2002-04, DIN EN 1343:2002-04	F 1 (beständig)
Abriebwiderstand[1]	DIN EN 1341:2002-04 DIN EN 1342:2002-04	14,5 mm
Verschleißprüfung[1]	DIN 52108:2002-07	6,7 cm³/50cm²
Frost-Tausalz-Beständigkeit[1]	ÖNORM B 3200:2005-12, ÖNORM B 3200:2002-06	beständig
Petrographische Prüfung	DIN EN 12407:2000-09	Granodiorit

Kurzfassung zum Prüfbericht-Nr : 1597/10[2] vom 22.02.2011

Kennwerte	Prüf-bzw. Produktnorm	Prüfergebnis
Wasseraufnahme[1]	DIN EN 13755:2008-06	0,2 M.-%
Offene Porosität[1]	DIN EN 1936:2007-02	0,5 %
Rohdichte[1]	DIN EN 1936:2007-02	2650 kg/m³
Biegefestigkeit[1]	DIN EN 12372:2007-02	17,7 MPa
Druckfestigkeit[1]	DIN EN 1926:2007-03	196 MPa
Frost-Tausalz-Beständigkeit[1]	TL Pflaster-StB 06, DIN EN 1367-6:2008-08 (Entwurf)	beständig
Frost-Tausalz-Beständigkeit[1]	RVS 08.18.01 ÖNORM EN 1367-6:2008-12	beständig

[1] Mittelwert gemäß Prüfvorschrift

[2] Wiederholungsprüfungen im Rahmen der werkseigenen Produktionskontrolle

Weitere Prüfergebnisse siehe Prüfbericht-Nr. 2949/03 und 1597/10

Wismar, den 22.02.2011

Dipl.-Ing. [illegible]
Leiterin der Prüfstelle

BAUSTOFFPRÜFSTELLE Wismar GmbH

ANNEX G CALIBRATION

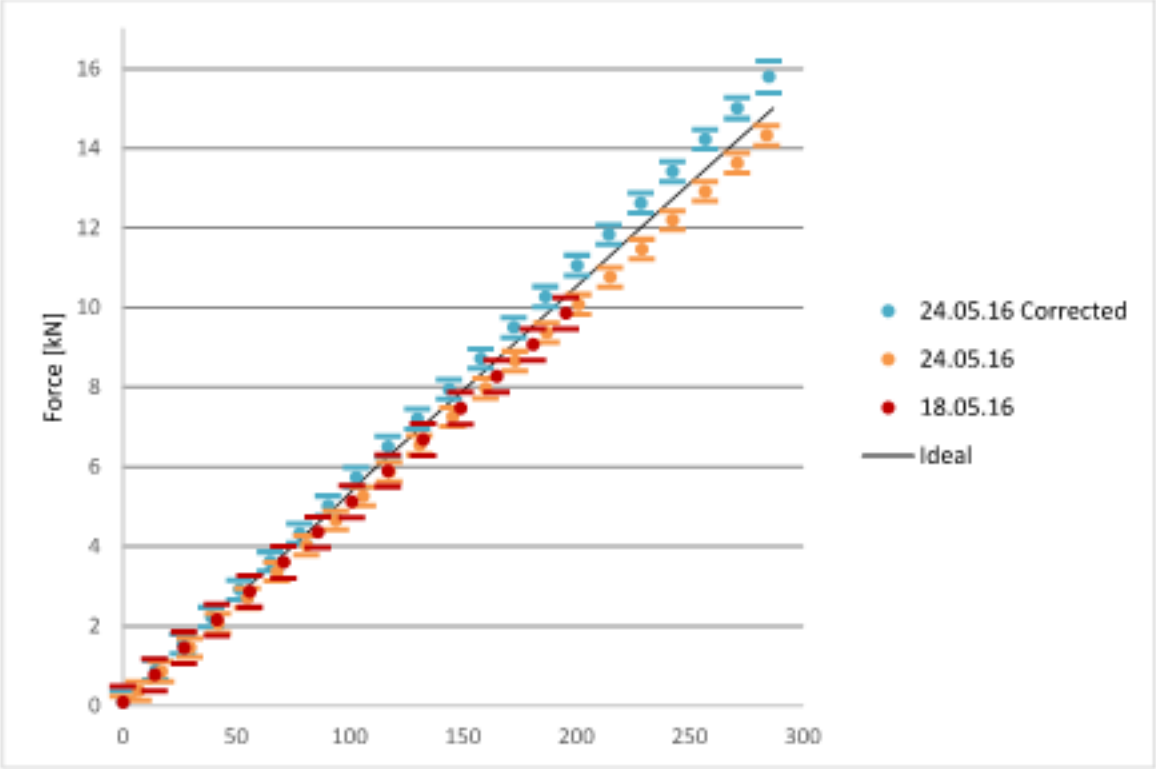

Figure Annex G-1 Results of calibration for axis X

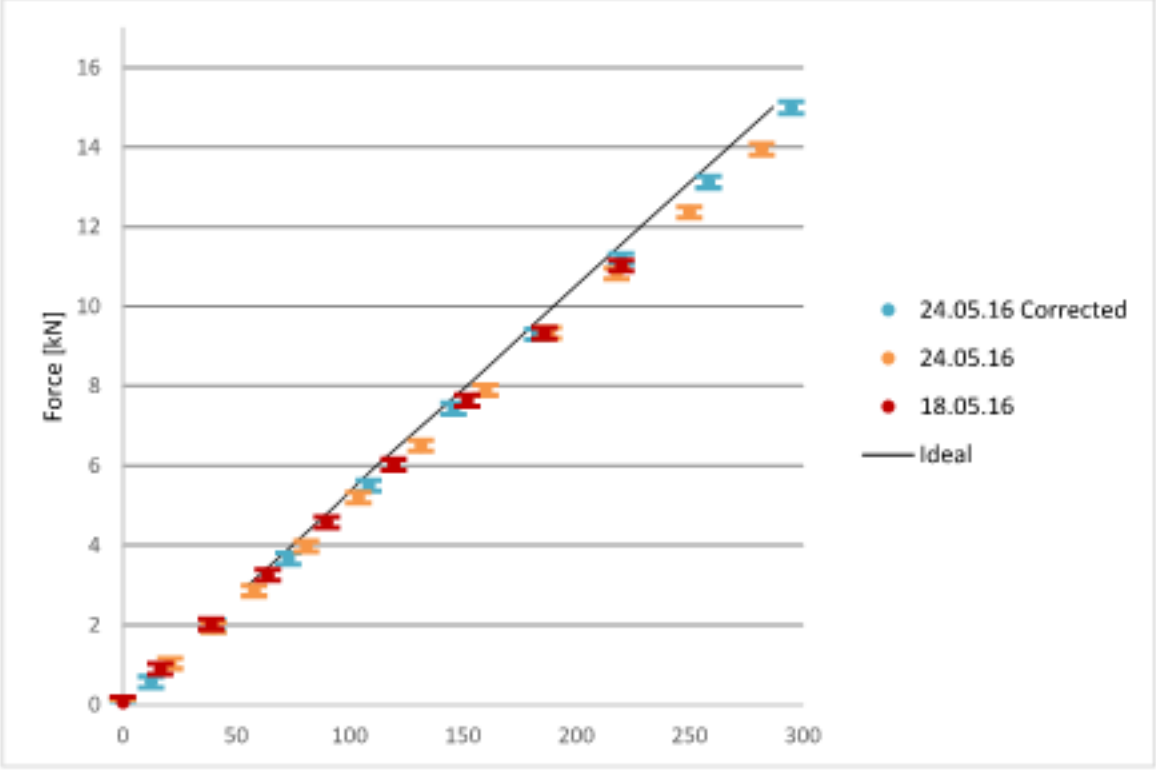

Figure Annex G-2 Results of calibration for axis Y

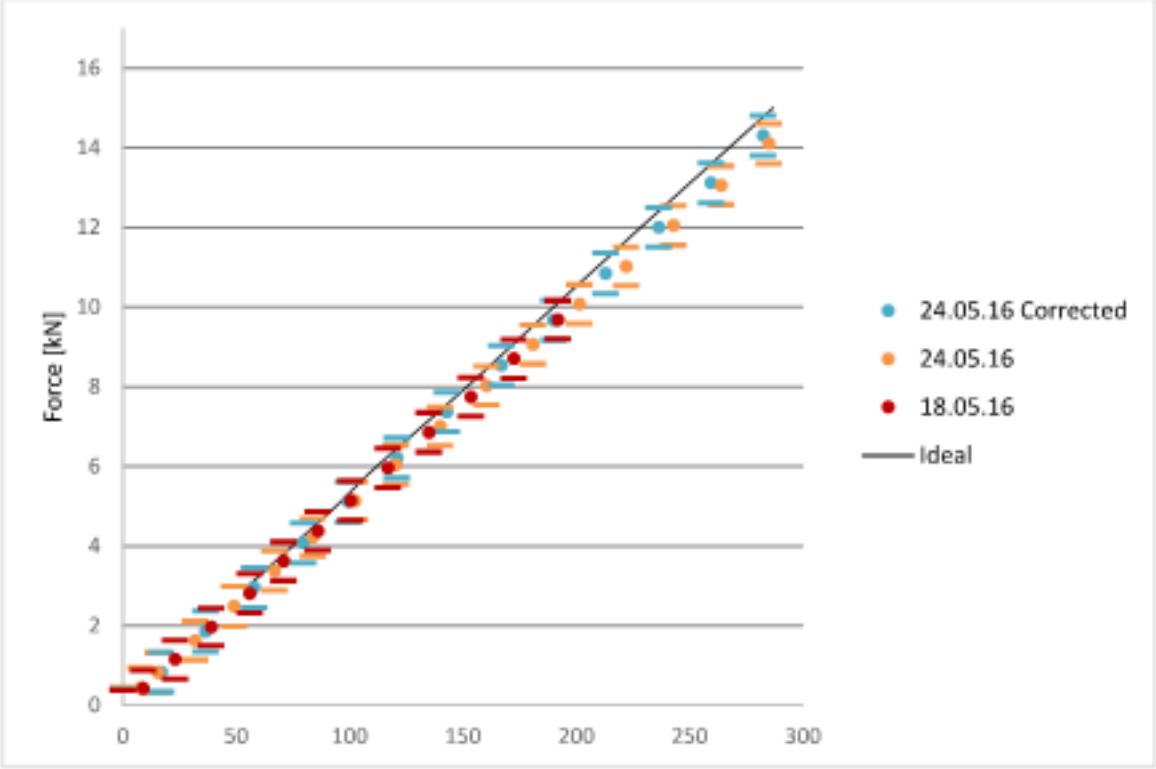

Figure Annex G-3 Results of calibration for axis Z

Force comparing to gauge index:

Force [kN]	Strain gauge sensor index
3	55.4
4	74.9
5	94
6	112
8	151.8
10	190
12.5	238.2
15	286.9
17.5	335.5

ANNEX H REGRESSION MODELS

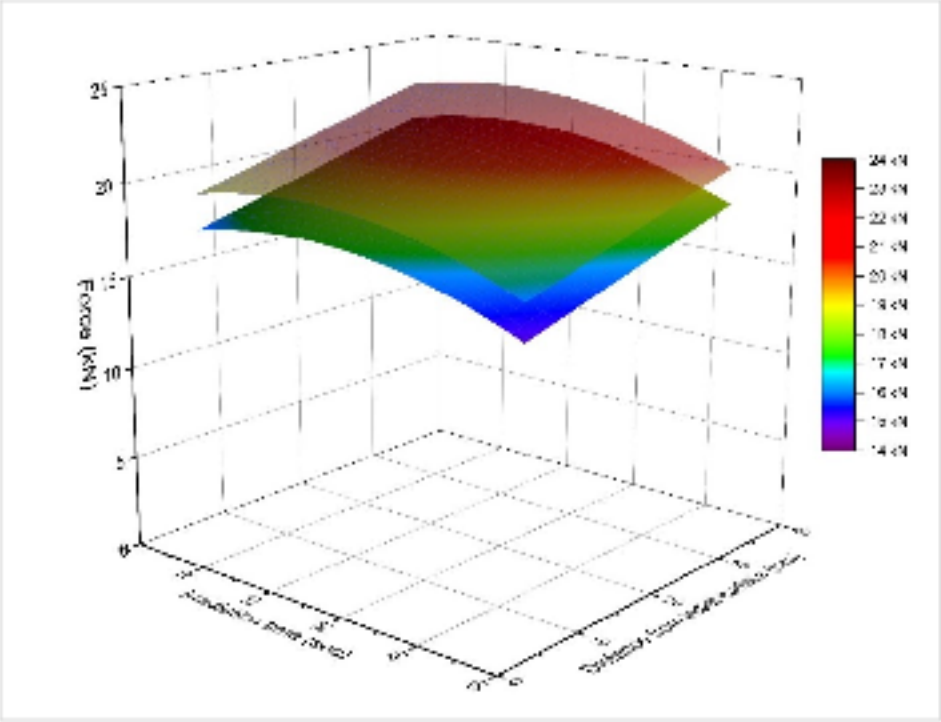

Figure Annex H-1 Response function of dependency of maximum cutting forces $F_{x_{max}}$ on irradiation time and distance from initial surface with spacing 8 mm (lower) and 12 mm (upper)

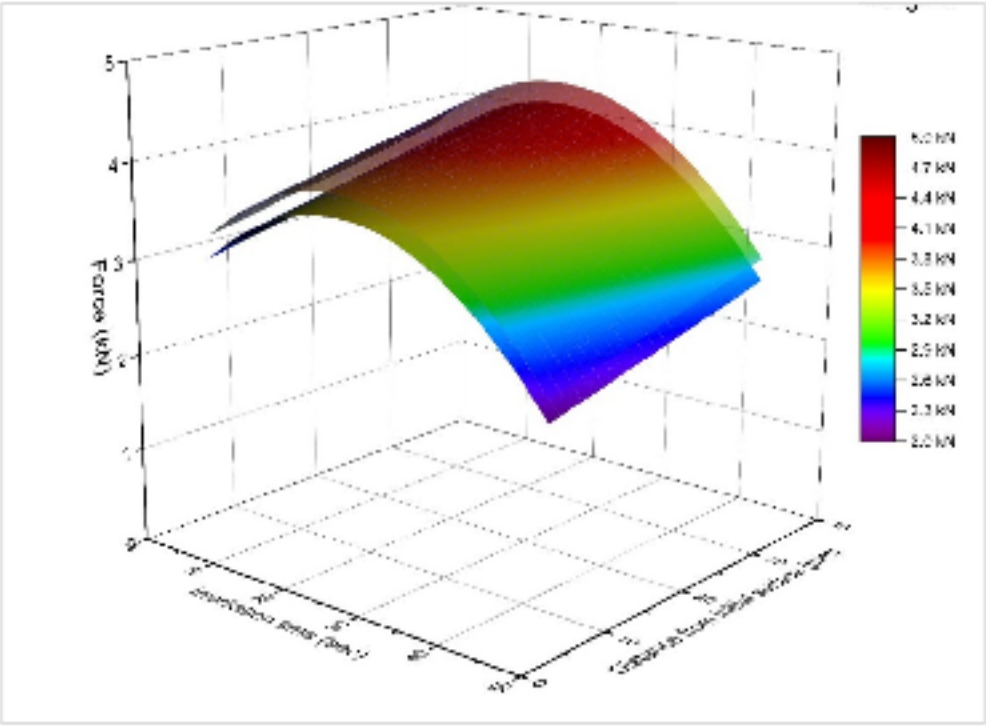

Figure Annex H-2 Response function of dependency of mean side forces $F_{y_{mean}}$ on irradiation time and distance from initial surface with spacing 8 mm (upper) and 12 mm (lower)

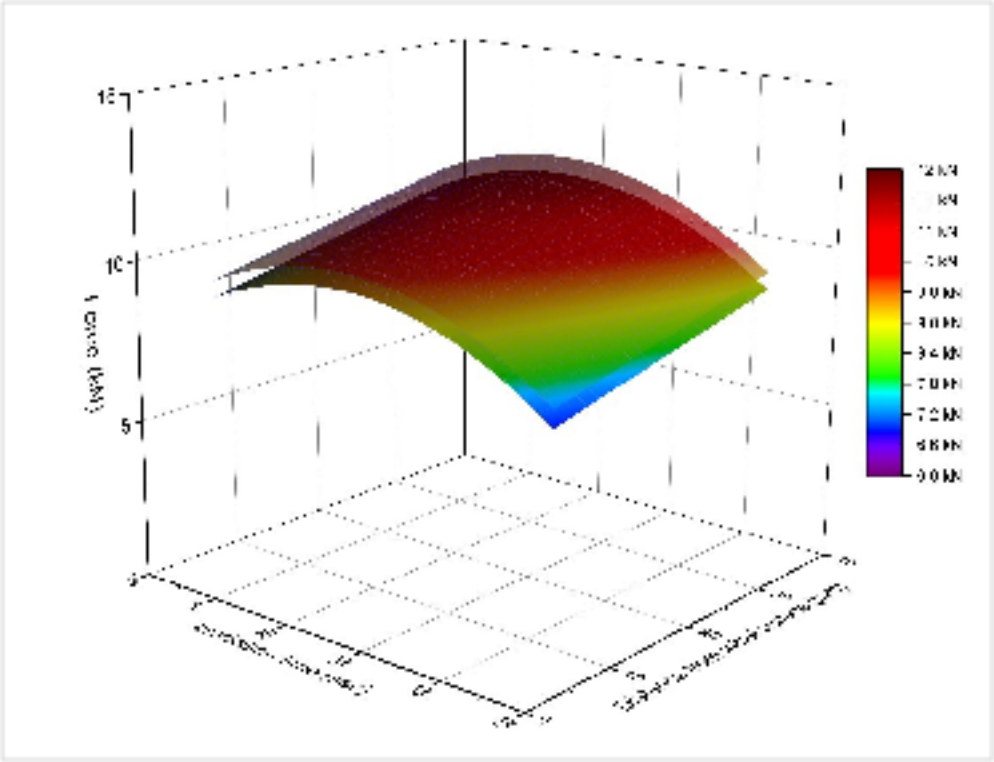

Figure Annex H-3 Response function of dependency of maximum cutting forces $F_{y_{max}}$ on irradiation time and distance from initial surface with spacing 8 mm (lower) and 12 mm (upper)

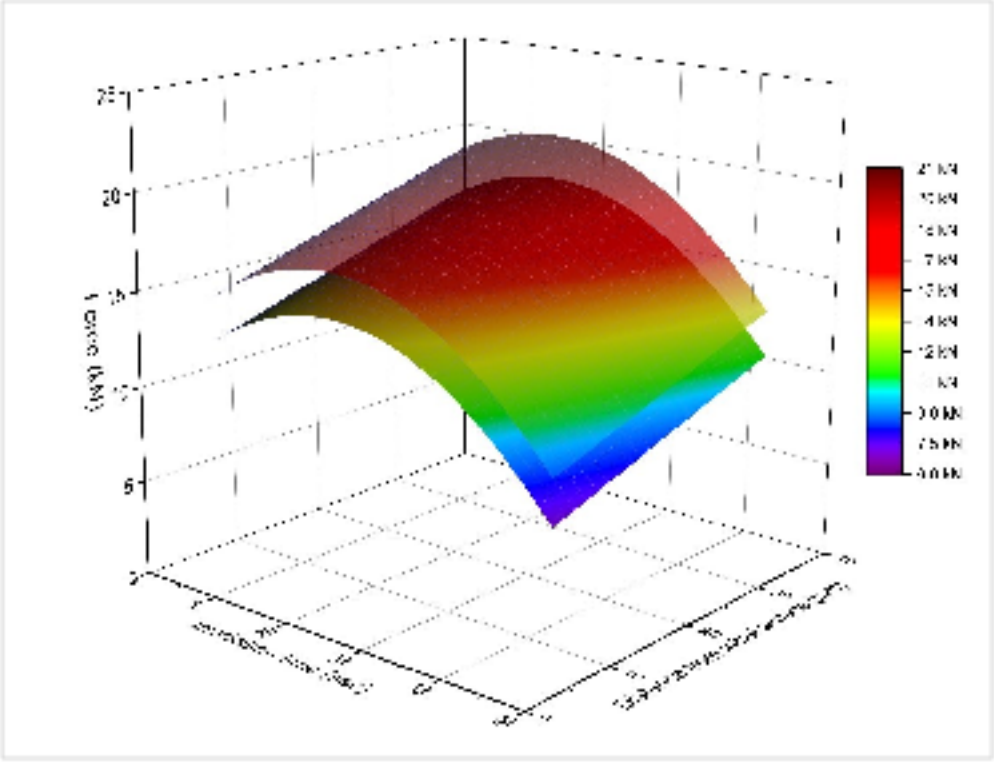

Figure Annex H-4 Response function of dependency of mean cutting forces $F_{z_{mean}}$ on irradiation time and distance from initial surface with spacing 8 mm (lower) and 12 mm (upper)

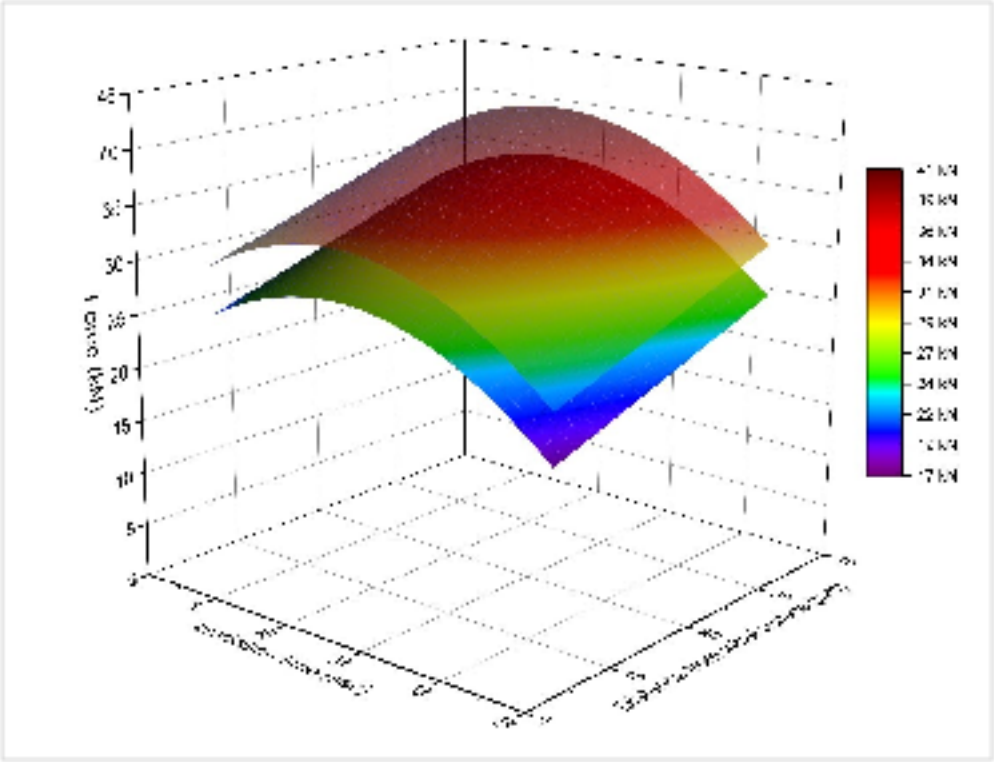

Figure Annex H-5 Response function of dependency of maximum cutting forces $F_{z_{max}}$ on irradiation time and distance from initial surface with spacing 8 mm (lower) and 12 mm (upper)

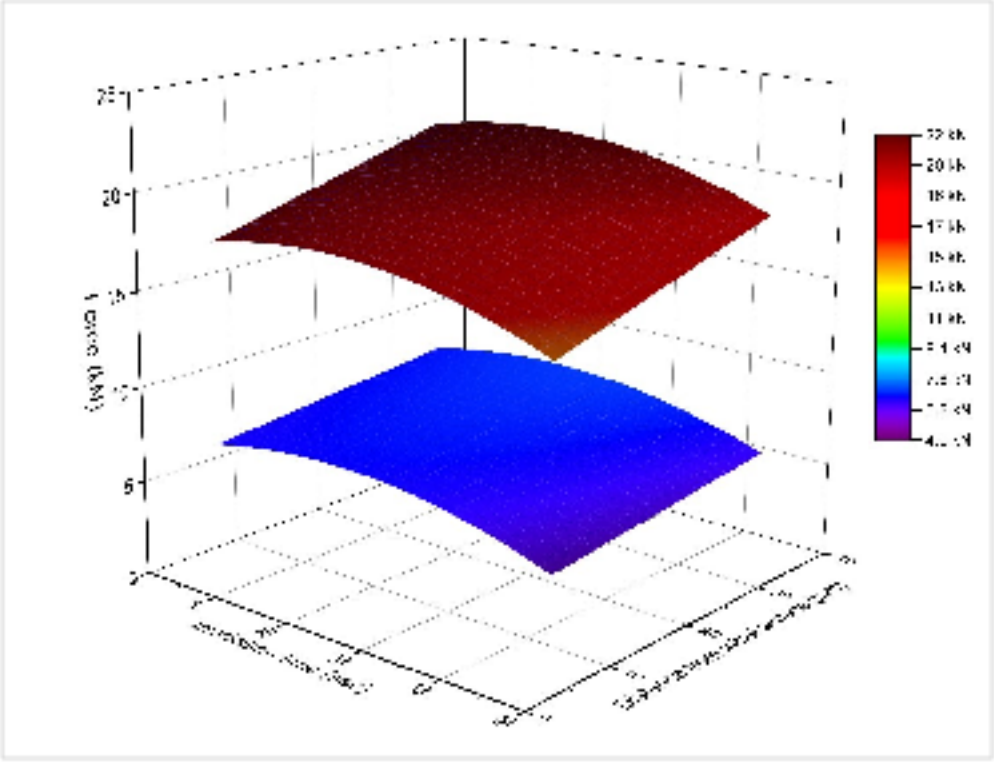

Figure Annex H-6 Comparing of response functions of mean (lower) and maximum (upper) cutting forces F_x for spacing 8 mm

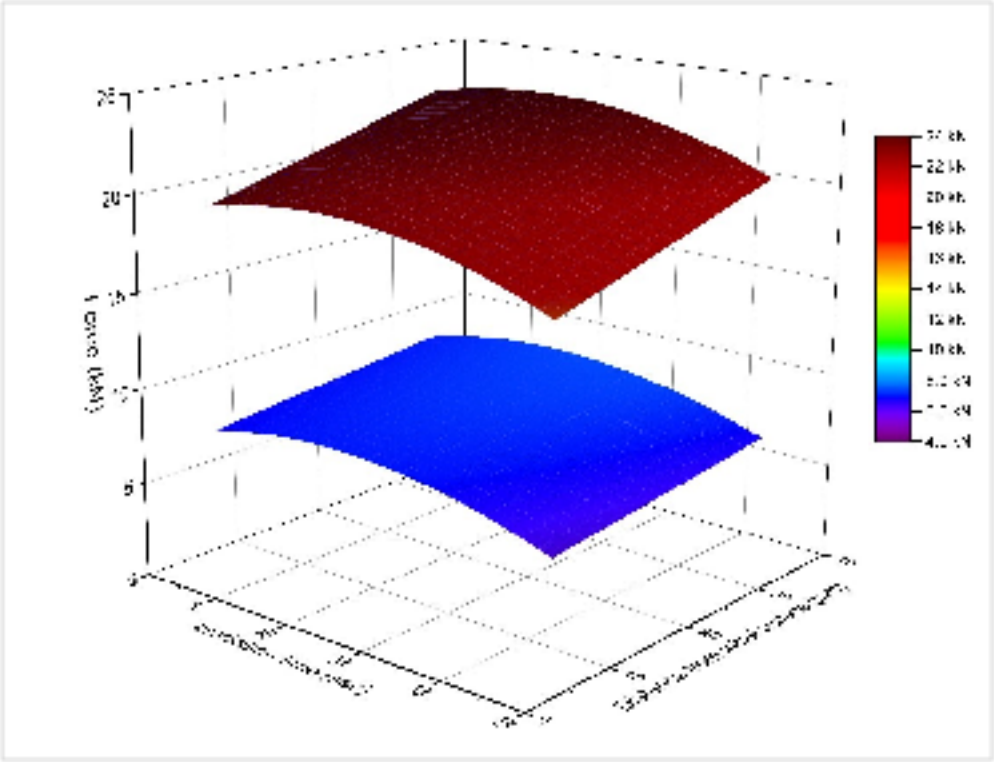

Figure Annex H-7 Comparing of response functions of mean (lower) and maximum (upper) cutting forces $\boldsymbol{F_x}$ for spacing 12 mm

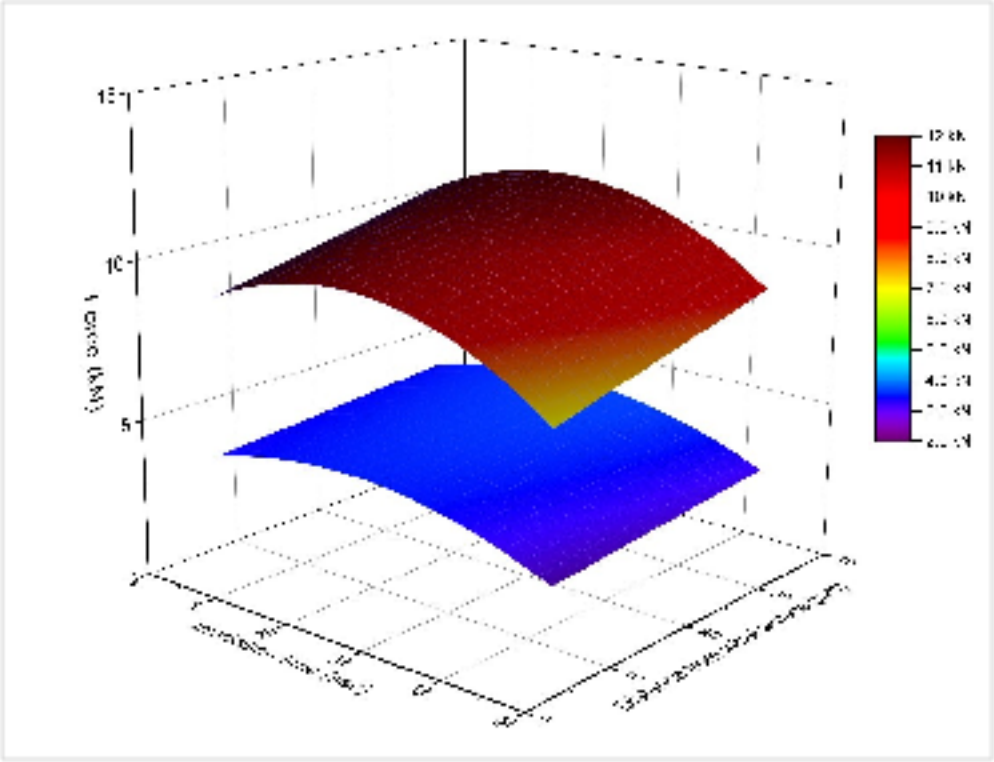

Figure Annex H-8 Comparing of response functions of mean (lower) and maximum (upper) side forces $\boldsymbol{F_y}$ for spacing 8 mm

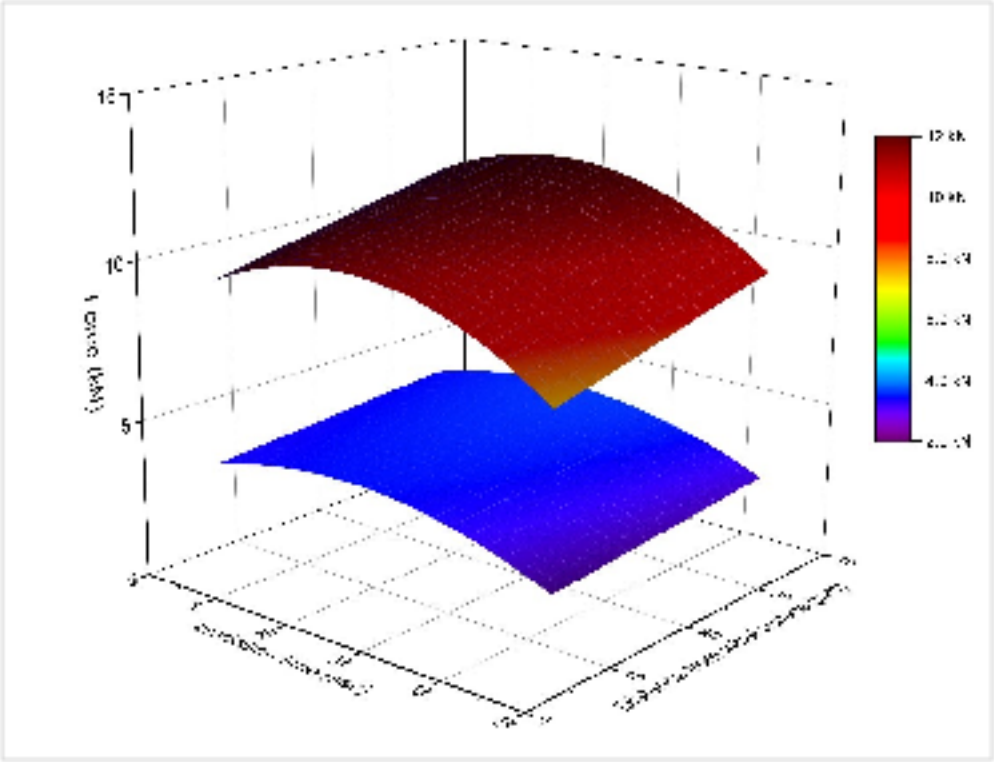

Figure Annex H-9 Comparing of response functions of mean (lower) and maximum (upper) side forces $\boldsymbol{F_y}$ for spacing 12 mm

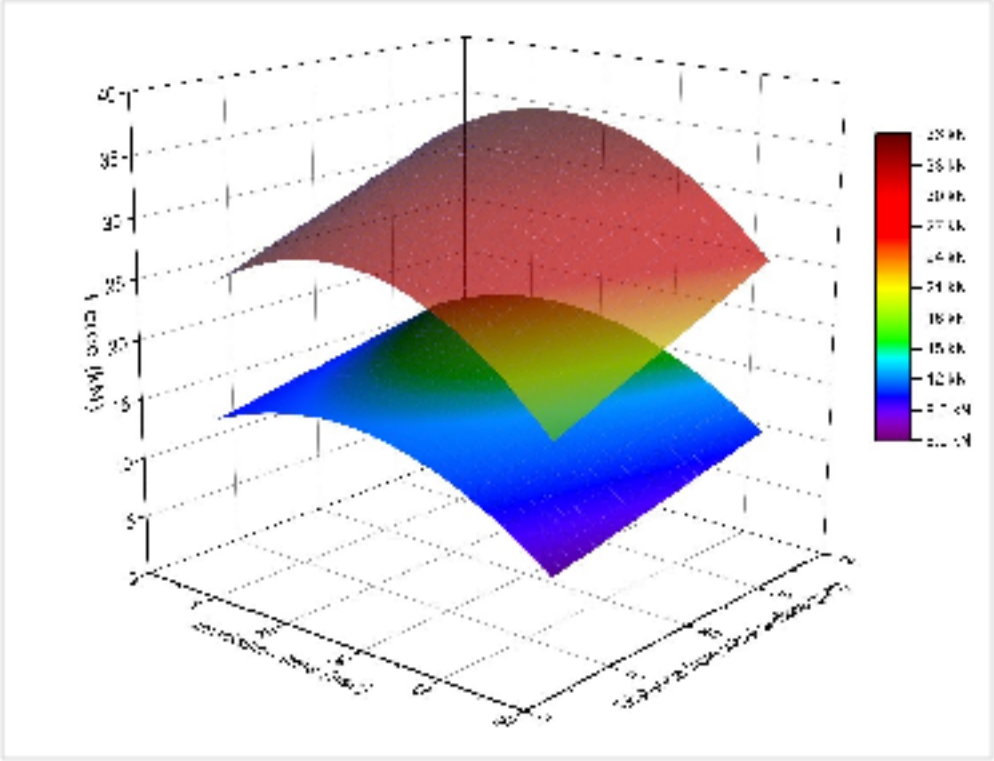

Figure Annex H-10 Comparing of response functions of mean (lower) and maximum (upper) normal forces $\boldsymbol{F_z}$ for spacing 8 mm

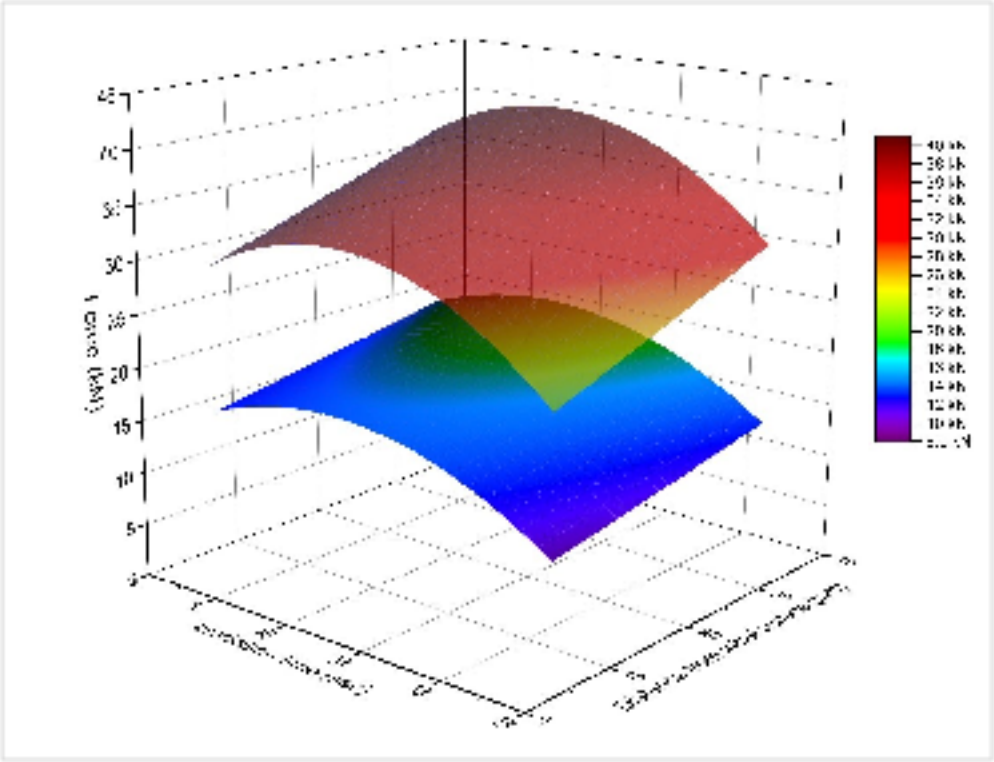

Figure Annex H-11 Comparing of response functions of mean (lower) and maximum (upper) normal forces $\boldsymbol{F_z}$ for spacing 12 mm

ANNEX I FORCE MAPPING

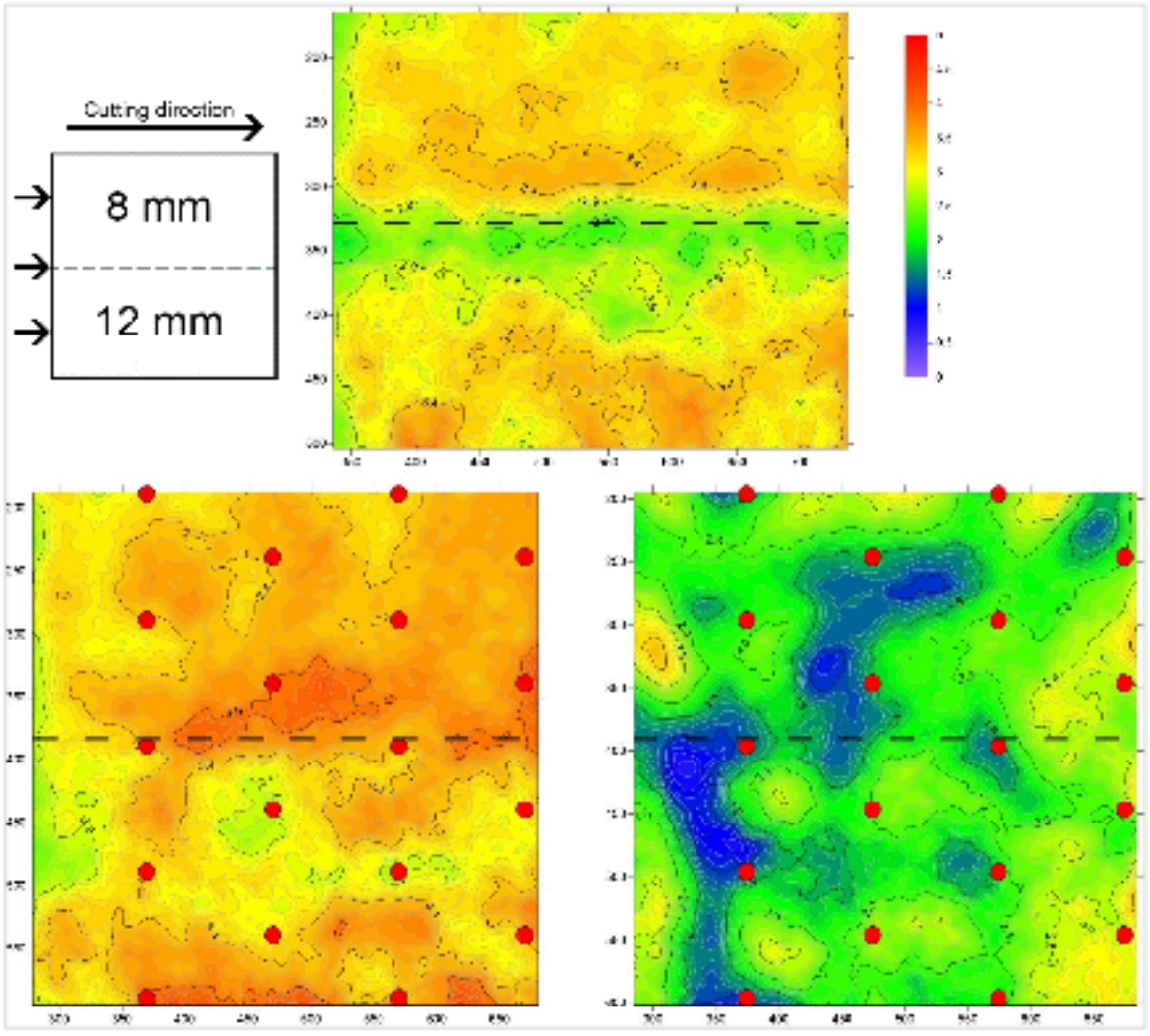

Figure Annex I-1 Force mapping of average side force F_y of three layers (2-4) for untreated sample (upper), 30 seconds irradiated sample (lower left) and 45 seconds irradiated sample (lower right)

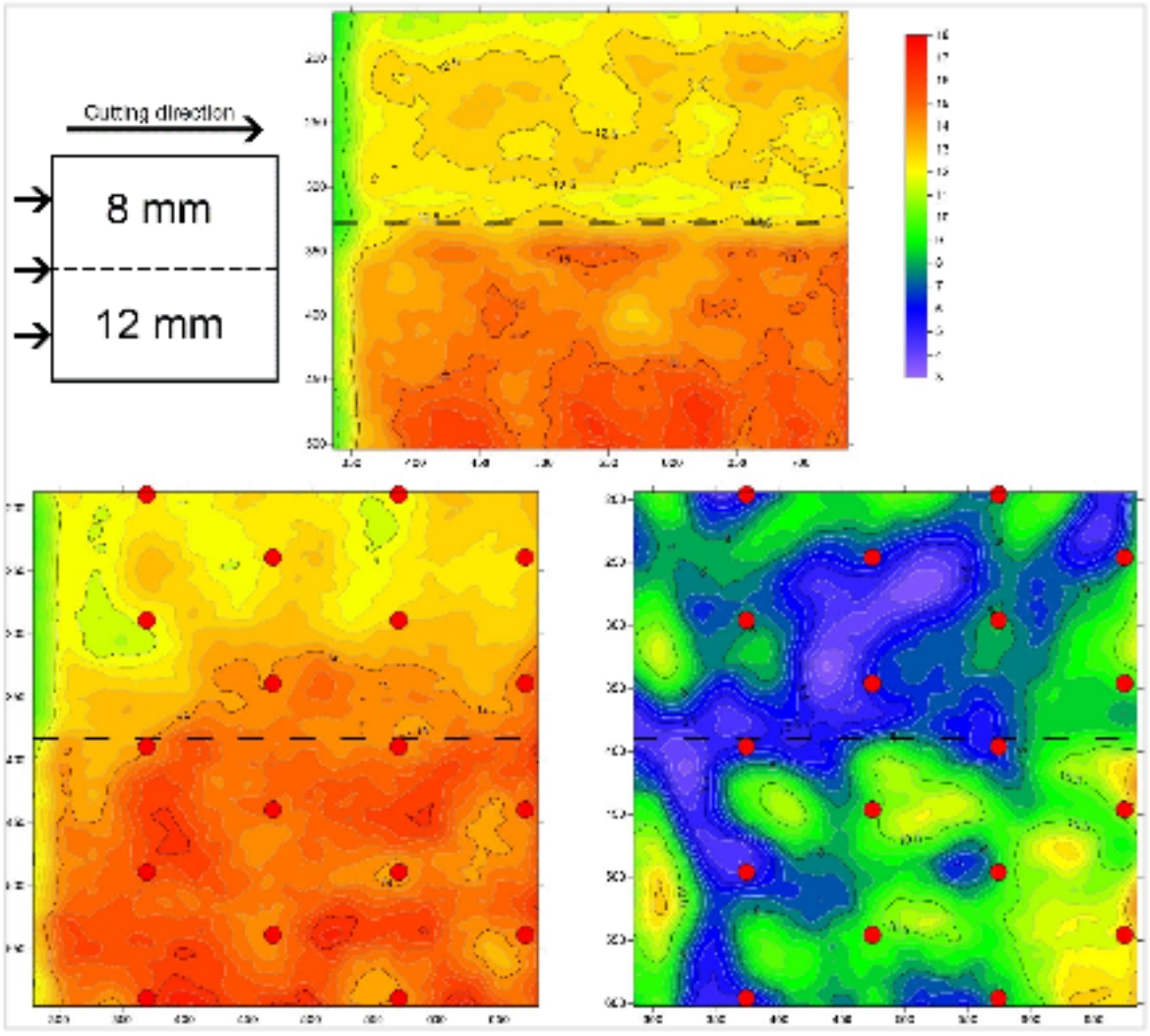

Figure Annex I-2 Force mapping of average normal force F_z of three layers (2-4) for untreated sample (upper), 30 seconds irradiated sample (lower left) and 45 seconds irradiated sample (lower right)

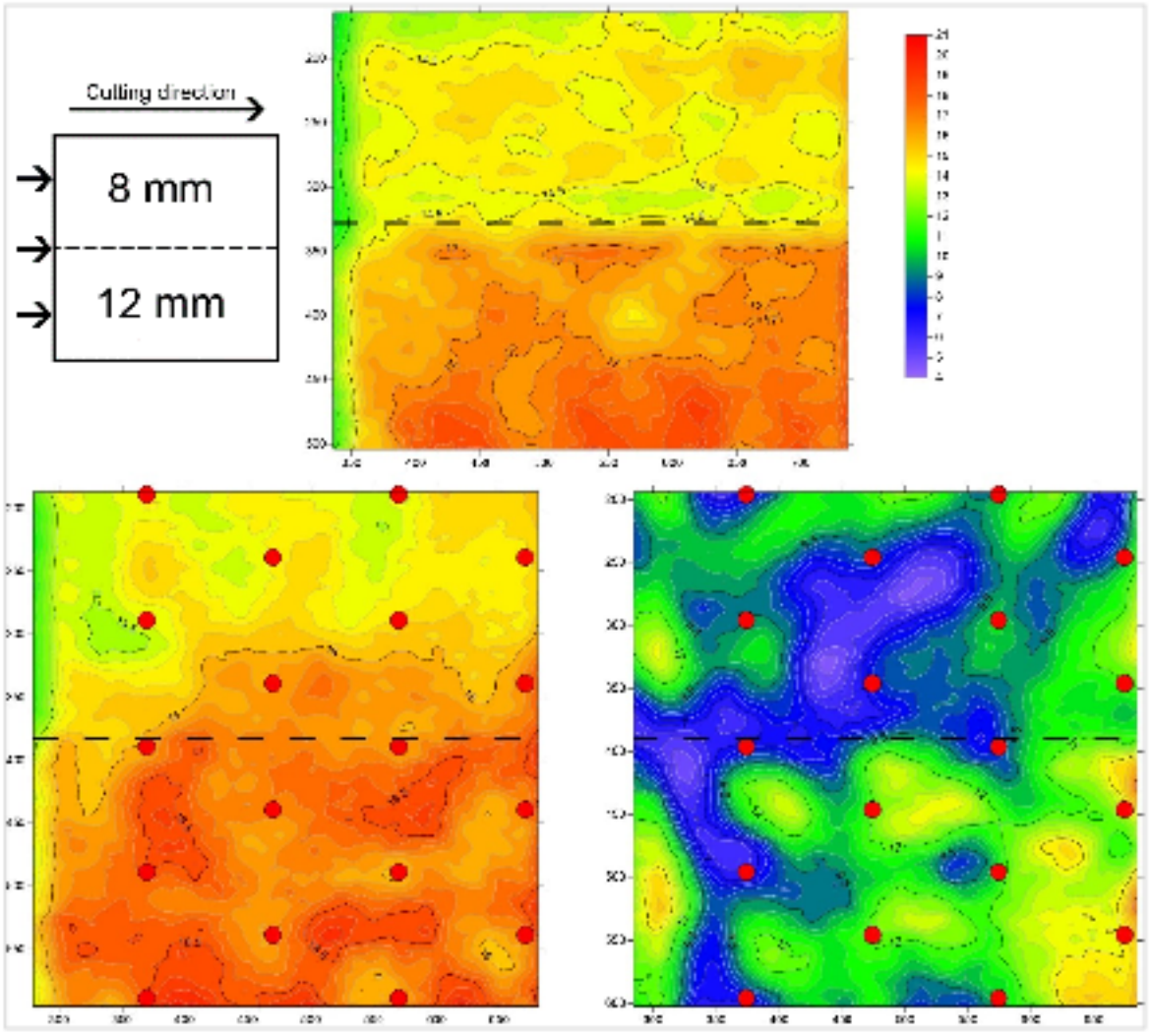

Figure Annex I-3 Force mapping of average total force $\boldsymbol{F_{Total}}$ of three layers (2-4) for untreated sample (upper), 30 seconds irradiated sample (lower left) and 45 seconds irradiated sample (lower right)

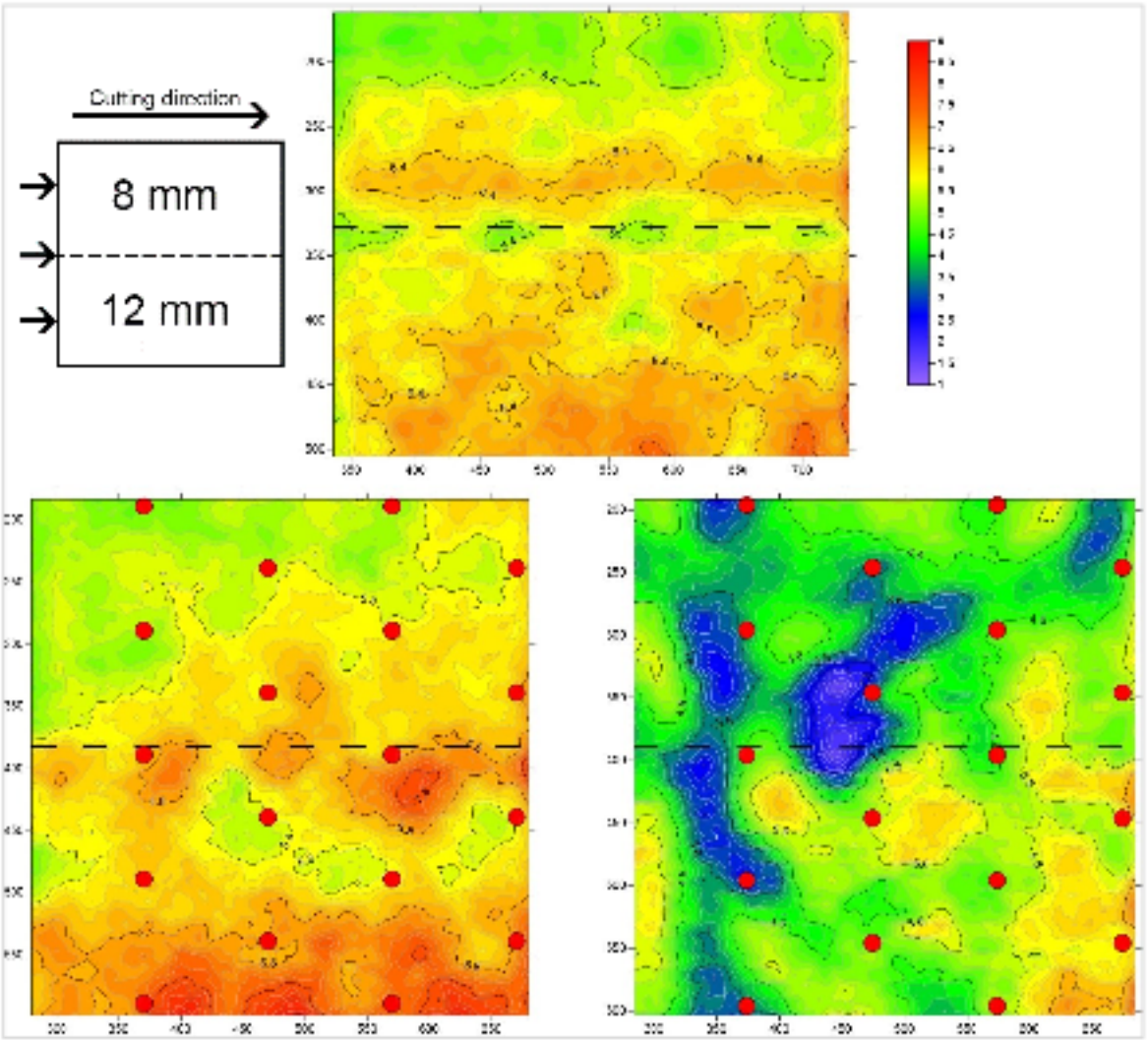

Figure Annex I-4 Force mapping of average cutting force $\boldsymbol{F_x}$ of layer 2 for untreated sample (upper), 30 seconds irradiated sample (lower left) and 45 seconds irradiated sample (lower right)

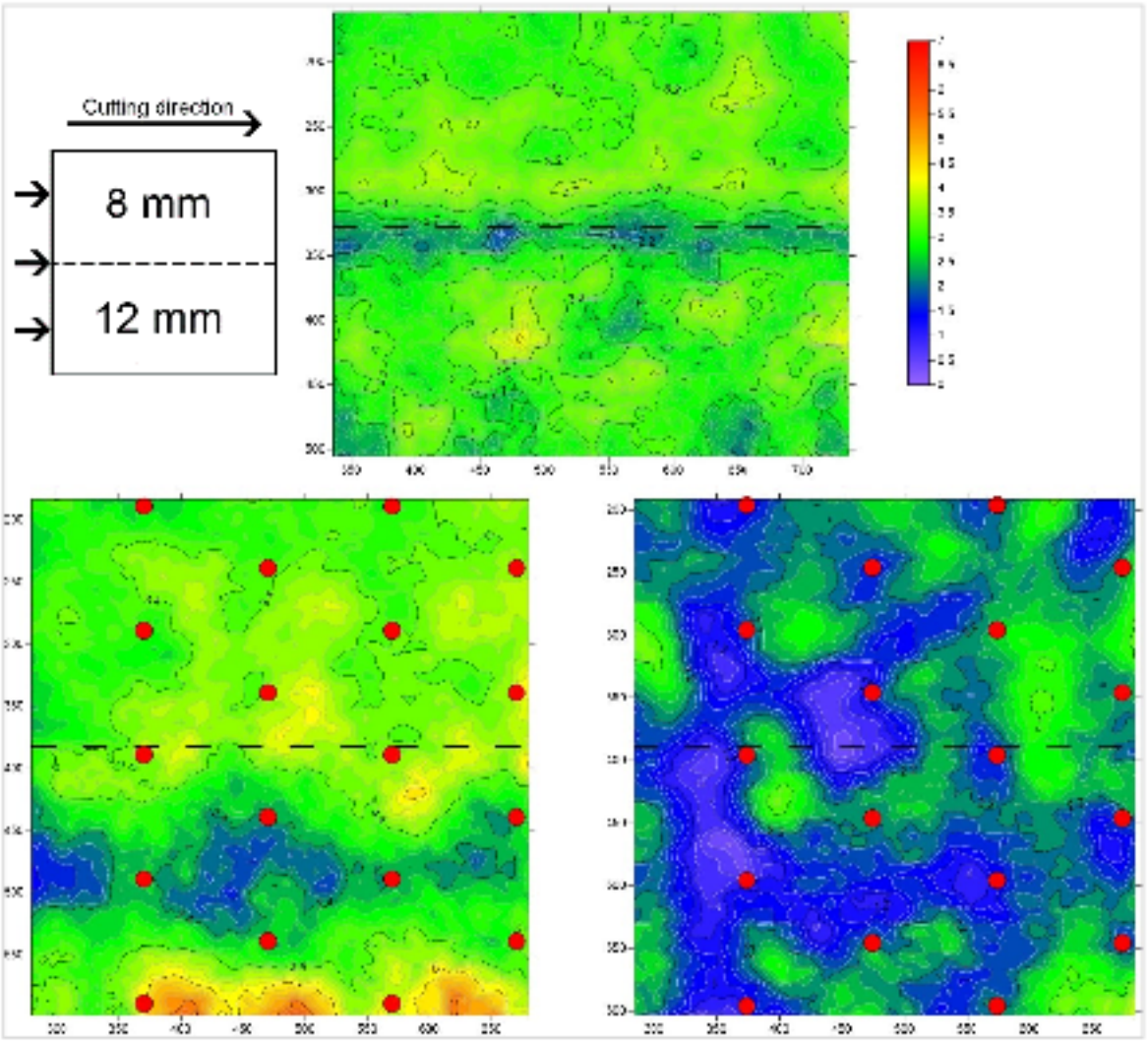

Figure Annex I-5 Y, layer 2 Force mapping of average side force F_y of layer 2 for untreated sample (upper), 30 seconds irradiated sample (lower left) and 45 seconds irradiated sample (lower right)

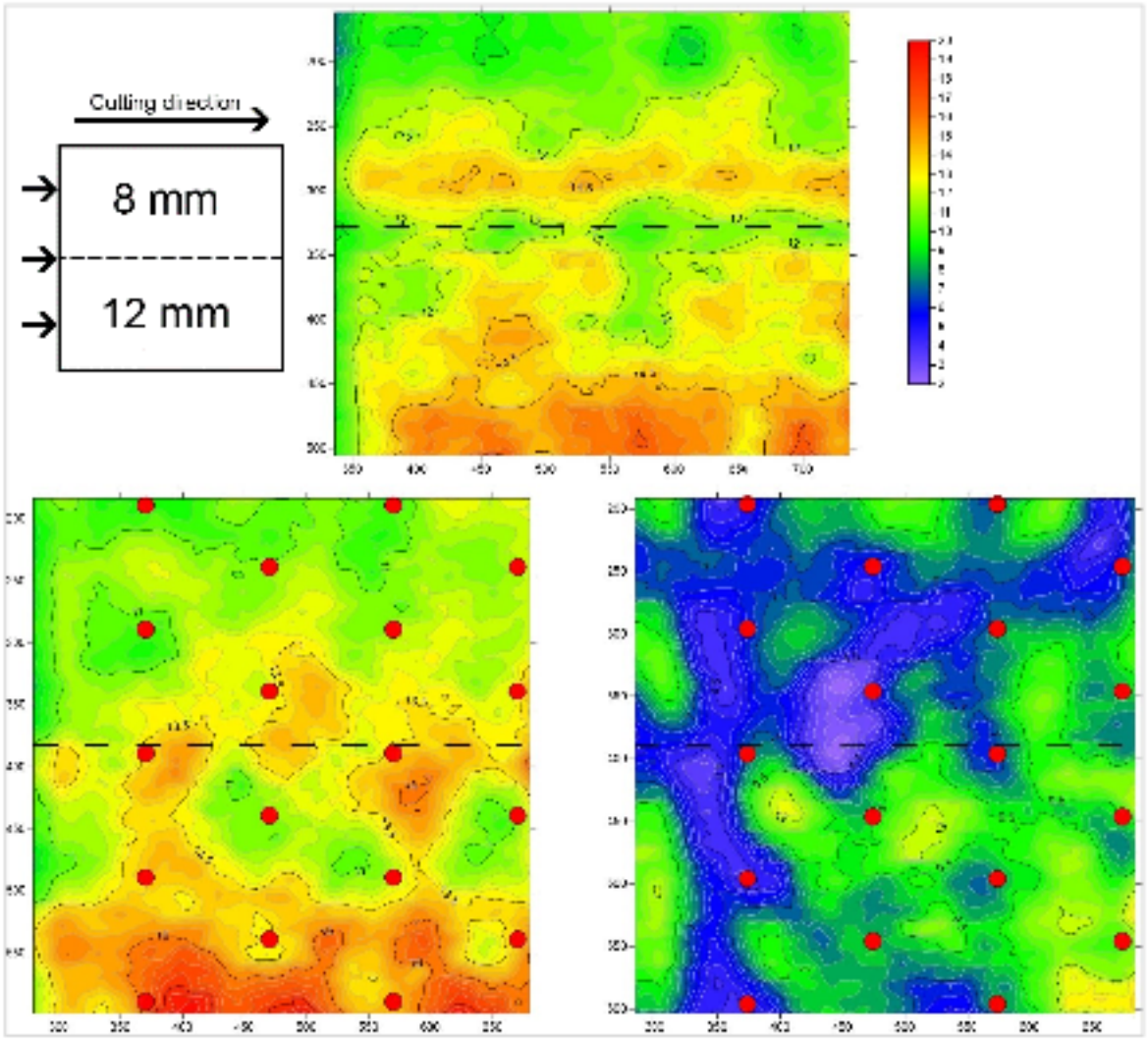

Figure Annex I-6 Z, layer 2 Force mapping of average normal force F_z of layer 2 for untreated sample (upper), 30 seconds irradiated sample (lower left) and 45 seconds irradiated sample (lower right)

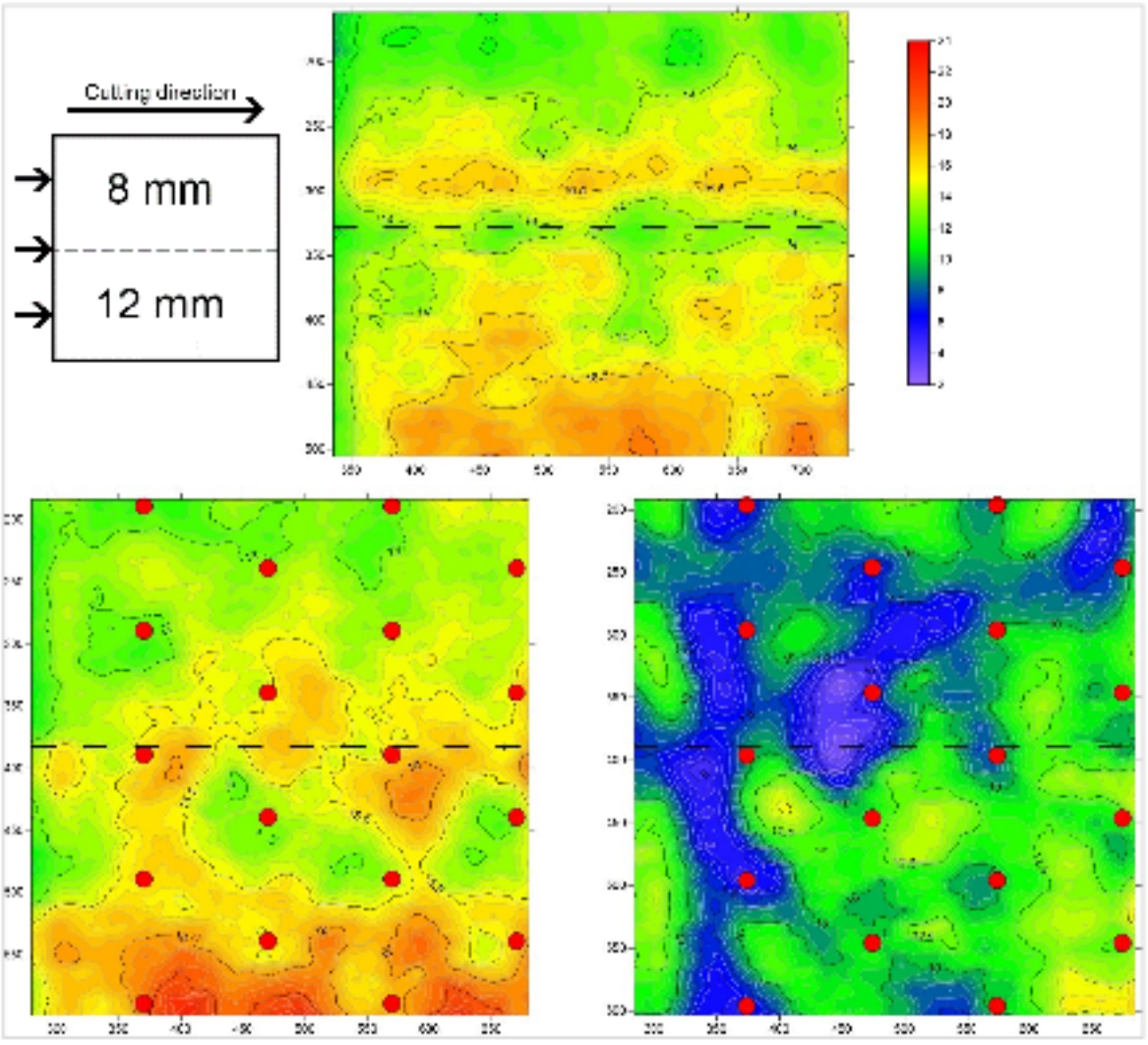

Figure Annex I-7 Total, layer 2 Force mapping of average total force F_{Total} of layer 2 for untreated sample (upper), 30 seconds irradiated sample (lower left) and 45 seconds irradiated sample (lower right)

ANNEX J CUTTING FORCES

45 seconds irradiated sample (layer 1, spacing 8 mm)

Cutting line	Mean forces [kN]				Maximum forces [kN]			
	Cutting	Side	Normal	Total	Cutting	Side	Normal	Total
2	4.72	2.59	7.36	9.12	14.03	7.48	15.71	22.35
3	4.22	2.43	6.77	8.34	13.80	6.61	15.07	21.48
4	4.09	2.23	6.64	8.11	14.44	6.95	16.88	23.27
5	4.54	2.52	6.66	8.45	12.87	6.75	14.92	20.83
6	4.17	2.35	6.34	7.94	13.15	7.30	15.15	21.35
7	4.60	2.76	7.35	9.10	13.31	7.75	15.63	21.94
8	4.40	2.24	6.82	8.42	13.11	6.18	13.63	19.90
9	4.41	2.50	6.39	8.16	13.09	7.22	15.05	21.22
10	4.66	2.84	7.02	8.89	13.38	7.76	15.59	21.96
11	4.83	2.90	7.47	9.36	14.45	7.56	15.99	22.83
12	4.55	2.78	7.04	8.83	13.88	7.59	14.88	21.72
13	4.96	3.06	8.12	9.99	14.34	7.61	15.27	22.28
14	4.79	2.88	7.71	9.53	13.88	7.87	16.06	22.64
15	4.85	2.90	7.89	9.70	14.53	7.73	15.78	22.80
16	4.88	3.02	8.07	9.90	15.10	8.16	18.19	25.01
17	4.45	2.59	7.53	9.12	14.79	7.77	18.21	24.71
18	4.73	2.67	8.29	9.91	14.51	7.09	17.26	23.64
19	4.66	2.39	7.83	9.42	14.75	7.65	18.22	24.66
20	4.75	2.69	8.16	9.82	15.09	7.08	17.95	24.50
21	5.21	2.79	9.00	10.77	14.81	6.83	18.35	24.55
22	4.15	2.11	7.09	8.48	14.63	7.19	18.71	24.81
23	4.55	2.51	7.59	9.19	14.53	6.56	17.34	23.55
24	4.63	2.21	7.77	9.31	14.41	6.16	17.15	23.23
25	4.48	2.21	7.35	8.89	14.35	6.63	16.44	22.81
26	4.63	2.36	7.27	8.94	13.98	6.49	16.03	22.23
27	4.31	2.28	7.07	8.59	13.78	6.48	15.22	21.53
Mean	**4.62**	**2.59**	**7.47**	**9.16**	**14.12**	**7.19**	**16.39**	**22.81**

45 seconds irradiated sample (layer 1, spacing 12 mm)

Cutting line	Mean forces [kN]				Maximum forces [kN]			
	Cutting	Side	Normal	Total	Cutting	Side	Normal	Total
1	5.72	2.42	9.52	11.37	18.46	8.65	26.45	33.40
2	5.31	2.49	9.20	10.91	16.12	7.64	21.71	28.10
3	5.11	1.97	9.01	10.55	15.89	6.92	22.92	28.73
4	5.92	2.41	11.06	12.78	17.07	7.52	25.08	31.26
5	4.99	1.93	8.44	10.00	14.82	6.84	18.52	24.69
6	5.57	2.52	9.57	11.35	16.29	7.21	21.87	28.21
7	5.13	2.20	9.02	10.61	16.15	7.63	23.76	29.72
8	5.28	2.46	8.89	10.63	15.74	8.00	21.41	27.75
9	5.28	2.35	8.83	10.56	15.72	7.09	21.37	27.46
10	4.30	1.86	7.07	8.49	14.99	6.08	18.52	24.59
11	4.79	2.04	7.44	9.08	15.30	7.33	21.00	26.99
12	5.09	2.25	8.44	10.10	15.11	6.99	19.92	25.96
13	4.74	2.00	7.50	9.09	14.87	6.64	18.69	24.79
14	4.31	1.82	6.45	7.97	14.44	5.64	16.90	22.93
15	4.58	2.04	7.14	8.72	14.22	6.21	17.65	23.50
16	4.74	1.93	7.72	9.26	14.56	5.97	18.66	24.40
17	4.93	1.90	7.68	9.32	14.73	5.55	18.16	24.03
18	4.73	1.49	7.33	8.85	14.12	4.89	17.76	23.21
19	4.84	1.61	7.68	9.22	15.56	6.03	22.98	28.40
Mean	**5.05**	**2.17**	**8.46**	**10.09**	**15.61**	**7.02**	**20.90**	**27.03**

45 seconds irradiated sample (layer 2, spacing 8 mm)

Cutting line	Mean forces [kN]				Maximum forces [kN]			
	Cutting	Side	Normal	Total	Cutting	Side	Normal	Total
2	4.79	2.39	8.55	10.09	14.83	7.14	18.74	24.94
3	4.43	1.99	7.77	9.16	14.64	6.43	17.81	23.94
4	4.76	2.13	8.52	9.99	15.77	6.97	21.44	27.51
5	4.47	2.23	7.65	9.13	14.65	6.73	17.45	23.75
6	4.40	2.21	7.34	8.84	14.34	6.64	16.08	22.56
7	4.33	2.19	7.04	8.55	14.03	6.55	14.72	21.36
8	4.13	1.98	6.34	7.82	13.76	6.69	13.95	20.70
9	4.16	2.38	6.54	8.10	13.34	6.77	13.95	20.46
10	4.19	2.53	6.97	8.52	13.40	7.29	14.90	21.32
11	4.05	2.16	6.28	7.77	13.81	7.29	15.00	21.65
12	4.09	2.32	6.71	8.20	13.46	6.40	14.46	20.77
13	3.79	1.91	5.57	7.00	13.05	6.44	13.02	19.53
14	4.07	2.13	6.39	7.87	15.21	7.21	16.73	23.73
15	4.50	2.72	7.56	9.21	15.57	8.60	18.98	26.01
16	4.43	2.49	7.49	9.05	15.36	8.34	18.64	25.55
17	4.64	2.42	8.02	9.58	15.44	7.02	19.13	25.56
18	4.74	2.49	8.26	9.84	15.78	7.95	19.54	26.34
19	3.85	1.78	6.24	7.55	15.02	6.58	19.01	25.11
20	4.25	2.03	6.91	8.36	15.46	7.93	20.34	26.75
21	4.45	2.15	7.62	9.09	15.35	7.22	19.57	25.90
22	4.54	2.12	7.72	9.21	15.42	6.57	19.01	25.34
23	4.34	2.27	6.67	8.27	14.56	7.18	18.10	24.31
24	4.38	2.02	6.75	8.29	14.07	5.64	15.44	21.64
25	4.26	1.85	6.82	8.25	14.37	6.43	17.07	23.22
26	3.75	1.90	5.77	7.13	15.38	8.25	19.15	25.91
Mean	**4.29**	**2.19**	**7.01**	**8.51**	**14.63**	**7.07**	**17.20**	**23.70**

45 seconds irradiated sample (layer 2, spacing 12 mm)

Cutting line	Mean forces [kN]				Maximum forces [kN]			
	Cutting	Side	Normal	Total	Cutting	Side	Normal	Total
1	4.61	1.68	7.07	8.60	15.70	6.71	20.28	26.51
2	4.84	1.87	7.85	9.41	16.99	7.59	23.96	30.34
3	5.39	2.43	9.04	10.80	16.10	7.27	21.38	27.74
4	5.59	2.51	9.94	11.68	16.70	8.38	23.40	29.94
5	5.38	2.02	9.34	10.97	16.26	7.35	22.32	28.57
6	5.39	1.96	9.63	11.20	16.26	7.26	22.30	28.54
7	5.20	1.65	9.05	10.56	15.46	6.41	20.54	26.50
8	5.24	1.66	9.27	10.77	16.72	6.90	23.56	29.70
9	5.13	1.53	8.97	10.45	15.85	5.76	21.41	27.25
10	4.70	1.50	7.86	9.28	16.50	7.04	21.71	28.17
11	5.40	2.03	9.78	11.36	16.44	7.08	23.53	29.56
12	5.58	1.67	10.17	11.72	16.28	6.89	22.35	28.49
13	5.44	2.09	9.70	11.31	16.05	6.77	20.40	26.82
14	5.05	2.36	8.87	10.48	15.79	7.42	20.68	27.06
15	5.02	2.11	8.53	10.12	15.71	7.18	19.97	26.40
16	5.65	2.79	10.02	11.83	17.02	8.06	24.13	30.61
17	4.98	2.08	7.97	9.62	16.63	7.57	22.26	28.81
18	5.07	2.35	7.97	9.73	16.37	9.25	21.62	28.65
Mean	**5.22**	**1.99**	**9.07**	**10.66**	**16.24**	**7.13**	**21.99**	**28.26**

45 seconds irradiated sample (layer 3, spacing 8 mm)

Cutting line	Mean forces [kN]				Maximum forces [kN]			
	Cutting	Side	Normal	Total	Cutting	Side	Normal	Total
2	5.11	2.97	8.67	10.50	16.21	8.57	20.17	27.26
3	4.66	2.75	7.76	9.46	15.02	8.05	17.81	24.65
4	5.04	2.96	8.80	10.57	14.90	7.12	18.17	24.56
5	5.83	3.41	9.84	11.94	16.98	8.52	22.15	29.18
6	4.49	2.24	7.31	8.87	14.64	6.54	17.41	23.66
7	4.51	2.11	7.03	8.62	13.81	6.19	16.01	22.03
8	4.70	2.12	6.99	8.68	14.03	5.93	16.05	22.12
9	4.40	2.03	6.64	8.22	13.12	5.49	14.74	20.48
10	4.50	2.01	7.22	8.74	13.71	6.00	16.64	22.38
11	3.88	1.79	6.35	7.65	13.09	5.91	15.83	21.38
12	3.90	1.81	6.36	7.68	14.64	7.08	17.43	23.84
13	4.11	1.72	6.60	7.96	14.02	5.80	16.38	22.33
14	4.33	2.10	7.42	8.84	14.10	5.95	16.99	22.86
15	4.55	1.97	8.20	9.58	15.61	6.83	21.19	27.19
16	4.66	2.09	8.38	9.81	15.89	6.28	21.18	27.21
17	4.30	2.11	7.61	8.99	14.32	6.24	17.32	23.32
18	5.39	2.48	9.94	11.58	16.29	7.15	21.91	28.23
19	4.93	2.18	8.63	10.17	15.65	7.09	20.89	27.05
20	4.55	2.43	7.84	9.38	14.98	7.03	18.83	25.07
21	5.14	2.71	8.77	10.52	15.16	7.33	19.27	25.59
22	4.85	2.56	8.27	9.93	14.90	7.36	18.31	24.73
23	3.68	1.71	5.35	6.71	13.17	6.57	13.94	20.27
24	3.86	2.11	5.96	7.41	14.70	6.89	16.19	22.93
25	3.44	1.67	5.16	6.42	13.80	6.82	15.49	21.84
Mean	**4.51**	**2.22**	**7.50**	**9.03**	**14.63**	**6.70**	**17.83**	**24.04**

45 seconds irradiated sample (layer 3, spacing 12 mm)

Cutting line	Mean forces [kN]				Maximum forces [kN]			
	Cutting	Side	Normal	Total	Cutting	Side	Normal	Total
1	5.00	2.01	8.32	9.91	16.91	7.36	22.66	29.22
2	5.27	2.24	9.02	10.68	17.51	8.44	25.66	32.19
3	5.34	2.34	8.90	10.64	18.15	7.80	22.90	30.24
4	6.06	2.85	10.67	12.60	18.60	8.58	24.09	31.62
5	6.09	2.80	10.63	12.57	17.64	8.86	24.23	31.25
6	6.07	3.00	10.70	12.66	17.84	8.75	24.31	31.40
7	5.87	3.16	10.16	12.16	17.78	9.16	23.28	30.70
8	5.68	3.32	9.61	11.65	17.72	9.56	22.25	30.01
9	5.01	2.58	8.33	10.06	16.65	9.05	20.03	27.57
10	5.26	2.68	8.83	10.62	18.24	8.61	24.21	31.51
11	5.75	2.84	10.14	12.00	17.64	8.92	25.14	31.98
12	5.42	2.33	9.65	11.31	16.88	8.16	22.94	29.63
13	5.60	2.14	9.85	11.53	16.02	7.63	21.40	27.80
14	5.76	2.22	10.06	11.80	16.35	6.90	21.71	28.04
15	5.00	1.71	8.66	10.15	15.20	6.68	19.02	25.25
16	5.66	2.28	10.39	12.05	16.18	7.21	22.46	28.61
17	4.98	1.56	8.41	9.90	15.78	6.48	22.23	28.03
Mean	**5.55**	**2.53**	**9.62**	**11.40**	**17.21**	**8.23**	**22.89**	**29.81**

45 seconds irradiated sample (layer 4, spacing 8 mm)

Cutting line	Mean forces [kN]				Maximum forces [kN]			
	Cutting	Side	Normal	Total	Cutting	Side	Normal	Total
2	4.44	2.11	7.42	8.91	15.90	7.43	19.97	26.62
3	4.59	1.79	7.62	9.07	15.08	6.02	19.92	25.70
4	4.59	1.79	7.62	9.07	15.08	6.02	19.92	25.70
5	4.51	1.60	7.53	8.92	14.77	5.83	18.72	24.55
6	4.33	1.45	6.86	8.24	15.29	5.31	17.03	23.50
7	4.40	1.58	6.74	8.20	14.39	5.88	17.01	23.05
8	4.53	1.66	7.26	8.72	16.34	5.79	20.16	26.59
9	4.79	1.92	7.93	9.46	15.93	6.87	21.28	27.46
10	4.30	1.61	7.27	8.60	15.22	5.66	18.25	24.43
11	4.66	1.85	7.88	9.34	17.88	6.94	22.82	29.81
12	4.74	2.07	8.14	9.64	17.87	8.09	23.85	30.88
13	4.47	2.40	7.99	9.46	16.73	8.43	22.71	29.43
14	4.78	2.57	8.52	10.10	18.75	9.33	25.77	33.21
15	5.38	3.20	10.04	11.84	19.05	10.15	26.32	34.04
16	5.17	2.99	8.87	10.70	17.02	9.14	22.69	29.80
17	4.78	2.72	8.13	9.82	15.81	8.58	21.52	28.05
18	4.60	2.53	7.82	9.42	15.40	7.83	18.46	25.29
19	4.34	2.43	7.18	8.73	15.42	8.43	18.57	25.57
20	3.55	2.07	5.49	6.86	15.02	8.81	17.96	25.01
21	3.48	1.84	5.54	6.80	13.92	6.89	15.96	22.27
22	3.87	1.86	6.29	7.61	14.74	7.46	17.14	23.80
23	3.78	2.03	5.85	7.26	13.86	6.34	14.64	21.13
24	4.15	2.24	6.78	8.26	15.43	8.19	18.51	25.45
Mean	**4.44**	**2.10**	**7.43**	**8.91**	**15.87**	**7.37**	**19.96**	**26.58**

45 seconds irradiated sample (layer 4, spacing 12 mm)

Cutting line	Mean forces [kN]				Maximum forces [kN]			
	Cutting	Side	Normal	Total	Cutting	Side	Normal	Total
1	4.55	1.72	7.72	9.13	16.67	6.46	22.87	29.03
2	5.51	1.90	9.95	11.53	18.43	8.20	28.25	34.72
3	4.98	1.51	8.82	10.24	17.24	6.36	26.63	32.36
4	5.12	1.71	8.75	10.27	17.32	6.73	23.12	29.66
5	5.57	1.79	9.92	11.52	17.21	6.61	24.80	30.90
6	5.38	1.58	9.29	10.85	16.53	6.23	21.67	27.96
7	5.07	1.82	8.85	10.36	17.00	6.65	22.90	29.29
8	4.83	1.64	8.53	9.94	18.00	7.71	25.68	32.29
9	4.69	1.58	7.97	9.38	18.00	7.01	23.82	30.67
10	5.79	2.39	10.05	11.84	19.23	8.73	25.34	32.99
11	5.91	2.55	10.89	12.65	21.88	8.86	28.19	36.77
12	6.80	3.59	13.20	15.28	19.72	10.95	30.30	37.77
13	6.00	3.23	10.97	12.91	18.12	9.76	23.55	31.28
14	6.04	3.17	10.69	12.68	19.14	10.15	25.54	33.49
15	6.58	3.80	11.98	14.19	18.40	9.60	23.94	31.69
16	5.67	2.66	9.38	11.28	18.20	8.75	26.15	33.04
Mean	**5.53**	**2.29**	**9.81**	**11.50**	**18.19**	**8.05**	**25.17**	**32.12**

30 seconds irradiated sample (layer 1, spacing 8 mm)

Cutting line	Mean forces [kN]				Maximum forces [kN]			
	Cutting	Side	Normal	Total	Cutting	Side	Normal	Total
2	5.51	3.00	11.33	12.95	15.27	7.66	20.76	26.88
3	5.48	3.07	11.06	12.72	15.35	8.09	21.13	27.34
4	5.55	3.02	10.88	12.58	15.93	8.20	21.65	28.11
5	5.11	2.78	10.06	11.62	14.90	7.66	19.48	25.69
6	5.20	2.59	10.08	11.63	14.82	7.06	18.87	25.01
7	5.02	2.53	9.80	11.30	14.95	7.47	19.69	25.83
8	4.78	2.59	8.94	10.46	14.14	6.97	17.55	23.59
9	4.56	2.17	8.37	9.78	14.04	6.30	16.90	22.86
10	4.78	2.39	9.10	10.55	14.58	7.04	19.63	25.45
11	4.35	2.45	8.10	9.51	13.59	6.54	15.96	21.96
12	4.62	2.29	8.43	9.88	14.06	6.71	16.54	22.72
13	4.76	2.47	8.98	10.46	14.18	7.04	17.16	23.35
14	4.90	2.64	9.53	11.03	14.31	7.37	17.78	23.99
15	4.57	2.37	8.97	10.34	14.21	7.27	19.11	24.90
16	4.96	2.52	9.96	11.40	14.44	6.88	18.66	24.58
17	4.53	2.20	7.97	9.43	13.50	6.31	15.59	21.57
18	4.63	2.48	8.79	10.24	14.23	6.62	18.02	23.90
19	4.84	2.44	9.03	10.53	13.88	6.69	16.78	22.78
20	5.01	2.82	9.65	11.23	14.45	7.37	18.57	24.66
21	5.07	2.75	9.81	11.38	14.47	7.41	19.01	25.02
22	5.05	2.69	9.61	11.18	15.00	7.34	19.59	25.74
23	5.65	2.97	10.72	12.47	15.55	7.49	20.57	26.85
24	5.35	2.67	10.69	12.25	15.35	7.09	20.07	26.24
25	5.58	2.92	10.98	12.66	16.04	7.71	22.25	28.49
26	5.57	3.17	11.13	12.84	15.81	8.41	22.15	28.49
27	5.51	3.03	11.09	12.75	15.70	7.86	21.25	27.57
Mean	**4.97**	**2.61**	**9.56**	**11.08**	**14.62**	**7.16**	**18.75**	**24.84**

30 seconds irradiated sample (layer 1, spacing 12 mm)

Cutting line	Mean forces [kN]				Maximum forces [kN]			
	Cutting	Side	Normal	Total	Cutting	Side	Normal	Total
1	5.44	1.92	10.84	12.28	15.87	5.92	22.25	27.97
2	5.88	1.39	12.18	13.60	16.90	5.83	26.41	31.89
3	6.31	1.23	13.19	14.67	17.44	5.88	27.46	33.06
4	6.15	1.48	12.85	14.33	17.19	6.11	26.18	31.91
5	5.85	1.66	12.40	13.81	16.55	7.36	26.19	31.84
6	6.22	1.53	12.74	14.26	17.30	6.57	27.22	32.91
7	6.02	1.53	12.03	13.54	16.59	6.58	24.37	30.21
8	5.83	1.92	11.84	13.34	16.34	6.85	24.22	30.01
9	6.10	1.91	12.41	13.96	16.72	6.67	24.85	30.68
10	5.77	1.58	11.32	12.81	16.31	6.23	23.57	29.33
11	5.48	1.72	11.14	12.54	16.05	6.57	23.71	29.37
12	5.67	1.69	11.48	12.92	16.05	6.42	23.19	28.92
13	5.09	1.41	9.62	10.97	15.09	5.88	20.42	26.06
14	5.29	1.45	10.41	11.76	15.59	5.79	21.94	27.53
15	5.05	1.14	9.46	10.79	14.97	5.35	19.77	25.36
16	4.84	0.66	9.43	10.63	14.87	4.64	19.89	25.26
17	4.69	0.60	9.04	10.20	14.59	4.26	19.81	24.97
18	4.49	0.45	8.36	9.50	14.28	3.88	17.91	23.23
19	4.59	0.36	8.80	9.93	14.23	3.71	18.29	23.47
Mean	**5.69**	**1.51**	**11.46**	**12.89**	**16.24**	**6.17**	**23.85**	**29.52**

30 seconds irradiated sample (layer 2, spacing 8 mm)

Cutting line	Mean forces [kN]				Maximum forces [kN]			
	Cutting	Side	Normal	Total	Cutting	Side	Normal	Total
2	5.58	3.14	11.04	12.76	16.01	8.30	22.59	28.91
3	5.51	3.22	11.04	12.76	15.64	8.24	21.37	27.73
4	5.59	3.15	11.29	12.98	16.06	8.38	22.93	29.22
5	5.32	3.03	10.16	11.87	14.71	7.35	18.90	25.05
6	5.63	3.36	11.37	13.12	15.87	8.46	22.24	28.61
7	5.35	2.98	10.45	12.11	15.40	7.49	20.18	26.47
8	5.64	3.50	11.51	13.29	16.05	8.82	22.91	29.33
9	5.80	3.57	12.28	14.04	16.49	8.37	23.73	30.09
10	5.77	3.61	12.00	13.80	15.91	8.62	22.79	29.11
11	5.56	3.33	11.03	12.79	15.87	8.53	22.01	28.45
12	5.76	3.47	11.31	13.15	16.31	8.67	22.13	28.83
13	5.70	3.45	11.28	13.10	16.10	8.56	22.09	28.64
14	5.96	3.80	12.46	14.32	16.71	8.88	23.49	30.16
15	5.92	3.56	11.79	13.67	16.34	8.81	23.93	30.29
16	5.62	3.35	11.31	13.06	16.44	8.91	23.51	30.04
17	5.98	3.23	11.84	13.65	16.76	8.35	24.20	30.60
18	5.96	3.37	12.20	13.99	16.90	8.70	25.20	31.57
19	6.03	3.39	12.03	13.87	16.99	8.85	25.20	31.66
20	6.09	3.39	12.47	14.28	17.00	8.87	25.42	31.84
21	6.17	3.71	12.91	14.78	17.38	9.29	25.89	32.54
22	6.05	3.41	12.33	14.15	17.16	8.52	25.75	32.09
23	6.32	3.72	13.17	15.07	17.34	9.25	26.40	32.91
24	6.18	3.52	13.17	14.97	17.39	8.82	26.44	32.85
25	6.10	3.43	13.13	14.88	17.00	8.78	25.84	32.15
26	6.10	3.43	13.13	14.88	17.00	8.78	25.84	32.15
Mean	**5.85**	**3.42**	**11.94**	**13.73**	**16.49**	**8.61**	**23.78**	**30.20**

30 seconds irradiated sample (layer 2, spacing 12 mm)

Cutting line	Mean forces [kN]				Maximum forces [kN]			
	Cutting	Side	Normal	Total	Cutting	Side	Normal	Total
1	7.21	3.62	14.48	16.57	19.40	10.41	30.55	37.66
2	6.98	3.97	14.14	16.26	19.01	10.60	29.39	36.57
3	6.76	3.10	13.27	15.21	18.44	9.81	28.68	35.48
4	6.30	3.04	12.57	14.39	17.28	8.85	25.56	32.10
5	6.29	3.10	12.57	14.39	17.19	8.98	25.97	32.41
6	6.11	2.62	12.49	14.15	17.03	8.07	25.53	31.73
7	5.76	2.26	11.75	13.28	16.75	7.53	25.60	31.51
8	5.95	2.50	12.37	13.95	16.51	7.67	24.52	30.54
9	6.01	1.89	11.99	13.54	17.38	7.82	26.72	32.82
10	6.15	2.45	13.02	14.61	17.01	7.74	25.64	31.73
11	6.37	2.56	13.52	15.17	17.55	8.96	27.23	33.61
12	7.04	2.76	14.79	16.61	18.35	8.89	29.38	35.76
13	6.98	3.09	14.96	16.80	19.16	9.57	32.24	38.71
14	6.98	3.15	15.25	17.07	18.88	9.56	32.34	38.65
15	7.13	3.28	14.97	16.90	19.08	10.63	31.09	37.99
16	7.22	4.11	15.26	17.38	19.17	10.88	30.17	37.36
17	7.45	4.13	16.34	18.42	19.64	11.16	32.27	39.39
18	7.92	4.67	16.71	19.08	20.22	11.62	33.93	41.17
Mean	**6.58**	**2.97**	**13.59**	**15.39**	**18.01**	**9.12**	**28.16**	**34.67**

30 seconds irradiated sample (layer 3, spacing 8 mm)

Cutting line	Mean forces [kN]				Maximum forces [kN]			
	Cutting	Side	Normal	Total	Cutting	Side	Normal	Total
2	6.66	3.73	13.60	15.59	17.66	9.05	26.42	33.05
3	6.39	4.05	13.49	15.46	17.97	10.18	27.47	34.36
4	6.56	3.87	13.19	15.24	18.05	9.89	26.88	33.86
5	5.85	3.48	11.61	13.46	16.62	8.74	23.48	30.06
6	5.94	3.42	12.27	14.06	16.70	8.69	23.85	30.38
7	6.04	3.59	12.41	14.27	16.76	8.59	24.33	30.77
8	5.45	3.07	10.96	12.62	16.10	8.10	21.89	28.35
9	5.50	3.19	11.16	12.85	16.17	8.58	22.76	29.21
10	5.50	3.16	11.06	12.75	16.13	7.90	21.93	28.35
11	5.47	3.03	10.58	12.29	16.40	8.46	22.97	29.47
12	5.61	2.99	11.35	13.01	16.13	8.17	23.43	29.59
13	5.86	3.27	12.27	13.98	16.65	8.41	24.48	30.77
14	5.41	2.76	10.77	12.37	16.03	7.74	22.25	28.49
15	5.57	3.00	11.24	12.90	16.32	8.18	22.42	28.91
16	5.58	3.17	11.25	12.96	15.83	8.21	22.05	28.36
17	5.99	3.39	12.25	14.06	17.19	8.90	25.35	31.89
18	5.97	3.50	11.85	13.72	16.89	9.02	24.70	31.25
19	6.21	3.77	13.18	15.05	17.29	9.40	25.31	32.07
20	6.14	3.02	12.23	14.01	17.71	8.41	26.72	33.14
21	6.60	3.49	13.46	15.39	18.37	8.63	26.66	33.51
22	6.32	2.94	12.82	14.59	17.23	7.94	24.87	31.28
23	6.52	3.55	13.57	15.48	17.81	9.16	27.23	33.81
24	6.72	4.16	14.33	16.36	18.39	10.38	29.59	36.35
25	6.99	4.10	14.57	16.68	19.44	10.54	30.15	37.39
Mean	**6.01**	**3.39**	**12.26**	**14.07**	**17.05**	**8.79**	**24.82**	**31.38**

30 seconds irradiated sample (layer 3, spacing 12 mm)

Cutting line	Mean forces [kN]				Maximum forces [kN]			
	Cutting	Side	Normal	Total	Cutting	Side	Normal	Total
1	6.78	3.25	14.31	16.17	18.62	9.59	30.56	37.05
2	7.22	3.30	15.71	17.60	19.62	9.72	31.81	38.62
3	7.34	3.48	16.06	18.00	19.82	10.51	32.24	39.28
4	7.35	3.80	15.99	18.00	19.38	10.81	31.57	38.59
5	7.41	3.83	16.64	18.62	19.60	11.11	31.83	38.99
6	7.41	3.97	16.36	18.39	19.43	10.71	31.43	38.47
7	7.29	3.35	15.03	17.04	19.33	10.24	32.10	38.85
8	7.26	3.78	14.89	16.99	19.87	10.61	32.16	39.26
9	7.02	3.48	14.69	16.64	18.86	10.51	30.29	37.20
10	6.85	3.41	13.71	15.70	18.22	9.92	27.56	34.50
11	6.83	3.55	14.35	16.29	18.80	10.02	28.70	35.74
12	6.79	3.11	14.41	16.23	18.70	10.08	29.40	36.27
13	6.57	3.23	13.52	15.37	17.96	9.53	28.31	34.85
14	6.75	3.04	14.40	16.20	18.41	9.58	29.94	36.43
15	6.29	2.63	13.42	15.05	17.70	8.59	27.60	33.89
16	6.17	2.33	12.22	13.89	17.55	8.53	27.83	33.99
17	6.46	2.43	13.51	15.17	18.21	8.20	28.74	35.00
Mean	**6.96**	**3.35**	**14.73**	**16.64**	**18.87**	**10.00**	**30.21**	**37.00**

30 seconds irradiated sample (layer 4, spacing 8 mm)

Cutting line	Mean forces [kN]				Maximum forces [kN]			
	Cutting	Side	Normal	Total	Cutting	Side	Normal	Total
2	5.87	3.18	12.62	14.27	16.80	8.18	24.75	31.01
3	5.87	3.14	12.23	13.92	16.22	7.89	23.44	29.58
4	5.81	2.83	12.01	13.64	16.58	7.86	23.53	29.84
5	5.93	3.39	12.27	14.04	16.38	8.08	23.08	29.43
6	6.03	3.52	12.63	14.43	16.76	8.80	24.65	31.08
7	5.90	3.30	12.14	13.90	16.96	8.67	25.33	31.70
8	6.16	3.54	13.14	14.93	17.08	8.74	25.15	31.63
9	6.50	3.82	13.90	15.81	17.87	9.74	28.28	34.84
10	6.37	3.70	13.59	15.45	17.72	9.37	27.42	33.96
11	6.51	3.95	14.35	16.25	18.00	9.77	27.87	34.59
12	5.97	3.67	12.71	14.52	16.85	8.90	25.70	31.99
13	6.19	3.77	13.65	15.45	17.56	9.34	27.01	33.54
14	6.53	3.98	14.31	16.23	17.87	9.51	26.94	33.70
15	6.68	4.20	14.35	16.37	18.01	9.92	27.96	34.70
16	6.40	4.04	13.77	15.72	17.39	9.87	28.10	34.49
17	6.46	2.96	13.43	15.20	17.94	8.86	28.15	34.54
18	7.14	3.48	15.39	17.32	19.14	9.32	32.02	38.45
19	6.67	3.47	14.54	16.37	18.85	9.70	32.54	38.84
20	7.26	4.64	16.86	18.94	19.35	10.89	32.18	39.10
21	6.93	4.48	15.64	17.68	18.83	10.49	30.51	37.36
22	7.31	4.48	16.15	18.28	19.26	10.85	31.56	38.54
23	6.34	3.87	13.77	15.64	17.45	9.08	26.56	33.05
24	6.33	3.55	13.72	15.52	17.41	8.91	27.04	33.37
25	6.81	4.23	16.00	17.90	18.86	9.93	30.13	36.91
26	6.42	3.65	13.73	15.59	18.57	10.70	30.28	37.10
Mean	**6.46**	**3.76**	**14.00**	**15.88**	**17.86**	**9.45**	**27.91**	**34.47**

30 seconds irradiated sample (layer 4, spacing 12 mm)

Cutting line	Mean forces [kN]				Maximum forces [kN]			
	Cutting	Side	Normal	Total	Cutting	Side	Normal	Total
1	6.96	3.18	15.13	16.95	18.58	9.56	30.40	36.89
2	7.65	3.09	16.55	18.49	19.73	9.82	33.29	39.93
3	6.91	2.42	14.92	16.62	18.75	8.37	32.56	38.49
4	7.63	2.97	16.26	18.21	19.97	9.94	34.53	41.11
5	7.15	3.03	16.13	17.90	19.00	9.77	32.17	38.62
6	7.44	3.15	16.94	18.77	20.27	10.23	35.78	42.38
7	7.56	3.40	17.25	19.14	20.03	10.49	35.07	41.73
8	7.55	3.15	17.02	18.88	20.09	10.46	35.05	41.73
9	8.05	3.45	17.86	19.89	21.00	11.29	37.36	44.32
10	7.56	3.37	16.35	18.33	19.78	10.91	32.85	39.86
11	7.53	3.61	16.65	18.63	20.32	10.75	34.08	41.11
12	8.25	4.64	19.00	21.23	21.21	12.25	36.46	43.93
13	7.82	4.06	17.31	19.43	20.49	11.45	34.07	41.37
14	7.36	4.02	16.38	18.40	19.42	11.94	33.24	40.30
15	7.61	4.33	16.51	18.69	20.13	11.94	33.92	41.21
16	7.95	4.32	17.32	19.54	20.29	11.59	35.83	42.77
Mean	**7.56**	**3.51**	**16.72**	**18.69**	**19.94**	**10.67**	**34.17**	**40.99**

30 seconds irradiated sample (layer 5, spacing 8 mm)

Cutting line	Mean forces [kN]				Maximum forces [kN]			
	Cutting	Side	Normal	Total	Cutting	Side	Normal	Total
2	7.09	4.67	15.58	17.74	19.05	11.04	29.71	36.98
3	7.01	4.56	15.63	17.72	18.98	10.56	29.36	36.52
4	6.86	4.55	15.11	17.21	19.80	11.03	31.06	38.45
5	6.10	3.69	12.98	14.81	16.79	8.69	24.07	30.61
6	6.33	3.43	13.04	14.89	17.56	9.18	25.93	32.63
7	6.77	3.64	14.43	16.35	18.37	9.43	28.90	35.52
8	6.80	3.95	14.04	16.09	19.70	10.11	28.59	36.16
9	6.01	3.05	12.41	14.12	17.16	8.44	25.70	32.04
10	6.73	3.69	14.62	16.51	18.46	9.22	28.49	35.18
11	6.52	3.87	13.95	15.88	17.30	9.25	26.08	32.63
12	5.90	3.20	12.19	13.92	17.21	8.70	25.76	32.18
13	6.40	3.78	13.75	15.63	17.39	9.64	27.66	34.07
14	6.29	3.69	13.59	15.42	17.46	9.62	27.82	34.23
15	6.18	3.60	13.44	15.22	17.53	9.60	27.98	34.38
16	6.58	3.93	14.48	16.38	17.79	9.48	27.88	34.40
17	6.84	3.40	13.87	15.83	18.78	9.60	28.47	35.43
18	6.27	2.81	12.83	14.56	17.67	8.15	27.04	33.32
19	6.72	3.00	13.95	15.77	18.30	8.75	28.82	35.24
20	7.48	4.49	16.87	19.00	19.56	10.42	31.50	38.51
21	7.26	4.43	16.32	18.41	19.20	10.85	30.75	37.84
22	7.48	4.43	16.79	18.91	19.92	10.82	33.57	40.51
23	6.40	3.42	13.44	15.27	17.57	8.57	26.78	33.16
24	6.53	3.29	13.44	15.30	18.02	9.04	27.49	34.09
25	7.03	3.89	14.36	16.45	18.82	10.12	28.90	35.94
Mean	**6.63**	**3.73**	**14.15**	**16.07**	**18.23**	**9.53**	**28.20**	**34.91**

30 seconds irradiated sample (layer 5, spacing 12 mm)

Cutting line	Mean forces [kN]				Maximum forces [kN]			
	Cutting	Side	Normal	Total	Cutting	Side	Normal	Total
1	7.27	3.65	15.49	17.50	19.53	9.79	31.19	38.08
2	7.33	3.50	15.70	17.68	19.54	10.46	32.89	39.66
3	7.01	3.14	15.36	17.17	19.53	10.09	32.68	39.39
4	7.33	3.15	15.90	17.79	19.66	9.89	33.69	40.24
5	7.40	2.83	15.96	17.81	20.26	9.47	35.34	41.82
6	7.60	2.55	16.71	18.53	20.01	9.06	34.79	41.15
7	8.20	3.84	18.44	20.54	21.29	11.00	36.55	43.70
8	8.20	3.58	18.38	20.44	21.35	11.87	36.89	44.25
9	8.08	3.50	19.20	21.13	21.26	10.82	37.37	44.34
10	8.36	3.81	18.69	20.83	21.87	11.32	38.26	45.50
11	7.74	3.40	16.96	18.95	20.20	10.79	34.99	41.82
12	8.00	3.33	17.80	19.80	21.06	10.83	37.20	44.10
13	7.80	3.34	17.65	19.58	20.47	10.53	34.96	41.86
14	7.24	3.18	15.97	17.82	19.85	10.62	32.92	39.88
15	7.45	3.41	16.86	18.75	20.14	10.66	33.76	40.72
16	8.40	5.26	19.62	21.98	22.14	12.94	37.02	45.03
Mean	**7.71**	**3.47**	**17.17**	**19.14**	**20.51**	**10.63**	**35.03**	**41.97**

30 seconds irradiated sample (layer 6, spacing 8 mm)

Cutting line	Mean forces [kN]				Maximum forces [kN]			
	Cutting	Side	Normal	Total	Cutting	Side	Normal	Total
2	7.81	4.52	18.03	20.17	20.63	11.02	34.21	41.44
3	7.62	4.47	16.93	19.09	20.60	10.69	31.84	39.40
4	7.33	4.40	16.08	18.22	19.96	10.89	32.27	39.48
5	6.94	3.69	14.62	16.60	18.89	9.68	30.33	37.02
6	6.95	3.97	15.01	17.01	18.48	9.34	28.50	35.23
7	7.28	4.06	15.16	17.30	19.46	10.46	31.56	38.53
8	6.77	4.28	14.85	16.88	18.46	10.47	30.01	36.76
9	6.38	3.84	14.22	16.05	17.57	9.60	27.67	34.16
10	6.60	3.90	14.37	16.29	18.51	10.00	28.54	35.46
11	6.44	3.50	13.50	15.36	18.00	8.83	26.48	33.22
12	6.39	3.11	13.87	15.58	17.86	8.57	26.79	33.32
13	6.50	3.17	14.23	15.96	18.32	8.47	27.86	34.40
14	6.54	3.79	14.61	16.44	18.07	8.99	27.04	33.74
15	6.68	3.65	14.65	16.51	18.96	9.55	28.40	35.45
16	6.48	3.66	15.09	16.82	18.35	9.53	29.77	36.24
17	6.91	3.72	15.09	17.01	19.71	9.24	30.20	37.23
18	6.33	3.22	13.52	15.27	19.75	8.70	29.35	36.43
19	6.64	3.64	14.93	16.74	18.44	9.35	29.48	36.01
20	6.72	4.09	14.59	16.58	18.75	10.10	29.43	36.33
21	7.13	4.57	15.59	17.74	19.33	11.15	31.31	38.45
22	7.18	4.72	16.42	18.54	19.11	10.39	29.71	36.82
23	7.13	3.63	15.26	17.23	18.98	9.45	30.79	37.38
24	7.42	3.94	16.43	18.45	19.99	10.30	31.31	38.55
Mean	**6.88**	**3.89**	**15.09**	**17.04**	**18.96**	**9.77**	**29.69**	**36.57**

30 seconds irradiated sample (layer 6, spacing 12 mm)

Cutting line	Mean forces [kN]				Maximum forces [kN]			
	Cutting	Side	Normal	Total	Cutting	Side	Normal	Total
1	7.77	2.88	17.29	19.18	21.38	9.30	36.55	43.35
2	7.93	2.94	17.93	19.82	21.42	9.56	36.59	43.46
3	8.27	2.90	18.53	20.50	21.00	9.85	37.53	44.12
4	9.02	4.43	20.37	22.72	23.29	12.43	39.90	47.84
5	8.79	4.39	20.48	22.71	22.26	11.87	38.35	45.90
6	8.92	4.37	20.84	23.09	24.76	12.03	40.39	48.88
7	8.38	3.88	18.41	20.60	21.93	11.68	37.17	44.71
8	8.41	4.14	18.97	21.16	22.94	12.24	39.81	47.55
9	7.82	3.44	17.89	19.83	21.69	10.71	37.30	44.45
10	8.14	3.48	18.72	20.71	20.87	10.85	36.65	43.55
11	7.93	3.50	17.66	19.67	22.12	10.70	37.20	44.58
12	7.88	3.20	17.18	19.17	21.06	10.57	34.81	42.04
13	7.21	3.69	16.79	18.64	19.95	10.98	33.32	40.36
14	7.45	3.54	16.68	18.60	20.07	10.80	32.90	40.02
15	7.72	4.18	18.12	20.14	21.19	11.82	35.34	42.87
16	11.20	8.99	24.16	28.11	26.48	16.82	43.02	53.24
Mean	**8.30**	**4.00**	**18.75**	**20.92**	**22.03**	**11.39**	**37.30**	**44.81**

30 seconds irradiated sample (layer 7, spacing 8 mm)

Cutting line	Mean forces [kN]				Maximum forces [kN]			
	Cutting	Side	Normal	Total	Cutting	Side	Normal	Total
2	8.18	4.80	16.91	19.39	19.86	11.40	33.15	40.30
3	7.41	3.97	15.01	17.21	19.42	10.45	31.77	38.68
4	7.27	3.67	15.86	17.83	19.59	10.10	32.52	39.28
5	6.70	3.98	14.50	16.46	18.71	10.23	29.62	36.50
6	6.66	3.88	14.46	16.39	18.14	9.68	28.16	34.86
7	7.26	4.32	15.85	17.97	20.06	10.82	31.85	39.17
8	6.39	3.66	14.26	16.05	18.41	9.71	28.64	35.41
9	6.58	3.23	14.12	15.91	18.90	8.85	28.06	34.97
10	7.04	3.75	15.73	17.64	19.50	9.84	31.84	38.61
11	7.04	3.98	15.01	17.05	19.85	10.20	30.24	37.59
12	6.86	3.95	15.32	17.25	19.15	9.98	29.29	36.39
13	6.78	3.86	15.05	16.95	19.01	9.89	29.53	36.49
14	7.53	4.06	17.34	19.33	20.56	10.53	34.61	41.61
15	7.55	3.98	16.59	18.66	20.74	9.82	32.22	39.56
16	7.44	3.90	17.15	19.10	19.69	10.24	33.36	40.07
17	7.68	5.14	17.51	19.80	20.37	11.32	32.34	39.86
18	7.44	5.22	17.79	19.97	20.72	11.84	32.52	40.34
19	6.86	4.41	15.45	17.47	18.93	10.75	30.57	37.53
20	7.81	4.73	18.56	20.68	20.42	11.35	34.71	41.84
21	7.69	4.73	18.27	20.38	20.97	12.08	36.10	43.46
22	7.58	4.14	17.33	19.36	19.99	10.84	34.45	41.28
23	7.73	5.40	18.84	21.07	21.43	11.74	34.63	42.39
24	7.44	5.10	18.53	20.61	20.68	10.71	33.14	40.50
25	7.71	5.50	19.07	21.29	20.69	11.70	33.78	41.31
26	7.42	4.76	17.29	19.41	20.72	11.02	33.65	41.02
27	7.90	4.88	18.02	20.27	21.83	12.40	35.31	43.32
Mean	**7.27**	**4.37**	**16.61**	**18.65**	**19.98**	**10.68**	**32.11**	**39.31**

30 seconds irradiated sample (layer 7, spacing 12 mm)

Cutting line	Mean forces [kN]				Maximum forces [kN]			
	Cutting	Side	Normal	Total	Cutting	Side	Normal	Total
1	8.20	3.51	18.36	20.41	22.27	11.25	37.24	44.83
2	8.58	3.24	19.84	21.86	23.25	11.39	41.24	48.69
3	8.96	3.33	21.19	23.24	23.14	10.71	41.81	48.97
4	8.92	4.31	22.02	24.15	23.18	11.97	40.42	48.11
5	8.64	4.34	20.65	22.80	23.15	11.75	40.62	48.21
6	8.55	3.94	20.24	22.32	22.94	11.53	38.70	46.44
7	8.25	3.44	19.50	21.45	21.90	11.11	39.25	46.29
8	8.19	3.54	18.49	20.53	22.09	11.22	38.43	45.72
9	8.50	3.68	20.02	22.06	21.90	11.08	38.85	45.95
10	8.29	3.22	18.82	20.81	23.44	11.28	38.97	46.85
11	7.75	3.21	17.46	19.37	20.96	10.53	36.67	43.53
12	8.43	3.65	19.21	21.29	21.74	11.22	38.64	45.73
13	7.67	3.99	18.23	20.18	22.70	11.56	35.88	44.00
14	7.49	4.05	17.60	19.55	21.02	10.92	34.15	41.56
15	7.75	4.76	18.63	20.73	20.85	12.07	36.16	43.45
16	8.07	4.71	18.06	20.33	21.04	11.92	36.08	43.44
17	7.63	3.97	16.36	18.48	20.87	10.99	36.08	43.11
Mean	**8.23**	**3.82**	**19.10**	**21.15**	**22.14**	**11.32**	**38.19**	**45.58**

30 seconds irradiated sample (layer 8, spacing 8 mm)

Cutting line	Mean forces [kN]				Maximum forces [kN]			
	Cutting	Side	Normal	Total	Cutting	Side	Normal	Total
2	6.25	3.06	12.80	14.57	16.90	8.12	24.93	31.20
3	6.33	3.10	13.22	14.99	17.11	8.70	26.18	32.47
4	6.90	3.43	14.71	16.60	18.60	9.15	29.79	36.30
5	6.81	3.88	15.63	17.49	18.22	9.59	29.08	35.63
6	6.87	3.93	15.47	17.38	18.63	9.94	29.64	36.39
7	6.85	3.87	15.44	17.33	18.98	9.48	29.49	36.33
8	7.70	3.86	17.32	19.34	20.57	10.47	33.06	40.32
9	7.29	3.57	16.09	18.02	20.41	9.56	33.35	40.25
10	7.34	3.71	15.95	17.94	20.84	9.97	33.44	40.65
11	8.03	5.22	17.96	20.35	21.71	11.97	34.03	42.10
12	7.57	5.27	17.38	19.68	20.40	11.55	32.28	39.89
13	7.53	5.15	17.38	19.63	20.52	11.27	32.09	39.72
14	7.57	3.88	16.09	18.20	19.81	10.57	32.43	39.45
15	7.17	3.31	15.29	17.21	19.25	9.39	29.84	36.73
16	7.58	3.55	16.49	18.49	20.49	10.62	33.85	40.97
17	7.62	4.60	18.30	20.35	20.73	10.92	34.46	41.67
18	7.44	4.54	17.62	19.66	20.19	10.95	33.19	40.36
19	8.00	4.69	18.63	20.81	22.09	11.58	35.54	43.42
20	7.32	3.66	16.18	18.13	20.48	10.55	33.65	40.78
21	7.32	3.59	16.39	18.31	20.56	10.02	32.82	40.01
22	7.13	3.50	16.34	18.17	20.75	9.77	33.35	40.47
23	6.76	3.84	14.58	16.52	20.13	9.46	28.57	36.20
24	6.96	4.64	16.60	18.59	19.52	10.80	31.34	38.47
25	7.41	4.51	16.90	19.00	20.37	10.89	32.75	40.08
26	6.90	3.80	14.45	16.46	19.51	10.76	30.33	37.63
Mean	**7.31**	**4.09**	**16.40**	**18.42**	**20.12**	**10.40**	**32.10**	**39.30**

30 seconds irradiated sample (layer 8, spacing 12 mm)

Cutting line	Mean forces [kN]				Maximum forces [kN]			
	Cutting	Side	Normal	Total	Cutting	Side	Normal	Total
1	8.45	3.81	18.75	20.91	21.75	11.59	38.26	45.51
2	8.77	4.14	19.45	21.73	22.38	12.53	39.27	46.90
3	8.15	3.53	17.77	19.87	21.66	10.41	36.69	43.86
4	8.18	3.42	18.38	20.41	22.47	11.34	37.58	45.23
5	7.89	3.38	18.18	20.11	20.92	10.54	35.73	42.73
6	7.92	3.16	18.77	20.61	21.45	10.63	37.78	44.73
7	7.82	3.47	18.47	20.36	21.80	11.34	37.19	44.57
8	8.08	4.14	19.04	21.09	21.27	11.38	36.42	43.68
9	7.58	3.74	17.46	19.40	20.45	11.02	34.82	41.85
10	7.03	3.21	16.14	17.90	19.68	9.59	32.74	39.38
11	7.36	3.23	16.43	18.29	22.07	10.03	34.72	42.35
12	7.05	2.55	15.59	17.30	20.54	9.54	35.12	41.79
13	7.13	3.33	16.60	18.37	19.95	10.00	32.72	39.60
14	7.02	3.22	15.94	17.72	19.34	10.22	32.48	39.16
15	7.48	3.56	17.20	19.09	20.02	10.35	34.13	40.90
16	7.89	2.63	17.77	19.62	21.16	9.08	37.12	43.69
17	9.96	4.73	22.33	24.90	24.33	12.70	43.95	51.81
Mean	**7.74**	**3.41**	**17.62**	**19.55**	**21.06**	**10.60**	**35.80**	**42.87**

30 seconds irradiated sample (layer 9, spacing 8 mm)

Cutting line	Mean forces [kN]				Maximum forces [kN]			
	Cutting	Side	Normal	Total	Cutting	Side	Normal	Total
2	7.53	3.71	16.52	18.53	19.98	10.07	32.83	39.73
3	7.05	3.41	15.05	16.96	19.31	9.82	31.21	38.00
4	7.30	3.88	16.63	18.57	18.96	9.70	31.68	38.17
5	7.83	5.10	18.34	20.58	20.79	11.45	34.70	42.05
6	7.60	5.25	17.44	19.74	20.76	11.74	33.22	40.90
7	7.23	4.40	15.35	17.52	20.08	11.25	32.52	39.84
8	7.43	3.70	15.74	17.79	20.37	10.59	33.91	40.95
9	7.50	3.40	16.34	18.30	20.02	9.76	33.79	40.47
10	7.65	3.45	16.43	18.45	20.19	9.82	33.68	40.48
11	8.15	4.93	19.05	21.30	22.72	11.69	35.13	43.44
12	7.60	4.72	17.35	19.52	20.78	11.08	32.25	39.93
13	7.48	4.65	17.00	19.14	20.76	11.33	33.43	40.95
14	6.77	3.25	14.65	16.46	19.83	9.32	30.58	37.62
15	6.97	3.34	15.62	17.43	18.93	9.48	31.50	37.95
16	6.90	3.36	15.07	16.91	18.97	9.50	30.49	37.15
17	7.02	4.13	15.74	17.72	19.28	10.20	30.22	37.27
18	7.47	4.66	16.90	19.05	20.04	11.13	32.89	40.09
19	7.22	4.65	16.57	18.66	20.02	11.00	31.08	38.57
20	6.33	3.23	13.14	14.94	19.24	9.38	27.91	35.17
21	6.53	3.30	14.35	16.11	19.36	8.82	28.34	35.44
22	6.79	3.49	14.85	16.70	18.49	8.90	28.08	34.78
23	6.62	3.59	14.67	16.49	18.38	9.56	29.15	35.76
24	7.23	4.12	15.98	18.02	19.45	10.36	31.48	38.43
25	6.57	3.47	14.10	15.94	19.33	9.63	28.63	35.86
Mean	**7.18**	**3.98**	**15.93**	**17.93**	**19.83**	**10.24**	**31.56**	**38.66**

30 seconds irradiated sample (layer 9, spacing 12 mm)

Cutting line	Mean forces [kN]				Maximum forces [kN]			
	Cutting	Side	Normal	Total	Cutting	Side	Normal	Total
1	8.82	3.63	20.53	22.63	23.21	12.72	41.22	48.99
2	8.53	4.36	20.04	22.21	22.12	11.96	38.34	45.85
3	8.03	3.68	18.39	20.40	21.81	11.89	38.09	45.47
4	6.86	3.01	15.46	17.18	18.77	9.17	31.03	37.41
5	6.99	2.93	15.61	17.35	20.16	8.88	30.92	37.97
6	7.33	3.05	16.89	18.66	20.44	9.40	32.40	39.44
7	6.95	2.75	15.53	17.24	19.38	8.72	31.61	38.08
8	7.08	3.20	15.67	17.49	19.69	9.69	32.31	39.06
9	7.41	3.16	16.15	18.05	20.82	9.79	33.21	40.40
10	7.94	3.05	17.91	19.83	21.67	10.36	37.33	44.39
11	8.06	2.82	19.16	20.98	21.16	10.11	38.75	45.29
12	8.64	3.00	19.31	21.37	22.64	10.89	39.97	47.21
13	9.16	5.08	21.95	24.32	24.40	13.62	43.40	51.62
14	8.68	4.64	21.04	23.23	23.08	12.74	40.84	48.61
15	9.33	5.37	23.41	25.77	23.75	13.14	41.16	49.31
16	9.17	4.92	21.09	23.52	23.24	13.50	41.92	49.79
Mean	**8.06**	**3.67**	**18.63**	**20.64**	**21.65**	**11.04**	**37.03**	**44.31**

Non-irradiated sample (layer 1, spacing 8 mm)

Cutting line	Mean forces [kN]				Maximum forces [kN]			
	Cutting	Side	Normal	Total	Cutting	Side	Normal	Total
2	5.91	3.51	11.72	13.59	16.56	9.88	23.90	30.71
3	5.82	3.65	11.79	13.64	16.52	9.44	24.09	30.70
4	5.93	3.57	12.05	13.90	16.74	9.64	24.75	31.40
5	5.69	3.23	11.77	13.46	16.40	8.57	23.35	29.79
6	5.88	3.37	11.80	13.61	16.45	9.41	23.34	30.06
7	5.96	3.46	11.60	13.49	17.05	9.90	24.16	31.18
8	6.03	3.67	12.25	14.14	17.10	10.18	25.31	32.20
9	6.09	3.78	12.55	14.45	17.15	10.05	25.37	32.23
10	6.38	4.07	13.39	15.38	17.48	10.18	27.46	34.11
11	5.78	3.57	11.75	13.58	16.55	9.80	24.34	31.02
12	5.91	3.71	11.75	13.67	16.78	10.04	23.69	30.72
13	6.12	3.89	13.03	14.91	17.50	9.95	26.84	33.55
14	6.21	3.90	12.87	14.81	16.95	9.70	25.45	32.08
15	5.98	3.52	12.50	14.30	17.07	9.68	25.65	32.29
16	5.86	3.27	12.21	13.93	16.92	9.16	25.92	32.28
17	5.54	3.12	11.09	12.78	15.98	8.70	22.62	29.03
18	5.62	3.16	11.41	13.11	16.57	8.89	24.05	30.53
19	5.45	2.98	10.98	12.61	16.14	8.81	22.78	29.27
20	5.14	2.92	10.96	12.45	15.46	8.70	21.70	28.03
Mean	**5.85**	**3.48**	**11.99**	**13.79**	**16.72**	**9.48**	**24.50**	**31.15**

Non-irradiated sample (layer 1, spacing 12 mm)

Cutting line	Mean forces [kN]				Maximum forces [kN]			
	Cutting	Side	Normal	Total	Cutting	Side	Normal	Total
1	6.20	1.86	12.84	14.38	17.31	6.53	25.76	31.72
2	6.11	1.96	13.26	14.73	17.45	6.24	26.40	32.25
3	6.87	2.61	15.19	16.87	18.58	8.08	29.18	35.52
4	6.23	2.77	13.63	15.24	17.70	7.31	26.28	32.51
5	6.13	2.59	13.43	14.99	17.35	7.88	26.09	32.31
6	6.58	2.78	14.39	16.06	18.32	7.67	29.00	35.14
7	5.94	2.68	12.70	14.27	16.95	7.50	24.19	30.48
8	6.29	2.36	13.53	15.11	17.60	7.13	27.51	33.42
9	6.03	2.28	13.51	14.97	17.31	6.99	25.70	31.77
10	5.55	2.00	11.69	13.10	16.69	6.69	24.11	30.07
11	5.73	2.22	12.53	13.96	16.76	6.96	24.35	30.37
12	6.00	1.93	13.40	14.81	17.24	6.34	26.06	31.88
13	5.77	2.00	12.54	13.95	16.81	6.77	24.67	30.61
14	6.01	2.09	13.19	14.65	17.17	7.04	25.28	31.36
Mean	**6.15**	**2.37**	**13.34**	**14.88**	**17.46**	**7.18**	**26.23**	**32.32**

Non-irradiated sample (layer 2, spacing 8 mm)

Cutting line	Mean forces [kN]				Maximum forces [kN]			
	Cutting	Side	Normal	Total	Cutting	Side	Normal	Total
2	6.42	3.76	13.87	15.74	17.86	9.92	26.73	33.64
3	6.31	3.63	13.40	15.25	17.67	9.47	26.65	33.35
4	6.40	3.70	13.09	15.03	17.73	9.68	26.42	33.25
5	5.89	3.96	12.38	14.26	16.79	9.63	23.37	30.35
6	6.19	4.02	13.17	15.10	17.42	9.62	24.08	31.24
7	6.08	4.22	13.41	15.31	17.23	9.57	24.56	31.49
8	5.86	4.06	12.39	14.29	16.70	9.64	23.77	30.61
9	5.47	3.35	11.06	12.79	16.79	9.46	23.55	30.43
10	5.89	3.92	12.56	14.41	17.12	9.67	25.20	31.97
11	5.67	3.60	11.93	13.70	16.20	8.60	22.60	29.11
12	5.99	3.54	12.85	14.61	17.04	9.34	24.34	31.15
13	5.97	3.74	12.28	14.16	16.92	9.22	24.66	31.29
14	6.19	3.51	12.85	14.68	17.37	9.36	25.54	32.27
15	6.02	3.44	12.59	14.37	17.22	9.00	25.04	31.70
16	6.14	3.47	13.05	14.83	17.46	9.00	25.70	32.35
17	6.15	4.15	13.38	15.30	17.33	9.96	26.79	33.43
18	6.23	4.05	13.74	15.62	17.24	9.42	26.14	32.70
19	6.54	4.45	14.15	16.21	18.35	11.43	29.76	36.78
Mean	**6.04**	**3.82**	**12.80**	**14.67**	**17.18**	**9.54**	**25.10**	**31.88**

Non-irradiated sample (layer 2, spacing 12 mm)

Cutting line	Mean forces [kN]				Maximum forces [kN]			
	Cutting	Side	Normal	Total	Cutting	Side	Normal	Total
1	7.09	3.11	15.49	17.32	19.65	10.08	31.45	38.43
2	7.33	3.15	15.95	17.83	19.70	10.25	32.45	39.32
3	7.39	3.28	17.32	19.11	20.25	9.98	32.49	39.56
4	7.50	4.16	16.53	18.63	19.66	10.59	30.71	37.97
5	7.23	3.85	16.03	18.01	19.29	10.02	31.32	38.13
6	7.14	3.70	16.45	18.31	19.44	10.29	31.96	38.79
7	6.88	3.38	14.98	16.83	18.81	9.42	29.15	35.95
8	7.03	3.37	15.91	17.72	19.59	10.35	32.26	39.13
9	6.99	2.85	16.01	17.70	19.07	9.89	31.01	37.72
10	7.05	3.85	16.07	17.96	19.59	11.16	31.64	38.85
11	6.70	3.42	14.94	16.72	18.69	9.67	29.78	36.46
12	6.93	3.27	15.30	17.11	19.17	9.75	31.02	37.74
13	7.06	3.43	16.08	17.89	19.31	10.44	30.88	37.89
Mean	**7.12**	**3.46**	**15.97**	**17.83**	**19.43**	**10.15**	**31.29**	**38.21**

Non-irradiated sample (layer 3, spacing 8 mm)

Cutting line	Mean forces [kN]				Maximum forces [kN]			
	Cutting	Side	Normal	Total	Cutting	Side	Normal	Total
2	6.57	3.84	13.77	15.73	18.35	10.58	27.97	35.08
3	6.19	3.74	12.87	14.76	16.97	9.85	24.35	31.27
4	6.41	3.75	13.93	15.79	17.91	9.66	27.59	34.28
5	6.23	3.65	13.00	14.87	17.54	10.02	26.41	33.25
6	6.09	3.85	13.03	14.89	17.23	9.56	25.24	32.02
7	6.57	3.93	13.68	15.68	18.65	9.89	27.64	34.77
8	6.50	4.03	14.03	15.98	18.17	9.86	27.25	34.21
9	6.75	4.12	14.38	16.41	18.91	10.79	29.64	36.78
10	6.64	3.88	14.69	16.58	18.17	10.16	28.17	35.02
11	5.74	3.49	11.27	13.12	17.49	9.28	23.33	30.60
12	5.89	3.72	12.04	13.91	17.01	9.31	24.55	31.29
13	6.01	3.69	12.68	14.51	17.58	9.70	26.71	33.41
14	5.77	3.30	11.64	13.41	17.18	9.01	25.11	31.73
15	5.92	3.49	12.45	14.22	17.19	9.41	26.04	32.59
16	6.03	3.54	12.41	14.25	17.42	9.24	24.99	31.84
17	6.19	3.19	12.75	14.53	17.54	9.06	25.65	32.37
18	6.42	3.71	13.19	15.13	18.11	10.34	27.18	34.26
Mean	**6.21**	**3.69**	**13.00**	**14.88**	**17.69**	**9.70**	**26.24**	**33.11**

Non-irradiated sample (layer 3, spacing 12 mm)

Cutting line	Mean forces [kN]				Maximum forces [kN]			
	Cutting	Side	Normal	Total	Cutting	Side	Normal	Total
1	7.19	3.73	15.94	17.88	19.98	10.58	30.85	38.25
2	6.97	3.35	15.07	16.94	19.57	9.56	29.87	36.97
3	6.88	3.57	14.81	16.71	20.17	9.87	30.27	37.69
4	7.14	3.36	16.07	17.91	19.60	9.54	32.27	38.95
5	7.30	3.11	16.02	17.87	20.88	9.68	33.88	40.95
6	7.01	3.27	16.15	17.91	21.42	9.54	34.78	41.95
7	6.50	2.74	14.44	16.07	18.40	8.75	29.66	35.98
8	7.33	3.58	16.45	18.36	20.15	10.49	32.22	39.43
9	7.25	2.99	16.64	18.40	20.02	9.96	33.67	40.42
10	7.06	3.26	16.43	18.17	19.40	10.41	32.33	39.12
11	7.39	3.09	16.99	18.78	20.67	9.83	33.95	40.94
12	6.83	2.64	15.12	16.80	19.57	8.76	31.46	38.07
Mean	**7.09**	**3.28**	**15.91**	**17.73**	**20.02**	**9.84**	**32.16**	**39.15**

Non-irradiated sample (layer 4, spacing 8 mm)

Cutting line	Mean forces [kN]				Maximum forces [kN]			
	Cutting	Side	Normal	Total	Cutting	Side	Normal	Total
2	6.26	3.57	13.95	15.71	18.15	9.59	27.34	34.18
3	6.26	3.83	13.52	15.38	17.17	9.21	25.12	31.79
4	6.36	3.90	13.69	15.59	18.24	9.52	26.24	33.34
5	6.33	3.63	13.61	15.44	17.86	9.16	26.49	33.24
6	6.90	4.17	15.08	17.10	18.54	9.96	28.28	35.26
7	6.83	4.01	15.14	17.08	19.18	9.76	28.96	36.08
8	6.28	3.49	13.48	15.27	17.92	9.24	27.04	33.73
9	6.43	3.63	13.80	15.65	17.99	9.15	26.73	33.49
10	6.51	3.66	14.26	16.10	18.15	8.89	26.81	33.57
11	6.02	3.59	12.67	14.48	17.43	9.43	26.46	33.06
12	6.16	3.74	12.82	14.71	17.85	9.54	26.09	33.02
13	6.16	3.40	12.76	14.57	18.37	9.52	25.90	33.15
14	6.08	3.41	12.76	14.54	18.14	9.82	26.39	33.49
15	6.43	3.65	13.13	15.07	18.35	9.40	25.65	32.91
16	6.38	3.75	13.65	15.52	19.53	9.55	26.54	34.31
17	6.14	3.27	12.60	14.39	17.35	8.92	25.05	31.75
Mean	**6.34**	**3.67**	**13.56**	**15.41**	**18.14**	**9.42**	**26.57**	**33.52**

Non-irradiated sample (layer 4, spacing 12 mm)

Cutting line	Mean forces [kN]				Maximum forces [kN]			
	Cutting	Side	Normal	Total	Cutting	Side	Normal	Total
1	6.06	3.53	12.69	14.50	19.62	10.25	30.19	37.43
2	6.06	3.53	12.69	14.50	19.62	10.25	30.19	37.43
3	6.76	3.82	14.51	16.46	19.40	10.72	29.23	36.68
4	6.76	3.82	14.51	16.46	19.40	10.72	29.23	36.68
5	7.08	4.26	15.06	17.17	19.80	11.33	31.51	38.90
6	7.08	4.26	15.06	17.17	19.80	11.33	31.51	38.90
7	6.84	3.69	13.90	15.93	20.07	10.48	29.85	37.46
8	6.89	3.82	14.39	16.40	19.30	10.75	30.17	37.39
9	6.84	3.49	14.32	16.25	19.17	9.71	29.36	36.38
10	7.34	3.53	15.68	17.67	19.84	9.98	31.57	38.60
11	7.21	3.67	16.19	18.10	20.13	9.97	33.63	40.44
Mean	**6.81**	**3.76**	**14.45**	**16.42**	**19.65**	**10.50**	**30.58**	**37.85**

Non-irradiated sample [additional] (layer 1, spacing 8 mm)

Cutting line	Mean forces [kN]				Maximum forces [kN]			
	Cutting	Side	Normal	Total	Cutting	Side	Normal	Total
5	5.31	3.13	10.40	12.09	15.85	8.96	23.10	29.41
6	4.90	2.77	9.72	11.23	15.25	7.86	21.33	27.37
7	4.78	2.66	9.58	11.04	15.13	8.47	21.44	27.57
8	4.54	2.55	8.35	9.84	15.50	8.37	20.96	27.38
9	4.74	2.26	8.55	10.03	15.15	7.60	20.05	26.25
10	5.18	2.74	9.76	11.39	15.74	7.94	22.41	28.51
11	4.74	2.50	9.32	10.75	14.55	7.23	19.08	25.06
12	4.97	2.84	9.81	11.36	15.31	7.81	21.08	27.20
13	5.00	2.57	9.86	11.35	15.52	7.52	21.08	27.23
14	4.86	2.62	9.37	10.87	14.88	7.31	20.26	26.18
15	5.12	2.83	10.88	12.35	15.83	8.65	24.35	30.31
16	5.00	2.76	10.28	11.76	15.30	7.78	22.10	27.98
17	4.84	2.19	9.63	11.00	14.31	6.54	20.32	25.70
18	5.21	2.17	10.56	11.98	15.77	7.71	23.82	29.59
19	5.15	2.20	10.50	11.90	15.88	7.43	24.18	29.87
20	5.44	2.73	11.39	12.91	16.47	8.11	25.46	31.39
21	5.88	2.83	12.91	14.47	17.79	8.47	28.66	34.78
22	5.90	2.83	13.09	14.64	16.77	7.98	26.61	32.46
23	5.34	2.19	10.64	12.11	15.89	8.36	22.82	29.03
Mean	**5.16**	**2.55**	**10.44**	**11.92**	**15.68**	**7.76**	**22.82**	**28.77**

Non-irradiated sample [additional] (layer 1, spacing 12 mm)

Cutting line	Mean forces [kN]				Maximum forces [kN]			
	Cutting	Side	Normal	Total	Cutting	Side	Normal	Total
1	7.07	2.54	14.03	15.92	19.19	10.05	29.50	36.60
2	6.20	3.61	12.26	14.20	18.01	9.76	26.13	33.20
3	6.53	3.53	12.78	14.77	18.48	10.06	26.47	33.82
4	6.88	3.63	14.02	16.04	18.87	9.85	27.75	34.97
5	6.85	3.62	14.56	16.49	18.51	10.07	28.73	35.62
6	6.88	3.48	14.75	16.64	18.85	9.65	28.53	35.53
7	6.94	3.48	14.74	16.66	18.81	9.56	28.82	35.72
8	6.81	3.34	15.06	16.86	18.57	9.03	28.87	35.49
9	7.07	3.12	15.86	17.64	19.24	9.05	29.94	36.72
10	7.25	3.45	16.36	18.22	19.34	9.69	30.39	37.30
11	7.33	3.11	16.90	18.68	19.71	9.42	31.43	38.28
12	7.86	3.63	17.73	19.73	20.62	10.58	34.14	41.27
13	7.14	3.47	15.32	17.25	19.25	9.94	30.81	37.67
14	7.23	3.00	15.47	17.34	19.47	9.35	31.96	38.58
15	7.46	3.36	17.17	19.01	19.87	10.10	32.75	39.62
16	7.02	3.50	15.32	17.21	19.89	11.28	33.63	40.67
Mean	**6.85**	**3.38**	**14.44**	**16.35**	**18.79**	**9.68**	**28.51**	**35.50**

Non-irradiated sample [additional] (layer 2, spacing 8 mm)

Cutting line	Mean forces [kN]				Maximum forces [kN]			
	Cutting	Side	Normal	Total	Cutting	Side	Normal	Total
2	5.72	3.33	11.13	12.95	16.39	8.84	22.23	29.00
3	5.29	3.10	9.90	11.65	16.49	8.39	21.06	28.03
4	5.12	2.96	9.81	11.46	16.18	8.39	22.50	28.95
5	5.43	3.23	10.43	12.19	15.60	8.45	21.23	27.66
6	4.85	2.95	9.01	10.65	15.28	8.62	20.27	26.81
7	5.11	3.10	10.04	11.68	15.54	8.22	21.66	27.89
8	5.82	3.37	11.60	13.41	16.76	8.87	23.85	30.47
9	5.74	2.99	11.17	12.91	16.12	8.09	21.88	28.35
10	5.67	3.25	11.31	13.06	16.44	8.71	24.08	30.43
11	5.83	3.33	11.86	13.63	16.58	8.59	24.04	30.44
12	6.04	3.66	12.18	14.07	17.04	9.48	25.54	32.13
13	6.02	3.50	12.25	14.09	17.02	8.99	26.32	32.60
14	5.95	2.99	11.98	13.70	16.41	8.05	25.29	31.20
15	5.97	3.10	12.13	13.87	16.35	8.59	24.50	30.68
16	5.95	2.89	12.01	13.72	17.20	8.22	26.05	32.28
17	6.53	3.63	14.17	16.02	17.77	8.73	27.09	33.55
18	7.13	4.05	15.79	17.79	19.15	9.74	30.20	37.06
19	7.14	3.90	15.31	17.33	19.03	9.66	30.15	36.94
20	6.60	3.67	13.23	15.23	17.62	9.56	27.01	33.64
21	5.81	3.03	11.49	13.23	16.77	8.47	25.18	31.42
22	4.36	1.47	8.26	9.45	14.14	6.13	19.07	24.52
Mean	**6.04**	**3.25**	**12.32**	**14.10**	**16.96**	**8.66**	**25.35**	**31.71**

Non-irradiated sample [additional] (layer 2, spacing 12 mm)

Cutting line	Mean forces [kN]				Maximum forces [kN]			
	Cutting	Side	Normal	Total	Cutting	Side	Normal	Total
1	6.62	2.31	13.38	15.11	18.67	7.97	27.84	34.46
2	5.48	2.55	11.25	12.77	16.00	7.45	21.69	27.97
3	6.24	3.12	13.09	14.83	17.56	8.72	25.83	32.43
4	6.38	3.01	13.02	14.81	18.31	8.25	27.12	33.74
5	6.05	3.11	12.20	13.97	16.99	8.82	23.99	30.69
6	6.31	3.52	13.28	15.11	18.27	9.64	26.47	33.58
7	6.62	3.10	13.29	15.17	18.24	8.90	26.54	33.41
8	6.05	3.00	12.74	14.42	18.05	8.62	27.73	34.19
9	6.63	3.86	13.58	15.59	18.64	9.74	28.09	35.09
10	6.19	2.77	12.60	14.31	17.46	8.50	25.62	32.14
11	6.67	2.93	14.14	15.91	18.06	8.84	25.95	32.82
12	6.84	3.28	15.53	17.29	18.85	9.14	29.96	36.56
13	6.82	2.87	14.99	16.72	18.96	8.78	28.96	35.71
14	6.69	2.77	15.03	16.69	18.64	9.02	29.31	35.89
15	6.83	2.77	15.31	16.99	18.74	8.47	29.99	36.36
Mean	**6.26**	**3.04**	**12.84**	**14.61**	**17.82**	**8.66**	**26.09**	**32.77**

Non-irradiated sample [additional] (layer 3, spacing 8 mm)

Cutting line	Mean forces [kN]				Maximum forces [kN]			
	Cutting	Side	Normal	Total	Cutting	Side	Normal	Total
2	5.79	2.70	11.97	13.57	16.52	8.34	25.17	31.24
3	5.54	2.51	11.20	12.74	16.67	7.55	23.66	29.91
4	6.03	2.75	12.71	14.34	18.01	8.25	27.13	33.60
5	6.20	3.27	13.50	15.21	18.08	8.92	28.27	34.72
6	6.50	3.21	13.86	15.64	17.69	8.51	27.27	33.60
7	6.70	3.45	14.59	16.42	18.15	9.06	29.21	35.56
8	5.95	2.84	11.62	13.36	16.46	8.23	23.83	30.11
9	5.83	2.92	11.68	13.38	16.53	8.34	24.25	30.51
10	5.99	3.00	11.72	13.50	16.74	8.79	23.92	30.49
11	5.75	3.33	13.08	14.67	16.55	8.91	25.88	31.99
12	5.77	3.36	12.44	14.12	17.75	8.97	25.12	32.04
13	5.78	3.28	12.14	13.84	17.88	9.08	27.15	33.75
14	5.97	3.58	12.03	13.90	18.13	9.13	25.03	32.23
15	5.87	3.69	11.60	13.52	16.98	9.85	24.84	31.66
16	6.44	3.93	12.56	14.65	18.21	10.08	26.34	33.57
17	5.66	3.34	10.96	12.78	16.52	9.45	23.14	29.96
18	5.58	3.35	11.15	12.91	16.13	8.61	23.20	29.54
19	5.30	3.07	10.25	11.94	16.97	8.77	23.78	30.50
20	6.27	3.39	12.36	14.27	18.04	9.48	26.24	33.22
21	4.53	1.81	8.67	9.95	15.19	7.17	21.88	27.58
Mean	**5.83**	**3.22**	**11.79**	**13.55**	**17.08**	**8.93**	**24.92**	**31.51**

Non-irradiated sample [additional] (layer 3, spacing 12 mm)

Cutting line	Mean forces [kN]				Maximum forces [kN]			
	Cutting	Side	Normal	Total	Cutting	Side	Normal	Total
1	6.90	1.46	15.95	17.44	19.15	7.36	31.15	37.30
2	6.80	2.28	14.87	16.51	19.21	8.92	29.63	36.42
3	6.06	1.67	12.52	14.02	17.83	7.62	27.17	33.38
4	6.12	2.05	13.31	14.79	17.54	6.98	27.24	33.14
5	7.00	1.81	15.38	16.99	18.74	7.48	29.75	35.95
6	6.65	1.62	14.92	16.41	18.56	7.56	29.35	35.54
7	6.69	2.59	15.14	16.75	19.45	8.35	29.91	36.64
8	6.64	2.24	15.06	16.61	18.71	7.43	29.45	35.67
9	7.49	3.07	16.64	18.51	20.24	9.28	32.24	39.18
10	7.30	3.52	16.35	18.25	20.60	9.82	32.02	39.31
11	7.22	3.79	16.18	18.11	19.87	10.53	31.27	38.52
12	7.70	3.64	17.65	19.60	21.21	10.30	35.10	42.28
13	7.24	4.02	15.25	17.35	19.53	10.31	29.47	36.83
14	7.53	4.47	15.97	18.21	20.52	11.36	30.74	38.67
Mean	**6.76**	**2.23**	**15.01**	**16.63**	**19.00**	**8.08**	**29.79**	**36.25**

Non-irradiated sample [additional] (layer 4, spacing 8 mm)

Cutting line	Mean forces [kN]				Maximum forces [kN]			
	Cutting	Side	Normal	Total	Cutting	Side	Normal	Total
2	6.31	3.25	13.33	15.10	17.44	9.23	24.85	31.74
3	6.70	3.64	13.98	15.92	18.06	9.89	26.60	33.64
4	6.51	3.56	13.95	15.80	17.94	9.36	26.73	33.52
5	6.57	3.76	14.55	16.41	18.31	9.49	27.78	34.60
6	6.80	3.71	15.09	16.96	18.54	9.39	28.19	35.03
7	6.79	3.63	14.84	16.72	18.93	9.11	27.97	34.98
8	6.47	3.58	13.88	15.73	18.22	9.21	25.13	32.38
9	5.92	3.14	12.08	13.82	18.81	9.25	25.21	32.79
10	6.34	3.40	13.62	15.40	17.54	9.38	26.66	33.26
11	5.54	2.92	12.03	13.56	16.37	8.53	23.77	30.10
12	5.65	2.84	12.57	14.07	17.13	8.29	25.26	31.63
13	5.81	2.99	12.84	14.40	16.91	8.36	24.18	30.67
14	5.79	3.38	11.68	13.47	16.87	9.06	23.10	30.00
15	5.42	3.02	11.06	12.69	16.05	8.87	21.88	28.55
16	6.03	3.66	12.65	14.49	18.04	9.38	24.74	32.02
17	5.66	3.07	11.08	12.82	17.67	8.40	21.61	29.15
18	5.48	3.21	10.94	12.65	16.14	8.75	21.41	28.21
19	5.45	3.07	10.56	12.28	16.01	8.74	20.56	27.49
20	5.75	3.06	11.58	13.28	17.23	9.98	25.16	32.09
Mean	**5.93**	**3.25**	**12.43**	**14.16**	**17.36**	**8.98**	**24.32**	**31.22**

Non-irradiated sample [additional] (layer 4, spacing 12 mm)

Cutting line	Mean forces [kN]				Maximum forces [kN]			
	Cutting	Side	Normal	Total	Cutting	Side	Normal	Total
1	7.92	2.91	17.65	19.56	20.27	8.44	33.01	39.64
2	7.62	2.80	16.75	18.62	20.46	8.61	31.76	38.75
3	7.72	3.17	16.63	18.61	22.22	9.04	32.36	40.28
4	7.58	3.84	15.12	17.34	22.60	9.86	29.90	38.76
5	7.57	4.31	16.04	18.25	19.83	10.33	28.81	36.47
6	7.10	3.75	14.87	16.90	20.17	10.25	30.33	37.84
7	6.93	3.76	14.25	16.29	20.14	9.73	28.06	35.89
8	7.00	4.05	14.19	16.33	20.28	10.03	27.60	35.69
9	6.74	3.64	14.00	15.96	18.10	9.36	27.03	33.85
10	6.80	3.46	14.82	16.67	18.27	8.99	27.40	34.14
11	6.67	3.52	14.50	16.35	18.50	8.89	27.36	34.21
12	6.08	2.83	12.89	14.53	17.44	8.40	25.67	32.14
13	6.80	2.95	15.30	17.00	19.85	8.61	29.74	36.78
Mean	**7.30**	**3.57**	**15.43**	**17.45**	**20.23**	**9.46**	**29.63**	**37.13**

Non-irradiated sample [additional] (layer 5, spacing 8 mm)

Cutting line	Mean forces [kN]				Maximum forces [kN]			
	Cutting	Side	Normal	Total	Cutting	Side	Normal	Total
2	6.37	3.58	13.05	14.96	18.69	10.12	28.22	35.33
3	6.74	4.03	13.58	15.68	19.28	10.66	28.31	35.87
4	6.73	4.13	13.88	15.97	18.29	10.15	28.04	34.98
5	6.02	3.37	11.93	13.78	18.34	9.38	24.84	32.27
6	5.53	3.12	10.91	12.63	17.26	8.73	23.97	30.80
7	5.87	3.38	11.62	13.45	17.41	9.46	24.57	31.56
8	6.31	3.34	12.73	14.59	18.15	9.33	26.54	33.48
9	6.26	3.30	12.77	14.60	18.62	9.09	27.27	34.25
10	6.12	3.27	12.63	14.41	17.93	9.39	27.16	33.87
11	5.74	3.02	11.70	13.38	17.87	8.99	27.04	33.63
12	6.56	3.53	13.59	15.50	18.83	9.49	28.68	35.60
13	6.44	3.75	14.14	15.99	19.04	9.59	28.26	35.40
14	6.08	2.90	12.57	14.26	17.41	8.63	26.59	32.94
15	6.28	2.91	13.46	15.13	18.15	8.72	28.18	34.63
16	6.41	2.93	13.63	15.35	18.87	8.76	28.82	35.55
17	6.52	3.11	13.59	15.39	18.12	8.38	27.22	33.76
18	6.77	3.10	13.91	15.78	19.18	9.32	30.54	37.25
19	6.31	2.85	13.12	14.84	17.75	8.38	26.71	33.15
Mean	**6.21**	**3.19**	**12.82**	**14.60**	**18.19**	**9.04**	**27.09**	**33.88**

Non-irradiated sample [additional] (layer 5, spacing 12 mm)

Cutting line	Mean forces [kN]				Maximum forces [kN]			
	Cutting	Side	Normal	Total	Cutting	Side	Normal	Total
1	8.30	2.91	17.96	20.00	21.49	9.56	34.99	42.16
2	8.09	3.31	17.52	19.58	21.89	10.03	35.02	42.50
3	7.22	2.51	15.85	17.60	20.55	8.42	32.51	39.37
4	7.37	3.36	16.90	18.74	21.46	9.82	32.16	39.89
5	7.42	3.08	17.16	18.94	23.38	9.42	33.98	42.31
6	7.46	2.77	16.73	18.53	25.91	9.02	35.30	44.70
7	6.67	2.50	13.90	15.62	22.37	9.21	28.93	37.72
8	6.78	2.78	14.56	16.30	19.60	8.44	27.72	34.98
9	6.70	2.87	14.65	16.36	19.28	9.11	30.59	37.29
10	6.64	3.10	14.69	16.42	20.16	9.83	28.94	36.61
11	6.81	3.31	14.71	16.54	20.13	9.09	29.20	36.61
12	7.03	3.72	15.33	17.27	19.76	10.24	29.66	37.08
Mean	**7.27**	**2.92**	**15.99**	**17.81**	**21.61**	**9.29**	**32.01**	**39.75**

Non-irradiated sample [additional] (layer 6, spacing 8 mm)

Cutting line	Mean forces [kN]				Maximum forces [kN]			
	Cutting	Side	Normal	Total	Cutting	Side	Normal	Total
2	6.83	3.37	13.65	15.64	18.46	9.45	29.37	35.95
3	6.10	3.03	12.42	14.17	19.43	8.79	27.31	34.65
4	6.46	3.16	12.86	14.73	19.55	9.41	29.47	36.59
5	6.37	3.50	13.28	15.14	18.22	9.06	26.93	33.76
6	6.69	3.72	14.30	16.22	19.45	9.54	28.89	36.11
7	6.60	3.48	13.66	15.56	18.89	9.11	28.08	35.05
8	6.45	3.17	12.96	14.82	19.37	8.89	27.77	35.01
9	6.39	3.08	12.97	14.79	19.06	9.18	27.20	34.46
10	6.41	3.11	13.13	14.94	19.69	9.09	28.50	35.81
11	6.59	2.95	13.01	14.88	19.48	8.68	29.16	36.12
12	6.86	3.22	14.60	16.45	18.98	9.24	29.88	36.58
13	7.46	3.44	15.50	17.54	20.66	9.87	32.79	39.99
14	6.79	3.80	13.78	15.83	18.52	9.97	28.33	35.29
15	6.84	4.07	14.07	16.17	19.33	10.80	29.44	36.84
16	7.06	4.38	14.81	16.98	19.82	10.29	30.39	37.71
17	6.18	3.47	12.61	14.46	17.98	9.72	28.07	34.72
18	5.53	2.54	11.00	12.57	17.24	8.13	23.93	30.60
Mean	**6.58**	**3.41**	**13.50**	**15.41**	**19.08**	**9.40**	**28.59**	**35.64**

Non-irradiated sample [additional] (layer 6, spacing 12 mm)

Cutting line	Mean forces [kN]				Maximum forces [kN]			
	Cutting	Side	Normal	Total	Cutting	Side	Normal	Total
1	8.12	2.24	17.99	19.86	23.37	9.72	36.44	44.37
2	7.29	3.01	16.49	18.28	19.69	8.96	30.83	37.67
3	7.16	2.77	15.55	17.34	19.36	9.43	31.63	38.27
4	7.17	2.85	15.50	17.31	19.43	9.21	30.69	37.47
5	7.43	2.97	16.42	18.27	20.56	9.12	31.81	38.96
6	7.12	2.25	16.38	18.00	19.81	8.33	32.58	39.03
7	7.39	2.39	16.13	17.90	20.79	8.04	31.77	38.81
8	7.59	2.34	16.92	18.70	22.18	8.12	33.41	40.92
9	7.56	1.98	16.97	18.68	20.59	7.56	32.90	39.54
10	7.56	3.17	17.53	19.35	21.31	9.41	32.62	40.09
11	7.68	3.29	17.88	19.74	21.71	10.18	34.55	42.06
Mean	**7.44**	**2.60**	**16.59**	**18.37**	**20.71**	**8.79**	**32.47**	**39.51**

Non-irradiated sample [additional] (layer 7, spacing 8 mm)

Cutting line	Mean forces [kN]				Maximum forces [kN]			
	Cutting	Side	Normal	Total	Cutting	Side	Normal	Total
2	7.14	3.90	15.57	17.57	19.36	10.24	30.00	37.14
3	7.01	3.78	14.71	16.72	19.38	10.53	30.84	37.92
4	6.62	3.61	13.88	15.80	19.03	10.24	29.22	36.34
5	6.83	3.85	14.07	16.10	19.55	10.20	29.64	36.94
6	7.12	3.98	14.51	16.65	19.86	10.20	28.79	36.43
7	6.78	3.87	14.26	16.26	18.65	9.86	28.83	35.72
8	6.64	3.85	14.24	16.17	18.87	10.65	29.85	36.88
9	6.88	3.89	14.47	16.49	19.30	11.06	31.05	38.20
10	7.14	4.21	15.46	17.54	19.50	10.57	30.96	38.09
11	6.58	3.24	13.28	15.17	19.22	9.45	28.77	35.86
12	6.77	3.30	14.26	16.13	18.52	9.99	30.67	37.20
13	6.85	3.56	14.62	16.53	18.81	9.80	29.01	35.94
14	6.91	3.23	14.38	16.28	19.06	9.46	30.68	37.34
15	7.16	3.28	15.53	17.41	19.42	9.72	31.06	37.90
16	6.60	2.66	13.68	15.42	19.14	8.93	29.53	36.31
Mean	**6.87**	**3.61**	**14.46**	**16.42**	**19.18**	**10.06**	**29.93**	**36.95**

Non-irradiated sample [additional] (layer 7, spacing 12 mm)

Cutting line	Mean forces [kN]				Maximum forces [kN]			
	Cutting	Side	Normal	Total	Cutting	Side	Normal	Total
1	7.73	2.85	16.60	18.53	21.05	9.63	34.38	41.45
2	6.81	3.54	14.33	16.26	19.21	10.14	31.37	38.16
3	7.74	3.99	16.68	18.82	21.08	10.54	32.26	39.95
4	7.76	4.33	16.70	18.92	21.40	11.89	33.40	41.42
5	6.87	3.91	14.64	16.64	19.30	11.05	30.04	37.37
6	7.58	4.25	16.19	18.38	20.92	11.17	31.71	39.60
7	7.05	3.70	15.16	17.12	19.18	11.25	29.98	37.33
8	7.14	3.97	15.29	17.33	19.70	11.04	29.75	37.35
9	6.39	3.18	13.22	15.02	18.13	9.21	28.39	34.92
10	6.97	3.10	15.56	17.33	19.18	9.42	29.58	36.49
Mean	**7.20**	**3.68**	**15.44**	**17.44**	**19.91**	**10.53**	**31.09**	**38.40**